Cosmic structure formation in non-Copernican cosmological model
(非コペルニクス的宇宙モデル上の構造形成)

Ryusuke Nishikawa
(西川 隆介)

Cosmic structure formation in non-Copernican cosmological model
(非コペルニクス的宇宙モデル上の構造形成)

大阪市立大学理学研究科
数物系専攻

平成25年度

Ryusuke Nishikawa
(西川 隆介)

PhD Thesis

Cosmic structure formation in non-Copernican cosmological model

Ryusuke Nishikawa

Department of Mathematics and Physics, Graduate School of Science, Osaka City University

Abstract

Copernican Principle which states "*we are not living in a special position in our universe*" is the most fundamental assumption in modern cosmology, and thus its observational test is one of biggest challenges. Recent technological developments have enabled us to pursue observational tests of the Copernican Principle. Therefore, theoretical studies of non-Copernican cosmological models which drop the Copernican Principle have gathered much attention in recent years.

In this thesis, in order to develop observational tests of the Copernican Principle, we study cosmic structure formation in a non-Copernican cosmological model. We focus on an inhomogeneous and isotropic Lemaître-Tolman-Bondi (LTB) cosmological model which is the most popular model in the study of non-Copernican cosmological models.

Firstly, we consider relativistic linear perturbations in a LTB cosmological model. It is known that perturbation equations in LTB spacetimes are hard to solve analytically. To avoid the difficulty, we focus on a LTB cosmological model of which radial inhomogeneity is small, and treat it as an isotropic linear perturbation around a FLRW universe. In this case, linear perturbation equations in a LTB cosmological model can be reduced to nonlinear perturbation equations in a FLRW universe. We solve the reduced equations order by order, and obtain density perturbations up to the second order around a FLRW universe. By computing a two-point correlation function of density perturbations, we show that it has a distortion (local anisotropy) due to the existence of tidal fields in a LTB cosmological model. Since no tidal force exists in homogeneous and isotropic FLRW universe models, our result suggests that we can test the non-Copernican cosmological model by observing a statistical distortion of the galaxy distribution.

Secondly, we consider nonlinear structure formation at subhorizon scales in a LTB cosmological model of a huge void. It is not clear how a relativistic huge void affects to Newtonian structures such as galaxies and clusters. To reveal the effects, we derive equations of non-relativistic hydrodynamics and Newtonian gravity for a fluid in a LTB cosmological model, by applying Cosmological Newtonian approximation to perturbations and a local approximation to a background LTB spacetime. From the derived equations, we show that local anisotropic volume expansion of a LTB cosmological model significantly affects to the evolution of Newtonian structures. Our result suggests that observations involved in Newtonian structure formation can give a strong constraint for non-Copernican cosmological models.

Acknowledgments

I would like to thank Prof. Ken-ichi Nakao for his continuous encouragement, meaningful discussions, and genuine support throughout my post graduate study. I am thankful to my collaborator Dr. Chul-Moon Yoo for his many useful and helpful discussions and his constant encouragement. I am also grateful to Prof. Hideki Ishihara and colleagues in the astrophysics and gravity group of Osaka City University, especially, Shunichiro Kinoshita, Masashi Kimura, Takahisa Igata, Ryotaku Suzuki, Hiroyuki Abe, Takamitsu Tatsuoka, Masato Takada, Tatsuya Uno, Atsuki Masuda and Hiroyuki Negishi, for many useful discussions and valuable advice.

I appreciate Prof. Hideki Ishihara and Prof. Ken-ichi Nakao for sending me to AstroParticle and Cosmology laboratory (University of Paris 7), which has benefited my research life. I would like to thank Prof. David Langlois for his kind hospitality and valuable discussions during one year of my student life in University of Paris 7. I also wish to thank Dr. Shuntaro Mizuno, Dr. Atsushi Naruko and Dr. Takahisa Igata for their useful discussions and kind supports during my stay in Paris.

This work was supported by a Grant-in-Aid through the Japan Society for the Promotion of Science (JSPS), and by the JSPS Strategic Young Researcher Overseas Visits Program for Accelerating Brain Circulation "Deepening and Evolution of Mathematics and Physics, Building of International Network Hub based on OCAMI".

Finally, I would like to thank my parents for their every support for my long student life.

Contents

Chapter 1

Introduction

1.1 Copernican Principle

Modern physical cosmologies commonly assume that our universe is spatially isotropic and homogeneous on large scales ≥ 1 Gpc. Accordingly, the background spacetime is described by the Friedmann-Lemaître-Robertson-Walker (FLRW) universe model. The Big Bang theory based on the FLRW universe model has been succeeded in predicting cosmological observations, including the expansion of the universe according to Hubble's law, the existence of the Cosmic Microwave Background (CMB) radiation and the relative abundances of light elements. In addition, perturbation theory in the FLRW universe accounts for almost all observations about the cosmic structure formation, including the CMB temperature fluctuations and the galaxy clustering, with a few parameters called the cosmological parameters. The success of the FLRW universe model seems to imply that our universe is isotropic and homogeneous on large scales. However, we should not blindly rely on the assumption without observational justifications, and should test it in all ways possible.

The isotropy of our universe can be confirmed directly, and the observed isotropy of the CMB radiation with high accuracy of about 10^{-5} implies the isotropy of our universe[1]. By contrast, the homogeneity of the universe cannot be confirmed directly, since we observe the universe from effectively one spacetime event. In order to lead to FLRW universe model from the observed isotropy, we commonly assume the *Copernican Principle* which states we are not living in a special position in the universe. The Copernican Principle is a weaker assumption than the *Cosmological Principle* that our universe is spatially isotropic and homogeneous on

[1]To prove the isotropy of spacetime, the isotropy of the CMB radiation is not enough and other observations – angular diameter distances, number counts, lensing distortion and transverse velocities – on the past lightcone are needed. See Ref. [5] in detail.

large scales. Thanks to the observed CMB isotropy, we can employ the Copernican Principle as a fundamental working hypothesis of the FLRW universe model instead of the Cosmological Principle.

Since observational data are usually interpreted under the assumption of homogeneity of the background spacetime, modern cosmology would contain systematic errors that arise from the inhomogeneities never perceived. The systematic errors may mislead us when we consider major issues in modern cosmology such as probing Dark Energy abundance and testing General Relativity at cosmological scales. Therefore, it is an unavoidable task to test the Copernican Principle in observational cosmology.

We cannot prove the Copernican Principle or homogeneity of the universe for now. However, we can progress observational tests for consistency of the Copernican Principle and the homogeneity, and their possibility has been discussed since many years ago [1, 2]. Recently, a few observational tests of the homogeneity have been proposed (see comprehensive reviews [3, 4, 5]). We give concrete examples of them as follows. First, a consistency relation between the luminosity distances and the expansion rates, which must be satisfied for all FLRW models can be used [6]. Second, a consistency relation between the radial and transverse Baryon Acoustic Oscillation (BAO) scales, which must be satisfied for all FLRW models can also be used [5]. Third, the non-perturbative thermal or kinetic Sunyaev-Zeldovich (SZ) temperature effect can show a violation of homogeneity [7]. Fourth, the time drift of cosmological redshifts can be used as a test of homogeneity [8]. If we find no violation from the homogeneity, we can strengthen our confidence in the Copernican Principle. By contrast, if we find any violation from the homogeneity, we should relinquish the Copernican Principle and modify the FLRW universe model.

Thanks to recent technological developments, we have begun to be able to test the Copernican Principle observationally as given above, and thus theoretical studies of cosmological models which drop the Copernican Principle are receiving much attention in recent years. We call such models the non-Copernican cosmological models. The non-Copernican models commonly assume that we live close to the center in an isotropic spacetime since the universe is observed to be nearly isotropic around us. We can see such models are contradict to the Copernican Principle, since it is assumed that we are living at a special position (near the symmetric center) in the universe. The most common way to describe the non-Copernican models is to use the Lemaître-Tolman-Bondi (LTB) [9, 10, 11] solution for the Einstein equations, which describes the motion of spherically symmetric dust. Thus, we call such non-Copernican cosmological models the LTB cosmological models throughout

this thesis. The LTB cosmological models have also been studied as an alternative to Dark Energy, as we will review in the next section.

Here, it should be noted an observational constraint concerning our location in the LTB cosmological models. The observed dipole component of the CMB temperature anisotropy limits the position of the observer, and some studies showed that the observer has to be located within about a radius of 15Mpc from the symmetric center [12, 13].

1.2 Dark Energy and non-Copernican cosmological model

The ΛCDM model, which can account for almost all observational results with a suitable values of the cosmological parameters, contains unknown souses of Cold Dark Matter (CDM) and Dark Energy in the form of a cosmological constant Λ. Although there exist a large number of Dark Energy models that attempt to provide a dynamical explanation for the cosmological constant, there seems to be no satisfactory theory that can naturally explain the existence or the abundance of the observed Λ. This motivates us in dropping the Copernican Principle to construct an alternative cosmological model that mimic the observations without introducing Dark Energy.

The observational results of the magnitude-redshift relation for distant Type Ia supernovae (SNIa) [14, 15, 16, 17] have played a central role in the study of Dark Energy and Copernican Principle. As long as we assume a homogeneous and isotropic universe model, the observation of SNIa indicates an acceleration of the cosmic volume expansion. This implies the existence of Dark Energy that acts as a source of a repulsive gravitational force, if we assume General Relativity at cosmological scales. However, if we relinquish homogeneity of the universe at cosmological scales, the observed magnitude-redshift relation can be interpreted as the spatial inhomogeneity of the volume expansion instead of the accelerating expansion. This is essentially understood as follows. Since the observational data is given on our past light cone, an expansion rate increasing in time can be hard to distinguish from an expansion rate decreasing in the radial coordinate of the observer. In the last decade, many LTB cosmological models which are compatible with SNIa observations have been constructed by many authors [18, 19, 20, 21, 22, 23, 24, 25, 26, 27, 28, 29, 30, 31].

LTB spacetime is governed by two free radial functions, the curvature function $k(r)$ and the Big-Bang time $t_{\mathrm{B}}(r)$ (we will define these in Chap. 2), where r is the radial coordinate of the observer at the spherical symmetric center. The curvature

function and the Big-Bang time correspond to the growing and decaying modes respectively, if we linearize the LTB spacetime around the FLRW spacetime (we will show it in Chap. 2). Many of LTB cosmological models assume the homogeneous Big-Bang time, $t_{\rm B}(r) = 0$, in order not to contradict to the standard inflationary scenario at sufficiently early times. In the case of inhomogeneous Big-Bang time, $t_{\rm B}(r) \neq 0$, since LTB cosmological models contradict to the inflationary scenario, it seems to be difficult to analyze perturbations which seed all cosmic structures.

The free radial function $k(r)$ can be adjusted to account for the observational data of the magnitude-redshift relation. Thus, other observations are needed to distinguish LTB cosmological models from the ΛCDM model. A number of papers for this purpose have appeared, giving constraints from various observations including the CMB acoustic peaks [32, 33, 34, 35, 36, 37, 38, 39, 40, 41, 42, 43], the present Hubble parameter H_0 [34, 35, 37, 38, 40], the BAO scale of the galaxy correlations [34, 44, 45], the kinematic Sunyaev-Zeldovich (kSZ) effect [46, 47, 48, 49, 50, 51] and others [52, 53, 54, 55, 56, 57, 58, 59, 60, 61, 62, 63, 64, 65, 66, 67, 68, 69, 70, 71, 72, 73]. Constraints arising from a combination of these observations have also been discussed [34, 35, 37, 38, 40, 45]. It is notable that observational results of the kSZ effect ruled out a simple LTB cosmological model, which assumes the homogeneous Big-Bang time and the adiabatic perturbation scenario. However, LTB cosmological models with non-adiabatic (isocurvature) perturbations or the inhomogeneous Big-Bang time have not yet been ruled out from the observations mentioned above. Therefore, further studies testing LTB cosmological models are needed. Future observations of the cosmological redshift drift are expected to give strong constraints on a wide class of LTB cosmological models, including models with the inhomogeneous Big-Bang time and with the isocurvature mode [8, 74, 75].

huge void model

It is worthwhile to review a huge void model that is the most popular model among the non-Copernican cosmological models proposed as an alternative to Dark Energy. A huge void model assumes that we are living close to the center in a nonlinear huge void of which size is about 1Gpc. This model is induced from a LTB cosmological model which assumes the simultaneous Big-Bang time and is consistent with the SNIa observations (we will see it in Chap. 2). Here, let's see a few philosophical questions concerning a huge void universe model. First, one may ask how does the inflationary scenario produce such a nonlinear huge void. One possible origin is that the void exists as a rare and large amplitude perturbation within the primordial Gaussian random field produced during inflation. Then, one may ask why are

we living very close to a center of the void. One possible explanation for this is given from highly speculative quantum cosmological ideas [76]. Apart from these questions, it is important to develop consistency tests of the homogeneity based on observations rather philosophical objections.

ΛLTB cosmological model

Recently, some papers have appeared studying a ΛLTB cosmological model, which contains the cosmological constant Λ and the spherically symmetric dust [77, 78]. These studies try not to give an alternative explanation for dark energy, but to investigate a systematic error arising from a non-Copernican inhomogeneity on the equation of state for dark energy. It is important to test the ΛLTB model by using various observations, in order to construct precision and accurate cosmology that eliminates the systematic error coming from the inhomogeneity and determines the cosmological parameters with higher accuracy than before.

1.3 Cosmic structure formation as a test of cosmological models

As we saw in the previous section, the background dynamics of non-Copernican cosmological models has been studied well. Accordingly, various observational quantities which are determined from the background dynamics have been used in testing these models. However, the growth of perturbations in the non-Copernican models has not been fully studied, and hence observational quantities involved in the *cosmic structure formation* have not been adequately considered as a test of these models. In this thesis, in order to develop a test of the Copernican Principle by using observations of the cosmic structure formation, we study the evolution of fluctuations in the LTB cosmological model.

Many observational results on the cosmic structure formation have been compared with the prediction of cosmological perturbation theory in the homogeneous and isotropic FLRW models. In this section, we review a few observations, including the Baryon Acoustic Oscillation (BAO) scales, the Redshift Space Distortions (RSD) and the gravitational weak lensing, which have given constraints for the cosmological parameters. Then, we discuss a possibility to test the non-Copernican cosmological models by using these observations.

1.3.1 Baryon Acoustic Oscillations

Before the last scattering, the tightly coupled photon-baryon plasma oscillates under the competing effects of gravitational collapse and radiation pressure. This is called the Baryon Acoustic Oscillations (BAO), and the imprint of BAO scales have observed in the galaxy clustering. In the study of the FLRW universes, the BAO scale is used as a *standard ruler*, which is an object of a known size at different redshifts. This is because that the BAO scale at the decoupling time is predicted via well-understood linear perturbation theory in the pre-decoupling era, and after the decoupling the comoving BAO scale is frozen that is justified by linear perturbation theory after the decoupling epoch. Thus, by observing the BAO scales at different redshifts, we can determine the history of volume expansion in the universe.

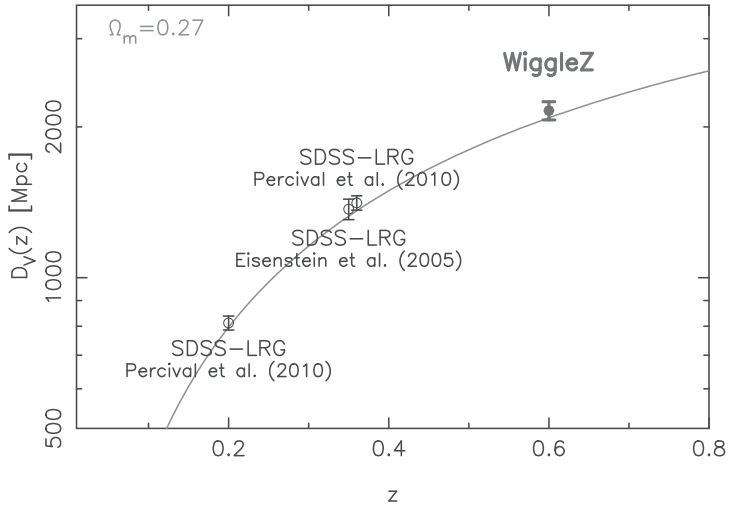

Figure 1.1: Measurements of a distance-redshift relation using the BAO standard ruler from SDSS-LRG and WiggleZ analysis (From Blake et al. [79]). The results are compared to a fiducial flat ΛCDM cosmological model with the matter density $\Omega_{\rm M} = 0.27$.

Fig. 1.1 shows measurements of an averaged distance $D_{\rm V}$ and the redshift z relation by observing the BAO scales at different redshifts [79], where $D_{\rm V}(z)$ is defined from the angular distance $D_{\rm A}(z)$ and the Hubble function $H(z)$ as $D_{\rm V}(z) = [(1+z)^2 D_{\rm A}(z)^2 (cz/H(z))]^{1/3}$. From fig. 1.1, we can see that the observational results are consistent with a concordant ΛCDM model with $\Omega_{\rm M} = 0.27$, where $\Omega_{\rm M}$ is a cosmological parameter of the matter density. The BAO observations have given a strong constraint for the cosmological parameters.

In the case of the LTB cosmological models, it is not clear whether the BAO scale should be considered as a standard ruler. In other words, it is not clear whether the comoving BAO scales in the LTB models are frozen after the decoupling. This is because that the growth rate of structures in the LTB models can be different at different places, and consequently the evolution of the BAO scales can differ from that of the volume expansion of the background LTB spacetime. We need a knowledge of perturbations to reveal this, and will discuss it in Chap. 5.

1.3.2 Redshift Space Distortions

In redshift surveys of galaxy distributions, positions of galaxies are specified by the redshift that contains the cosmological redshift and the peculiar velocities of each galaxies. In the study of the FLRW universes, it is known that the peculiar velocities distort the clustering pattern of galaxies which is called as Redshift Space Distortions (RSD) [80]. The RSD on the linear power spectrum and on the linear two-point correlation function have been investigated by cosmological perturbation theory in the FLRW models (for review, see Ref. [81]). Since the growth of peculiar velocities of linear perturbations significantly depends on the background dynamics, we can use observations of RSD for major issues in observational cosmology, such as determining the cosmological parameters, testing various dark energy models and testing General Relativity at cosmological scales.

Fig. 1.2 shows observational results on $f(z)\sigma_8(z)$ [82] by measuring the RSD, where $f(z)$ is the growth rate of the matter density fluctuations and $\sigma_8(z)$ is the rms amplitude of the mass fluctuations at the comoving scale $8h^{-1}$Mpc (h is the normalized Hubble constant defined as $H_0 = 100h$ kms^{-1}Mpc^{-1}). The solid lines denote $f(z)\sigma_8(z)$ for dark energy models with $c_{\rm s}^2 = 1$ and (a)$w = -1.2$, (b)$w = -1$, (c)$w = -0.8$, (d)$w = -0.6$, (e)$w = -0.4$, respectively, where w and c_s^2 are the parameters for dark energy and defined as $w = p/\rho$ and $c_s^2 = \delta p/\delta\rho$. From fig. 1.2, we can see that the observational results of the RSD have given constraints for a nature of dark energy.

In order to apply these observational data to the LTB cosmological models, we have to solve perturbation equations in the LTB background. We will solve perturbations and show that the two-point correlation function in the LTB model has a distortion in the real space and its effect appears in the observations of the RSD in Chap. 4.

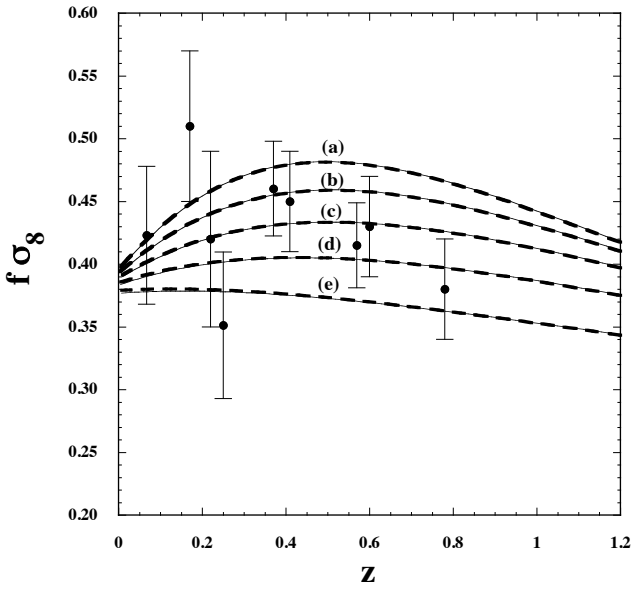

Figure 1.2: Measurements of $f(z)\sigma_8(z)$ versus z from the current RSD data; 2dFGRS, SDSS LRG, WiggleZ, BOSS CMASS and 6dFGRS (From Tsujikawa-Felice-Alcaniz [82]). The solid lines denote $f(z)\sigma_8(z)$ for dark energy models with $c_{\rm s}^2 = 1$ and (a)$w = -1.2$, (b)$w = -1$, (c)$w = -0.8$, (d)$w = -0.6$, (e)$w = -0.4$, respectively.

1.3.3 Weak gravitational lensing

Galaxy images are slightly distorted due to the bending of the light by the intervening large-scale structure. This effect is known as the *weak gravitational lensing*, and has become one of the principal probes of the FLRW cosmologies. The statistics of the weak lensing is usually described by the two-point correlation functions of the ellipticity of the galaxy images. The observed ellipticity correlation functions can be separated into two independent components, an E-mode and B-mode, which correspond to curl-free and divergence-free of the shear field. These components directly reflect gravitational fields of the large-scale structure, and their values can be predicted by cosmological perturbation theory in the FLRW models. As a result of perturbation theory, it is known that the weak lensing E-mode is produced by a scalar mode (Newtonian potential) of perturbations, and the B-mode by vector and tensor modes of perturbations. Since the vector and tensor modes do not contain the growing mode, the B-mode should be zero at late times. By contrast, observations of the E-mode can give a constraint for the cosmological parameters, since the growth of scalar perturbations strongly depends on the background dynamics.

Fig 1.3 shows cosmological constraints from weak gravitational lensing data,

adopted from Canada-France-Hawaii Telescope Legacy Survey (From Fu et al. [83]). Upper panel shows that measurements of the E- and B- modes of the shear correlation functions, where filled circles denote observations of the E-mode and open circles the B-mode. We can see that B-modes are consistent with zero. Lower panel shows that likelihood contours (1σ) from the observed shear correlation functions in the $\Omega_{\rm M}$-σ_8 plane. From fig. 1.3, we can see that the weak lensing survey have given constraints for the cosmological parameters.

In the case of the LTB cosmological models, we expect that the growth rate of the gravitational potential can depend on the positions, and thus the weak lensing E-modes may significantly differ from those in the FLRW models. We also note that it is not clear whether the B-modes vanish in the LTB models. We will solve perturbations in the LTB models, and discuss these issues in Chap. 5.

1.4 Perturbations in Lemaître-Tolman-Bondi cosmological model

We have to solve perturbation equations in the LTB cosmological models to predict the observations of large-scale structures reviewed in the previous section. Unfortunately, it is quite difficult to solve perturbations in the LTB cosmological models. This is because that the isometries in the LTB spacetime are less than those in the homogeneous and isotropic FLRW universe. Although master equations for perturbations for general spherically symmetric spacetimes have been derived a long time ago [84], these equations for the LTB solution cannot be reduced to ordinary differential equations. This is a very different situation from the case of the homogeneous and isotropic universe.

Recently, some papers have appeared [60, 85, 86, 87, 88, 89, 90] studying perturbations and related observations in the LTB cosmological models. Zibin [90] and Dunsby-Goheer-Osano-Uzan [60] solved perturbations by using a "silent approximation" that neglects the magnetic part of the Weyl tensor. However, we should note that the magnetic part of the Weyl tensor usually plays an important role even in Newtonian situations [91]. Clarkson-Clifton-February [87] classified perturbations into the "scalar", "vector" and "tensor" degrees of freedom by taking the limit to FLRW models, and solved perturbation equations by neglecting the "vector" and "tensor" modes. However, in the case of LTB spacetimes, the vector and tensor modes couple to the scalar mode in general. We will discuss this issue in Chap. 3. Alonso et al. [86] performed numerical simulations for non-Copernican models including only cold dark matter. They studied the perturbed Einstein-deSitter uni-

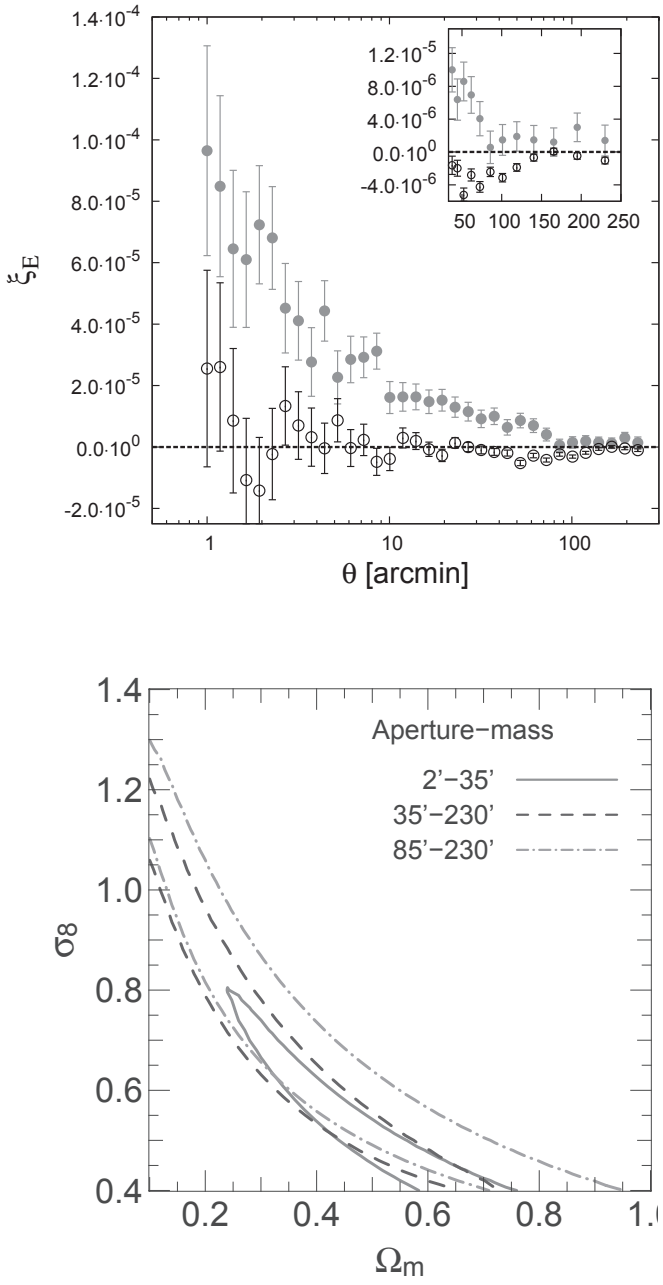

Figure 1.3: Cosmological constraints from weak lensing data, adopted from Canada-France-Hawaii Telescope Legacy Survey (From Fu et al. [83]). Upper panel: measurements of the E-mode (filled circles) and B-mode (open circles) of the shear correlation functions. B modes are consistent with zero. Lower panel: Likelihood contours (1σ) from the observed shear correlation functions (upper panel) in the $\Omega_{\rm M}$-σ_8 plane.

verse with two kinds of perturbations: one forms a spherical void, and the other is a non-spherical perturbation with a random phase Gaussian probability distribution. They followed the growth of these perturbations using Newtonian N-body simulations. However, in order to confirm the validity of the numerical simulations, analytic complementary studies are necessary. Hence, in this thesis, we propose another complementary analytic approaches for solving perturbations.

Some authors studied a test of LTB cosmological models from observations of the BAO scales such as SDSS-LRG and WiggleZ (see fig. 1.1) by applying a "geometric approximation" that assumes the BAO scale is stretched by the background cosmic expansion. The geometric approximation is justified by perturbation theory in the case of FLRW universes. However, in the case of LTB models, we need a knowledge of perturbation theory to clarify whether we can apply the approximation.

This thesis is organized as follows. In Chap. 2, we review the LTB spacetimes by focusing on the cosmological applications: light propagation, physical degrees of freedom and $1+3$ covariant formalism. We also give a brief review on LTB cosmological models proposed by some authors as an alternative to the ΛCDM model. In Chap. 3, we study relativistic perturbations in the LTB cosmological models based on our paper [92]. First we review perturbation theory in LTB spacetimes and a previous work on solving perturbations by February, Clarkson and Maartens [88] (FCM). Then we propose our approximation scheme which is essentially based on a linearization of the LTB background around a FLRW spacetime. We solve perturbation equations under the approximation, and obtain density fluctuations in the LTB cosmological models. We compare our results with the previous work by FCM. In Chap. 4, we study stochastic properties of density perturbations in the LTB cosmological models based on our papers [92] and [93]. First we derive two-point correlation functions of density perturbations in the LTB cosmological models. Then, by using the two-point correlation functions, we show that the galaxy clustering has a statistical distortion due to the tidal force that exists in the LTB background. We also study the growth rate of density perturbations in a huge void model proposed by Clarkson and Regis, and reveal a difference of it from the ΛCDM model. In Chap. 5, we study Newtonian self-gravitating system in the LTB cosmological models based on our paper in preparation [94]. First we propose a local approximation to the LTB cosmological models by using a Fermi-normal coordinate expansion. Then we add local inhomogeneity which represents Newtonian structures in the universe to the approximated LTB models. By applying the Cosmological Post-Newtonian expansion, we derive Newtonian hydrodynamical equations. We solve the derived equations under a linear approximation, and investigate the growth rate of linear

density fluctuations. We discuss a consistency between our approximation scheme in Chap 3 and that in Chap. 5. Chap. 6 is devoted to summary of this thesis.

In this thesis, we use the geometrized units in which the speed of light and Newton's gravitational constant are one, respectively. The Latin indices denote the spatial components, whereas the Greek indices represent the spacetime components.

Chapter 2

Lemaître-Tolman-Bondi (LTB) spacetime as non-Copernican cosmological model

We describe non-Copernican cosmological model by using Lemaître-Tolman-Bondi (LTB) spacetime throughout this thesis. In § 2.1 we review LTB spacetime from a cosmological point of view concerning light propagation, physical degrees of freedom and 1+3 covariant approach. In § 2.2 we review LTB cosmological models which account for the cosmological observations without introducing dark energy, by focusing on the time evolution of the energy density and the volume expansion.

2.1 LTB spacetime

2.1.1 Derivation of LTB solution

LTB spacetime [9, 10, 11] is an exact solution of the Einstein equations and describes the motion of spherically symmetric dust. In general, the line element and the stress-energy tensor of spherically symmetric spacetimes for dust, in the synchronous-comoving coordinate, can be written as

$$ds^2 = -dt^2 + X^2(t,r)dr^2 + R^2(t,r)\left(d\theta^2 + \sin^2\theta d\phi^2\right), \tag{2.1}$$

$$T^{\mu\nu} = \rho(t,r)u^\mu u^\nu, \tag{2.2}$$

where $X(t,r)$ and $R(t,r)$ are functions of the time and radial coordinates, and $\rho(t,r)$ and $u^\mu = (1,0,0,0)$ are the energy density and the 4-velocity of the dust, respectively. By substituting Eqs. (2.1) and (2.2) into the Einstein equations $G_{\mu\nu} =$

$8\pi T_{\mu\nu}$, independent differential equations are obtained as

$$-2\frac{\partial_r^2 R}{RX^2}+2\frac{(\partial_r R)(\partial_r X)}{RX^3}+2\frac{(\partial_t R)(\partial_t X)}{RX}+\frac{1}{R^2}+\left(\frac{\partial_t R}{R}\right)^2 - \left(\frac{\partial_r R}{RX}\right)^2-8\pi G\rho = 0, \tag{2.3}$$

$$\frac{\partial_t\partial_r R}{\partial_r R}-\frac{\partial_t X}{X} = 0, \tag{2.4}$$

$$2\frac{\partial_t^2 R}{R}+\frac{1}{R^2}+\left(\frac{\partial_t R}{R}\right)^2-\left(\frac{\partial_r R}{RX}\right)^2 = 0. \tag{2.5}$$

By solving Eq. (2.4), we obtain

$$X(t,r)=\frac{\partial_r R(t,r)}{\sqrt{1-k(r)}}, \tag{2.6}$$

where $k(r)$ is an arbitrary function of the radial coordinate, and is called as the curvature function. By substituting Eq. (2.6) into Eq. (2.5) and by integrating Eq. (2.5) with respect to the time coordinate, we obtain

$$\left(\frac{\partial_t R(t,r)}{R(t,r)}\right)^2=\frac{M(r)}{R^3(t,r)}-\frac{k(r)}{R^2(t,r)}, \tag{2.7}$$

where $M(r)$ is an arbitrary function of the radial coordinate, and is called as the mass function. By substituting Eqs. (2.6) and (2.7) into Eq. (2.3), the energy density is described as

$$8\pi G\rho(t,r)=\frac{1}{R^2(t,r)\partial_r R(t,r)}\frac{dM(r)}{dr}. \tag{2.8}$$

Here, it should be noted that $M(r)/2$ coincides with the Misner-Sharp mass that is the quasi-local mass naturally introduced into the spherically symmetric spacetime. By integrating Eq. (2.7), we obtain

$$R(t,r)=(3M(r))^{1/3}(t-t_{\rm B}(r))^{2/3}S(x), \tag{2.9}$$

where $t_{\rm B}(r)$ is an arbitrary function of r called as the Big-Bang time function, x is defined by

$$x:=k(r)\left(\frac{t-t_{\rm B}(r)}{3M(r)}\right)^{2/3}, \tag{2.10}$$

and, by defining η as

$$x=:\begin{cases}\dfrac{-(\sinh\sqrt{-\eta}-\sqrt{-\eta})^{2/3}}{6^{2/3}} & \text{for} \quad x<0,\\[2ex] \dfrac{(\sqrt{\eta}-\sin\sqrt{\eta})^{2/3}}{6^{2/3}} & \text{for} \quad x>0,\end{cases} \tag{2.11}$$

the function $S(x)$ is given by

$$S(x) = \begin{cases} \dfrac{\cosh\sqrt{-\eta}-1}{6^{1/3}(\sinh\sqrt{-\eta}-\sqrt{-\eta})^{2/3}} & \text{for} \quad x<0, \\ \dfrac{1-\cos\sqrt{\eta}}{6^{1/3}(\sqrt{\eta}-\sinh\sqrt{\eta})^{2/3}} & \text{for} \quad x>0, \end{cases} \tag{2.12}$$

and $S(0) = (3/4)^{1/3}$. From Eqs. (2.6), (2.8) and (2.9), we can see that the LTB spacetime are determined by three arbitrary functions: $k(r)$, $M(r)$ and $t_{\rm B}(r)$. One of them is a gauge degree of freedom for rescaling of the radial coordinate, and the remaining two functions represent physical degrees of freedom which correspond to the growing and the decaying modes (we will see it later in this section).

For later convenience, we rewrite the LTB spacetime in a cosmological form similar to the FLRW spacetime. The line element (2.1) together with Eq. (2.6) can be described as

$$ds^2 = -dt^2 + \frac{\left(\partial_r R(t,r)\right)^2}{1-k(r)}dr^2 + R^2(t,r)\left(d\theta^2+\sin^2\theta d\phi^2\right), \tag{2.13}$$

$$:= -dt^2 + \frac{a_{||}^2(t,r)}{1-k(r)}dr^2 + a_\perp^2(t,r)r^2\left(d\theta^2+\sin^2\theta d\phi^2\right), \tag{2.14}$$

where we defined $a_{||}(t,r)$ and $a_\perp(t,r)$ as the radial and azimuthal scale factors. Then, we define the radial and azimuthal Hubble rates as

$$H_\parallel(t,r) := \frac{\partial_t a_{||}(t,r)}{a_{||}(t,r)} \quad \text{and} \quad H_\perp(t,r) := \frac{\partial_t a_\perp(t,r)}{a_\perp(t,r)}, \tag{2.15}$$

and the density-parameter function as

$$\Omega_{\rm M}(r) := \frac{M(r)}{H_\perp^2(t_0,r)a_\perp^3(t_0,r)}, \tag{2.16}$$

where t_0 denotes the present time. By using Eqs. (2.14), (2.15) and (2.16), we can rewrite Eq. (2.7) in a form similar to the Friedmann equation:

$$H_\perp^2(t,r) = H_\perp^2(t_0,r)\left[\Omega_{\rm M}(r)\left(\frac{a_\perp(t_0,r)}{a_\perp(t,r)}\right)^3 + (1-\Omega_{\rm M}(r))\left(\frac{a_\perp(t_0,r)}{a_\perp(t,r)}\right)^2\right]. \tag{2.17}$$

Here, we also denote two useful relations from Eqs. (2.3)–(2.5) as

$$\frac{1}{3}\frac{\partial_t^2 a_\parallel(t,r)}{a_\parallel(t,r)} + \frac{2}{3}\frac{\partial_t^2 a_\perp(t,r)}{a_\perp(t,r)} = -\frac{4\pi}{3}\rho(t,r), \tag{2.18}$$

$$\frac{\partial}{\partial t}\rho(t,r) + \left(H_\parallel(t,r)+2H_\perp(t,r)\right)\rho(t,r) = 0. \tag{2.19}$$

We will use the equations (2.18) and (2.19) in Chap. 5.

To see the inhomogeneity of the LTB cosmological models, we define the density contrast as

$$\Delta(t,r) := \frac{\rho(t,r) - \rho(t,0)}{\rho(t,0)}. \tag{2.20}$$

Similarly, we define the Hubble contrasts with respect to the parallel and the transverse direction of the line of sight as

$$\Delta_{\rm Hp}(t,r) := \frac{H_{||}(t,r) - H_{||}(t,0)}{H_{||}(t,0)}, \quad \text{and} \quad \Delta_{\rm Ht}(t,r) := \frac{H_{\perp}(t,r) - H_{\perp}(t,0)}{H_{\perp}(t,0)}. \tag{2.21}$$

where we note that $H_{||}(t,0) = H_{\perp}(t,0)$ is satisfied due to the spherical symmetricity. We also define the normalized shear which represents the local anisotropy of the volume expansion as

$$\Delta_{\sigma}(t,r) := \frac{H_{||}(t,r) - H_{\perp}(t,r)}{H_{||}(t,r) + 2H_{\perp}(t,r)}. \tag{2.22}$$

The quantities $\{\Delta, \Delta_{\rm Hp}, \Delta_{\rm Ht}, \Delta_{\sigma}\}$ characterize the LTB cosmological models, and all of them vanish in the limit to the homogeneous and isotropic FLRW models.

2.1.2 Light propagation in LTB spacetime

Basically, an observer can observe only on his/her past light cone through electromagnetic radiation[1]. Hence, in the case of non-Copernican cosmological model described by LTB spacetime, it is useful to consider quantities on the light cone of an observer who stays at the symmetry center of LTB spacetime at present. Hereafter, for simplicity, we call the observer who stays at the symmetry center at present "the central observer", and the past light cone of the central observer is denoted by $\Sigma_{\rm lc}$.

From the symmetry of the situation, it is clear that the light from the central observer can travel radially, that is, there exist geodesics with $d\theta = d\phi = 0$. Thus, the tangent vector of the past-directed outgoing radial null geodesics, k^{μ}, is given as

$$k^{\mu} = \left(\frac{dt}{d\lambda}, \frac{dr}{d\lambda}, 0, 0\right), \tag{2.23}$$

[1]The past light cone of an observer at the event p is defined by the boundary of the causal past of p, which is usually denoted by $\dot{J}^{-}(p)$ in general relativity. Strictly speaking, the observer can see the inside of the light cone through a congruence of the light rays which have experienced caustics caused by gravitational lens effects or scattering due to electromagnetic interactions in the real universe.

where λ is the affine parameter. The cosmological redshift z is defined by

$$z = \frac{u^\mu k_\mu|_{\rm source}}{u^\mu k_\mu|_{\rm observer}} - 1, \tag{2.24}$$

where $u^\mu k_\mu|_{\rm source}$ and $u^\mu k_\mu|_{\rm observer}$ are the values of the frequency at the time of the emission of a photon and that of the detection by the central observer, respectively. By using the cosmological redshift z instead of the affine parameter λ and by using Eq. (2.13), the geodesic equations $k_{\mu;\nu}k^\nu = 0$ for the generator of the past light cone $\Sigma_{\rm lc}$ are given by

$$\frac{dr}{dz} = \frac{\sqrt{1-k(r)}}{(1+z)\partial_t\partial_r R(t,r)}, \tag{2.25}$$

$$\frac{dt}{dz} = -\frac{\partial_r R(t,r)}{(1+z)\partial_t\partial_r R(t,r)}. \tag{2.26}$$

We can obtain the light propagation by solving the above equations in a given LTB model. We denote the solution of the above equations by

$$t = t_{\rm lc}(z) \quad \text{and} \quad r = r_{\rm lc}(z). \tag{2.27}$$

The angular diameter distance for the central observer is given as

$$d_{\rm A}(z) = R\left(t_{\rm lc}(z), r_{\rm lc}(z)\right). \tag{2.28}$$

In general, the luminosity distance is related to the angular diameter distance as $d_{\rm L}(z) = (1+z)^2 d_{\rm A}(z)$ and thus we have

$$d_{\rm L}(z) = (1+z)^2 R\left(t_{\rm lc}(z), r_{\rm lc}(z)\right). \tag{2.29}$$

2.1.3 Physical degrees of freedom of LTB spacetime

As we shown in the section, LTB spacetime has three free radial functions, $k(r)$, $M(r)$ and $t_{\rm B}(r)$, and one is the gauge degree of freedom and the others describe physical degrees of freedom. In this subsection, we clarify the physical meaning of the two free functions by considering a situation, where LTB spacetime is very close to the Einstein de-Sitter (EdS) universe model.

First of all, we review density perturbations in the EdS universe model. The evolution of linear density perturbation, in the synchronous comoving gauge, in the EdS universe is given by

$$\delta = \frac{\rho - \rho^{\rm EdS}}{\rho^{\rm EdS}} = t^{2/3}\delta^+(\mathbf{x}) + t^{-1}\delta^-(\mathbf{x}), \tag{2.30}$$

where ρ is the energy density in the perturbed universe, and $\rho^{\rm EdS}$ is the energy density in the EdS background and described as $\rho^{\rm EdS} \propto t^{-2}$. We note that δ^+ and δ^- represent physical degrees of freedom in the perturbed universe, and are known as the growing and decaying mode, respectively.

Vanishing decaying mode

We consider a LTB spacetime with $t_{\rm B}(r) = 0$, and expand the spacetime around $t \to 0$. In the situation, the function x defined in Eq. (2.10) satisfies

$$x = k(r) \left(\frac{t}{3M(r)} \right)^{2/3} \ll 1, \tag{2.31}$$

and accordingly the function $S(x)$ defined in Eq. (2.12) can be expanded as

$$S(x) = \left(\frac{3}{4} \right)^{1/3} \left[1 - \frac{3}{5} \left(\frac{3}{4} \right)^{1/3} x + \mathcal{O}(x^2) \right]. \tag{2.32}$$

By using Eqs. (2.31) and (2.32) together with Eq. (2.9), the metric function $R(t, r)$ is expanded as

$$R(t, r) = \left(\frac{9}{4} M(r) \right)^{1/3} t^{2/3} \left[1 - \frac{9}{20} k(r) \left(\frac{9}{4} M(r) \right)^{-1} t^{2/3} + \mathcal{O}(t^{4/3}) \right]. \tag{2.33}$$

By substituting Eq. (2.33) into Eq. (2.8), we obtain

$$\rho^{\rm LTB}(t, r) = \frac{1}{6\pi t^2} \left[1 + \frac{1}{5} \left(\frac{k(r)}{M(r)} + 3 \frac{dk(r)/dr}{dM(r)/dr} \right) t^{2/3} + \mathcal{O}(t^{4/3}) \right]. \tag{2.34}$$

From Eq. (2.34), we can see that the density of the LTB spacetime approaches to that of the EdS universe near $t \to 0$ as

$$\rho^{\rm LTB} \to \frac{1}{6\pi t^2} \ =: \bar{\rho}. \tag{2.35}$$

Then, by using Eqs. (2.34) and (2.35), we obtain the density perturbation of the LTB spacetime near $t \to 0$ as

$$\delta^{\rm LTB} := \frac{\rho^{\rm LTB} - \bar{\rho}}{\bar{\rho}} = \frac{1}{5} \left(\frac{k(r)}{M(r)} + 3 \frac{dk(r)/dr}{dM(r)/dr} \right) t^{2/3} + \mathcal{O}(t^{4/3}). \tag{2.36}$$

Comparing Eq. (2.36) with Eq. (2.30), we can see that the LTB spacetime with $t_{\rm B}(r) = 0$ does not have the decaying mode at sufficiently early times, where the spacetime can be treated as a linear perturbation from the EdS universe model. Thus, we conclude that the radial free function $t_{\rm B}(r)$ corresponds to the decaying mode.

Vanishing growing mode

We consider a LTB spacetime with $k(r) = 0$, and expand the spacetime around $t \to \infty$. From $k(r) = 0$ and Eq. (2.10), we can see that $x = 0$ is satisfied. As a result, the metric function $R(t, r)$ given in Eq. (2.9) is described as

$$R(t, r) = \left(\frac{9}{4}M(r)\right)^{1/3} (t - t_{\rm B}(r))^{2/3}. \tag{2.37}$$

By using Eq. (2.37) and by introducing an expansion parameter $t_{\rm B}(r)/t$, the energy density defined in Eq. (2.8) can be expanded around $t \to \infty$ as

$$\rho^{\rm LTB}(t, r) = \frac{1}{6\pi t^2}\left[1 + \left(2t_{\rm B}(r) + \frac{3}{2}\frac{M(r)}{dM(r)/dr}\frac{dt_{\rm B}(r)}{dr}\right) t^{-1} + \mathcal{O}\left(t_{\rm B}/t\right)^2\right]. \tag{2.38}$$

From Eq. (2.38), we can see that the density of the LTB spacetime approaches to that of the EdS universe near $t \to \infty$ as

$$\rho^{\rm LTB} \to \frac{1}{6\pi t^2} \quad =: \bar{\rho}. \tag{2.39}$$

Then, by using Eqs. (2.38) and (2.39), we obtain the density perturbation of the LTB spacetime near $t \to \infty$ as

$$\delta^{\rm LTB} := \frac{\rho^{\rm LTB} - \bar{\rho}}{\bar{\rho}} = \left(2t_{\rm B}(r) + \frac{3}{2}\frac{M(r)}{dM(r)/dr}\frac{dt_{\rm B}(r)}{dr}\right) t^{-1} + \mathcal{O}\left(t_{\rm B}/t\right)^2. \tag{2.40}$$

Comparing Eq. (2.40) with Eq. (2.30), we can see that the LTB spacetime with $k(r) = 0$ does not have the growing mode at sufficiently late times, where the spacetime can be treated as a linear perturbation from the EdS universe model. Thus, we conclude that the radial free function $k(r)$ corresponds to the growing mode.

2.1.4 1+3 covariant approach to LTB spacetime

In the Ellis's 1+3 covariant formalism (see, for reviews [95, 96, 97, 98]), every quantity has a natural interpretation in terms of fundamental worldlines with the fundamental 4-velocity u^μ, where $u_\mu u^\mu = -1$. In this subsection, we describe the LTB spacetime in terms of a set of fundamental quantities of the 1+3 formalism. This will be helpful in discussing Newtonian self-gravitating system in LTB cosmological model in Chap. 5.

The basic tensor is $P_{\mu\nu} := g_{\mu\nu} + u_\mu u_\nu$, and the fundamental kinematic quantities are given as

$$u_{\mu;\nu} = \frac{1}{3}\theta P_{\mu\nu} + \sigma_{\mu\nu} + \omega_{\mu\nu} - a_\mu u_\nu, \tag{2.41}$$

where ; denotes covariant derivative, and θ, $\sigma_{\mu\nu}$, $\omega_{\mu\nu}$ and a_μ are known as the expansion, shear, twist and acceleration of the congruence of worldlines and are defined as

$$\theta := P^{\mu\nu}u_{\mu;\nu},\ \sigma_{\mu\nu} := \left(P^{\kappa}_{(\mu}P^{\lambda}_{\nu)} - \frac{1}{3}P^{\kappa\lambda}P_{\mu\nu}\right)u_{\kappa;\lambda},\ \omega_{\mu\nu} := P^{\kappa}_{[\mu}P^{\lambda}_{\nu]}u_{\kappa;\lambda},\ a_\mu := u_{\mu;\rho}u^\rho.$$

As for the gravitational field, the electric, $\mathcal{E}_{\mu\nu}$, and the magnetic, $\mathcal{B}_{\mu\nu}$, parts of the Weyl tensor, $C_{\mu\alpha\nu\beta}$, are defined as

$$\mathcal{E}_{\mu\nu} := u^\alpha u^\beta C_{\mu\alpha\nu\beta}, \quad \mathcal{H}_{\mu\nu} := u^\alpha u^\beta {}^*C_{\mu\alpha\nu\beta}, \tag{2.42}$$

where $*$ denotes the Hodge dual and defined as ${}^*C_{\mu\alpha\nu\beta} := -\frac{1}{2}\eta_{\gamma\delta\alpha(\mu}C^{\gamma\delta}{}_{\nu)\beta}$, where we have used the fully antisymmetric tensor $\eta_{\mu\nu\kappa\lambda} := (-g)^{1/2}[\mu\nu\kappa\lambda]$ with the determinant of $g_{\mu\nu}$, g, and the completely antisymmetric Levi-Civita symbol, $[\mu\nu\kappa\lambda]$, defined by $[0123] = +1$. The energy-momentum tensor of a general fluid can be decomposed into its irreducible parts as

$$T_{\mu\nu} = \rho u_\mu u_\nu + pP_{\mu\nu} + 2q_{(\mu}u_{\nu)} + \pi_{\mu\nu}, \tag{2.43}$$

where ρ, p, q_μ and $\pi_{\mu\nu}$ are the matter enrgy density, the effective isotropic pressure of the fluid, the total energy-flux vector and the symmetric and trace-free anisotropic stress tensor, and are defined as

$$\rho = T_{\mu\nu}u^\mu u^\nu,\ p = \frac{1}{3}T_{\mu\nu}P^{\mu\nu},\ q_\mu = -P^\nu_\mu T_{\nu\lambda}u^\lambda,\ \pi_{\mu\nu} = \left(P^{\kappa}_{(\mu}P^{\lambda}_{\nu)} - \frac{1}{3}P^{\kappa\lambda}P_{\mu\nu}\right)T_{\kappa\lambda}.$$

A set of quantities, $\{\theta, \sigma_{\mu\nu}, \omega_{\mu\nu}, a_\mu, \mathcal{E}_{\mu\nu}, \mathcal{B}_{\mu\nu}, \rho, p, q_\mu, \pi_{\mu\nu}\}$, completely characterizes a spacetime in the 1+3 covariant formalism.

By choosing u^μ as the dust 4-velocity $u^\mu = (1, 0, 0, 0)$, we compute a set of quantities, $\{\theta, \sigma_{\mu\nu}, \omega_{\mu\nu}, a_\mu, \mathcal{E}_{\mu\nu}, \mathcal{B}_{\mu\nu}, \rho, p, q_\mu, \pi_{\mu\nu}\}$, in the LTB spacetime. By using Eq. (2.14), we obtain

$$\theta = H_{||}(t, r) + 2H_\perp(t, r), \tag{2.44}$$

$$\sigma^\mu{}_\nu = \begin{pmatrix} 0 & 0 & 0 & 0 \\ 0 & \frac{2}{3}\left(H_{||}(t,r) - H_\perp(t,r)\right) & 0 & 0 \\ 0 & 0 & -\frac{1}{2}\,\sigma^r{}_r & 0 \\ 0 & 0 & 0 & -\frac{1}{2}\,\sigma^r{}_r \end{pmatrix}, \tag{2.45}$$

$\omega_{\mu\nu} = a_\mu = 0$,

$$\mathcal{E}^\mu{}_\nu = \begin{pmatrix} 0 & 0 & 0 & 0 \\ 0 & \frac{2}{3}\left(\frac{\partial_t^2 a_{||}}{a_{||}} - \frac{\partial_t^2 a_\perp}{a_\perp}\right) & 0 & 0 \\ 0 & 0 & -\frac{1}{2}\,\mathcal{E}^r{}_r & 0 \\ 0 & 0 & 0 & -\frac{1}{2}\,\mathcal{E}^r{}_r \end{pmatrix}, \tag{2.46}$$

$\mathcal{B}_{\mu\nu} = 0$, $\rho = \rho(t, r)$ and $p = q_\mu = \pi_{\mu\nu} = 0$. From Eq. (2.45), we can see the shear field represents the anisotropy of the local volume expansion which vanishes in the FLRW limit. From Eq. (2.46), we can see that there exists the electric part of the Weyl tensor in the LTB spacetime which represents the tidal force, whereas there is no tidal force in the homogeneous and isotropic FLRW universes. We also note that the twist $\omega_{\mu\nu}$ and the magnetic part $\mathcal{B}_{\mu\nu}$ are zero in the LTB spacetime same as to the case of FLRW universes.

2.2 LTB cosmological models as an alternative to Dark Energy

2.2.1 Clarkson-Regis model

We consider a LTB cosmological model given by Clarkson and Regis [36], which we call the Clarkson-Regis (CR) model. The CR model can explain the SNIa data and peak positions of the fluctuations in the CMB radiation. The CR model has the uniform big-bang time $t_{\rm B}(r) = 0$, and the gauge condition is chosen so that $R(t_0, r) = r$. In the uniform big-bang model, one functional degree of freedom to specify the model remains. In the CR model, this degree of freedom is fixed so that the density-parameter function defined in Eq (2.16) is given by

$$\Omega_{\rm M}(r) = \Omega_{\rm M}^{(\rm out)} - (\Omega_{\rm M}^{(\rm out)} - \Omega_{\rm M}^{(\rm in)})e^{-r^2/(2\sigma^2)}, \tag{2.47}$$

where $\Omega_{\rm M}^{(\rm out)} = 0.7$, $\Omega_{\rm M}^{(\rm in)} = 0.242$ and $\sigma = 6$Gpc. The Hubble constant at the center is chosen as $H_\perp(t_0, 0) = 74 \mathrm{kms}^{-1}\mathrm{Mpc}^{-1}$.

In fig. 2.1, we plot the density contrasts $\Delta(t, r)$ defined in Eq. (2.20) in CR model on the spacelike hypersurfaces for $t = t_{\rm lc}(100)$, $t = t_{\rm lc}(1)$ and $t = t_0$, as functions of r. Here, we have used the cosmological redshift z to specify each constant time hypersurface given by $t = t_{\rm lc}(z)$. We can see that the CR model has a void structure which grows with time. The void size is about 12Gpc, and the vicinity of the center is locally the dust filled FLRW model with the cosmological density parameter $\Omega_{\rm M} = 0.242$, whereas the asymptotic region is almost the same as the dust filled FLRW model with $\Omega_{\rm M} = 0.7$. We can also see that the void structure becomes non-linear at the present time, that is, the density contrast exceeds 1 at t_0. In fig. 2.2, we plot the Hubble contrasts, $\Delta_{\rm Hp}(t, r)$ and $\Delta_{\rm Ht}(t, r)$ defined in Eq. (2.21), in CR model on the spacelike hypersurfaces for $t = t_{\rm lc}(100)$, $t = t_{\rm lc}(1)$ and $t = t_0$, as functions of r. We can see both $\Delta_{\rm Hp}$ and $\Delta_{\rm Ht}$ grow with time grows. The Hubble functions at the center is larger than those at off central region, since the matter

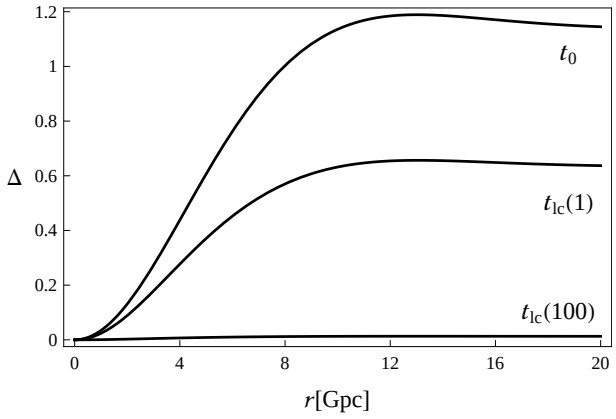

Figure 2.1: Density contrasts $\Delta(t, r)$ in CR model on the spacelike hypersurfaces for $t = t_{\rm lc}(100)$, $t = t_{\rm lc}(1)$ and $t = t_0$, as functions of r.

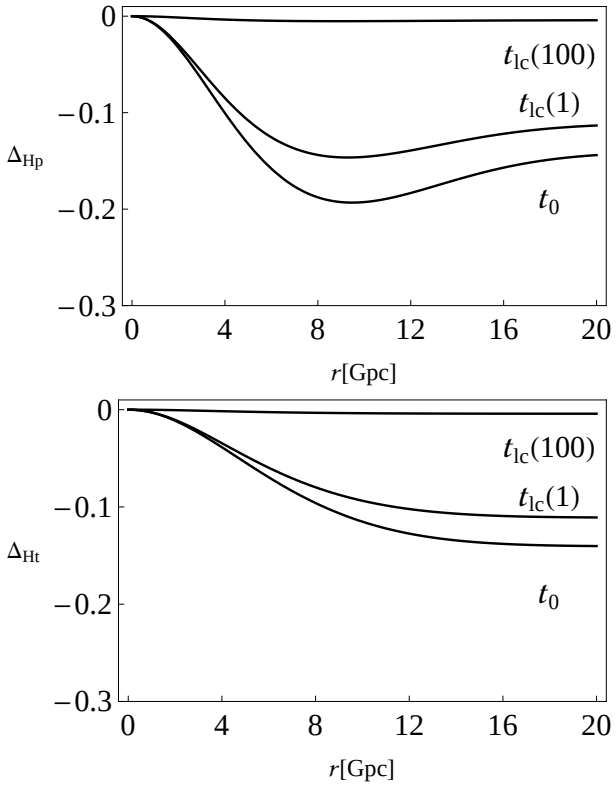

Figure 2.2: Hubble contrasts, $\Delta_{\rm Hp}(t, r)$ and $\Delta_{\rm Ht}(t, r)$, in CR model on the spacelike hypersurfaces for $t = t_{\rm lc}(100)$, $t = t_{\rm lc}(1)$ and $t = t_0$, as functions of r.

density at the center is least. In fig. 2.3, we plot the normalized shear, $\Delta_\sigma(t,r)$

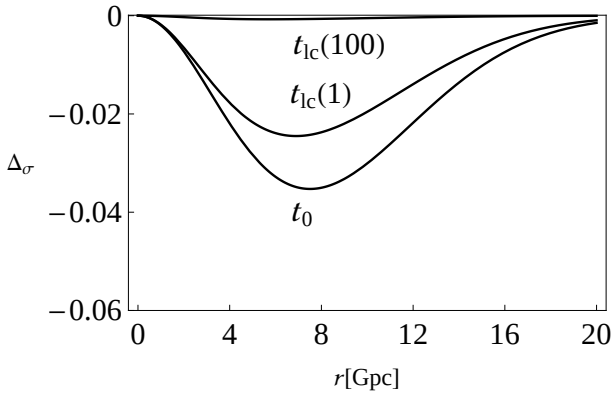

Figure 2.3: The normalized shear, $\Delta_\sigma(t,r)$, in CR model on the spacelike hypersurfaces for $t = t_{\rm lc}(100)$, $t = t_{\rm lc}(1)$ and $t = t_0$, as functions of r.

defined in Eq. (2.22), in CR model on the spacelike hypersurfaces for $t = t_{\rm lc}(100)$, $t = t_{\rm lc}(1)$ and $t = t_0$, as functions of r. We can see that the normalized shear grows as time grows, and this means the anisotropy of the expansion at off central region becomes important at late time. From fig. 2.3, we can also see that the peak position of the normalized shear is located around the edge of the void structure.

2.2.2 Yoo-Kai-Nakao model

We consider a LTB cosmological model proposed by Yoo, Kai and Nakao [30], which we call the Yoo-Kai-Nakao (YKN) model. The YKN model assumed the simultaneous big bang, i.e., $t_{\rm B}(r) = 0$, and fixed the gauge condition by setting

$$\frac{M(r)}{2} = \frac{4\pi}{3}\rho(t_0,0)r^3, \tag{2.48}$$

where the present matter density $\rho(t_0,0)$ is related to the present Hubble and the curvature function as

$$H^2(t_0,0) + \left.\frac{k(r)}{r^2}\right|_{r=0} c^2 = \frac{8\pi G}{3}\rho(t_0,0). \tag{2.49}$$

The remaining function, $k(r)$ was determined so that the distance-redshift relation of YKN model agrees with that of the concordance ΛCDM model with $(\Omega_{m0}, \Omega_{\Lambda 0}) = (0.3, 0.7)$. The fitting function is given as

$$\tilde{k}(\tilde{r}) = \frac{0.545745}{0.211472 + \sqrt{0.026176 + \tilde{r}}} - \frac{2.22881}{(0.807782 + \sqrt{0.026176 + \tilde{r}})^2}, \tag{2.50}$$

where $\tilde{r}$ and $\tilde{k}$ are defined as

$$\tilde{r} := \frac{H(t_0, 0)r}{c}, \quad \tilde{k}(\tilde{r}) := \frac{k(r)c^2}{H^2(t_0, 0)r^2}. \tag{2.51}$$

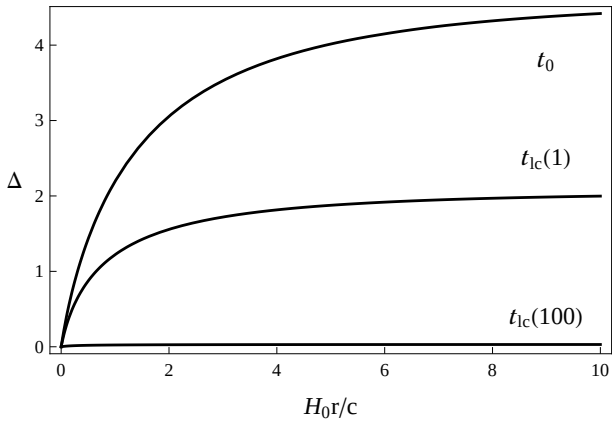

Figure 2.4: Density contrasts $\Delta(t, r)$ in YKN model on the spacelike hypersurfaces for $t = t_{\rm lc}(100)$, $t = t_{\rm lc}(1)$ and $t = t_0$, as functions of r.

In fig. 2.4, we plot the density contrasts $\Delta(t, r)$ defined in Eq. (2.20) in YKN model on the spacelike hypersurfaces for $t = t_{\rm lc}(100)$, $t = t_{\rm lc}(1)$ and $t = t_0$, as functions of r. We can see that the YKN model has a void structure which grows with time. The void size is about $2H_0r/c$, and the vicinity of the center is locally the dust filled FLRW model with the cosmological density parameter $\Omega_{\rm M} \simeq 0.1$, whereas the asymptotic region is almost the same as the dust filled FLRW model with $\Omega_{\rm M} = 1.0$. We can also see that the void structure becomes non-linear at sufficiently early times. In fig. 2.5, we plot the Hubble contrasts, $\Delta_{\rm Hp}(t, r)$ and $\Delta_{\rm Ht}(t, r)$ defined in Eq. (2.21), in YKN model on the spacelike hypersurfaces for $t = t_{\rm lc}(100)$, $t = t_{\rm lc}(1)$ and $t = t_0$, as functions of r. We can see both $\Delta_{\rm Hp}$ and $\Delta_{\rm Ht}$ grow with time grows. The Hubble functions at the center is larger than those at off central region, since the matter density at the center is least. In fig. 2.6, we plot the normalized shear, $\Delta_\sigma(t, r)$ defined in Eq. (2.22), in YKN model on the spacelike hypersurfaces for $t = t_{\rm lc}(100)$, $t = t_{\rm lc}(1)$ and $t = t_0$, as functions of r. We can see that the normalized shear grows as time grows. From fig. 2.6, we can also see that the peak position of the normalized shear is located around the edge of the void structure.

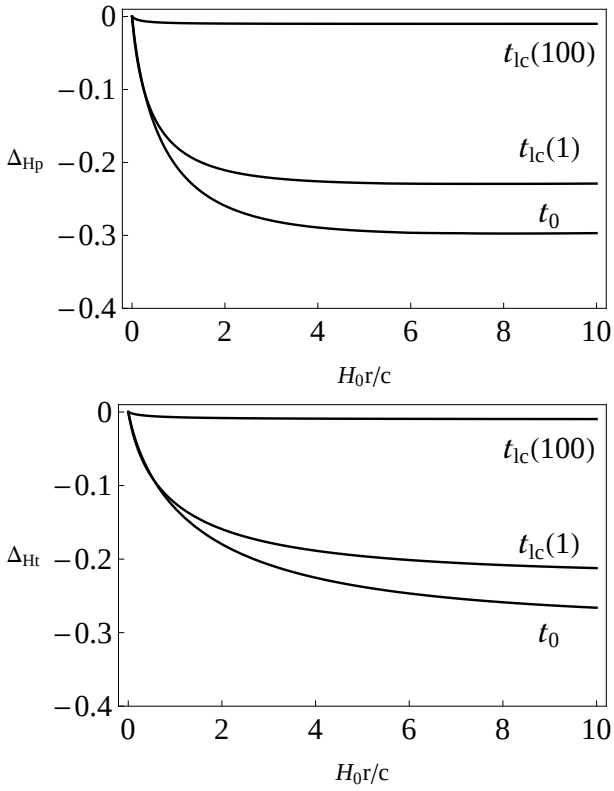

Figure 2.5: Hubble contrasts, $\Delta_{\mathrm{Hp}}(t,r)$ and $\Delta_{\mathrm{Ht}}(t,r)$, in YKN model on the spacelike hypersurfaces for $t = t_{\mathrm{lc}}(100)$, $t = t_{\mathrm{lc}}(1)$ and $t = t_0$, as functions of r.

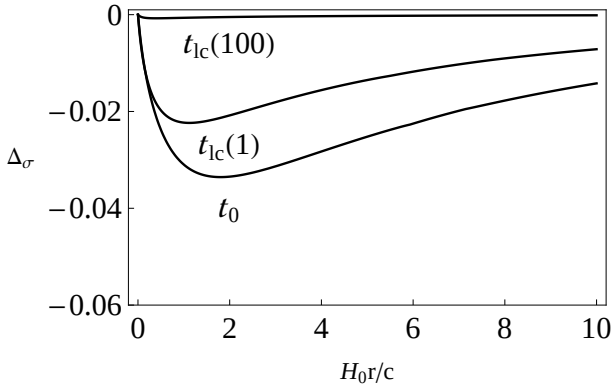

Figure 2.6: The normalized shear, $\Delta_\sigma(t,r)$, in YKN model on the spacelike hypersurfaces for $t = t_{\mathrm{lc}}(100)$, $t = t_{\mathrm{lc}}(1)$ and $t = t_0$, as functions of r.

2.2.3 Garcia-Bellido and Haugbølle model

We consider a LTB cosmological model proposed by Garcia-Bellido and Haugbølle [37], which we call the Garcia-Bellido and Haugbølle (GBH) model. The GBH model has the uniform big-bang time $t_{\rm B}(r) = 0$, and the gauge condition is chosen so that $R(t_0, r) = r$. In the uniform big-bang model, one functional degree of freedom to specify the model remains. In the GBH model, this degree of freedom is fixed so that the density-parameter function defined in Eq (2.16) is given by

$$\Omega_{\rm M}(r) = \Omega_{\rm out} + (\Omega_{\rm in} - \Omega_{\rm out}) \left(\frac{1 - \tanh[(r - r_0)/2\Delta r]}{1 + \tanh[r_0/2\Delta r]} \right), \tag{2.52}$$

where $\Omega_{\rm out} = 1.0$, $\Omega_{\rm in} = 0.13$, $r_0 = 2.5$Gpc, $\Delta r = 0.64 r_0$ and $H(t_0, 0) = 56 {\rm kms}^{-1}{\rm Mpc}^{-1}$.

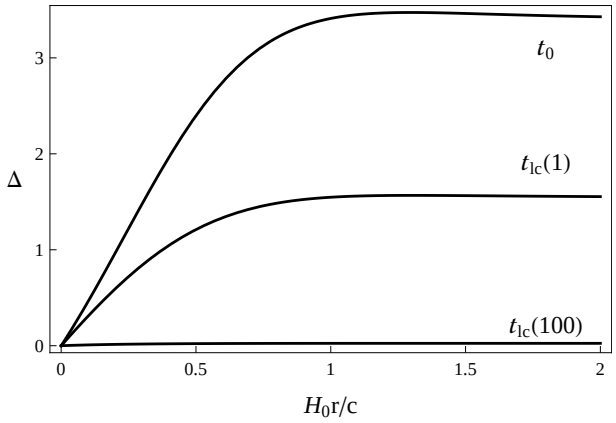

Figure 2.7: Density contrasts $\Delta(t, r)$ in GBH model on the spacelike hypersurfaces for $t = t_{\rm lc}(100)$, $t = t_{\rm lc}(1)$ and $t = t_0$, as functions of r.

In fig. 2.7, we plot the density contrasts $\Delta(t, r)$ defined in Eq. (2.20) in GBH model on the spacelike hypersurfaces for $t = t_{\rm lc}(100)$, $t = t_{\rm lc}(1)$ and $t = t_0$, as functions of r. We can see that the GBH model also has a void structure which grows with time. The void size is about $0.5 H_0 r/c$, and the vicinity of the center is locally the dust filled FLRW model with the cosmological density parameter $\Omega_{\rm M} = 0.13$, whereas the asymptotic region is almost the same as the dust filled FLRW model with $\Omega_{\rm M} = 1.0$. We can also see that the void structure becomes non-linear before the present time. In fig. 2.8, we plot the Hubble contrasts, $\Delta_{\rm Hp}(t, r)$ and $\Delta_{\rm Ht}(t, r)$ defined in Eq. (2.21), in GBH model on the spacelike hypersurfaces for $t = t_{\rm lc}(100)$, $t = t_{\rm lc}(1)$ and $t = t_0$, as functions of r. We can see both $\Delta_{\rm Hp}$ and $\Delta_{\rm Ht}$ grow with time grows. The Hubble functions at the center is larger than those at off central region. In fig. 2.9, we plot the normalized shear, $\Delta_\sigma(t, r)$ defined in Eq. (2.22), in GBH model on the spacelike hypersurfaces for $t = t_{\rm lc}(100)$, $t = t_{\rm lc}(1)$ and $t = t_0$, as

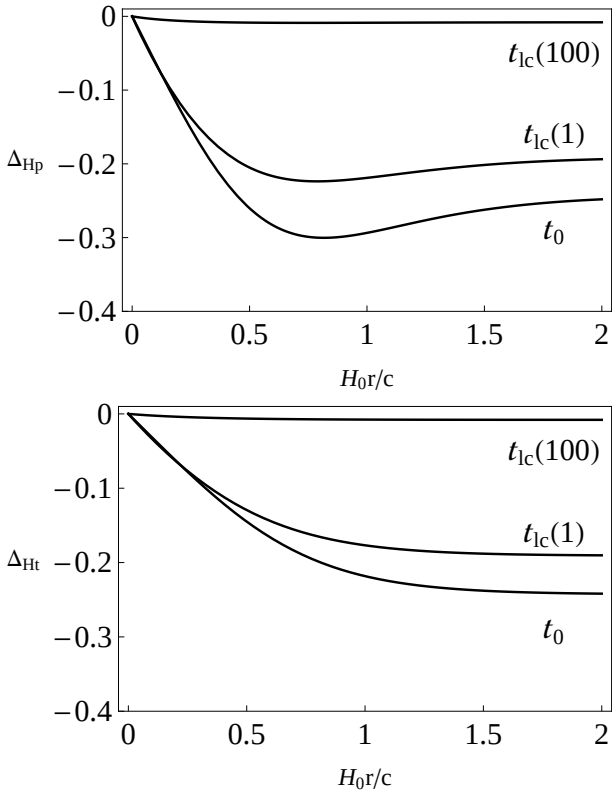

Figure 2.8: Hubble contrasts, $\Delta_{\mathrm{Hp}}(t, r)$ and $\Delta_{\mathrm{Ht}}(t, r)$, in GBH model on the spacelike hypersurfaces for $t = t_{\mathrm{lc}}(100)$, $t = t_{\mathrm{lc}}(1)$ and $t = t_0$, as functions of r.

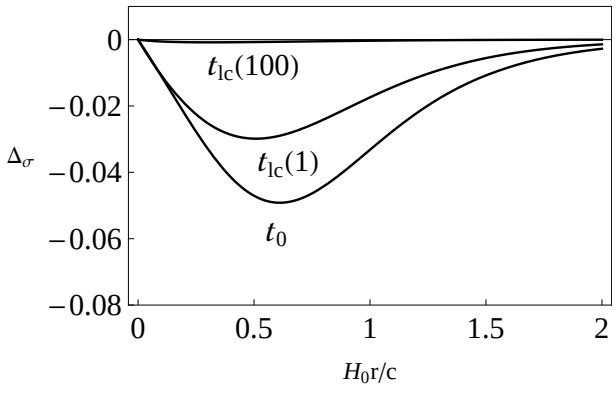

Figure 2.9: The normalized shear, $\Delta_\sigma(t, r)$, in GBH model on the spacelike hypersurfaces for $t = t_{\mathrm{lc}}(100)$, $t = t_{\mathrm{lc}}(1)$ and $t = t_0$, as functions of r.

functions of r. We can see that the normalized shear grows as time grows. From fig. 2.9, we can also see that the peak position of the normalized shear is located around the edge of the void structure. From figs. 2.3, 2.6 and 2.9, we expect that the feature about the peak position of the shear commonly appears in LTB cosmological models with a huge void structure.

Chapter 3

Relativistic perturbations in LTB cosmological model

As shown in the previous chapter, most of LTB cosmological models which account for the observations have a huge void structure that becomes nonlinear at the present time. However, Enqvist et al. [61] pointed out that the void inhomogeneity remains in a quasi-linear regime $\sim \mathcal{O}(0.1)$ inside a past light-cone of an observer at the center of the void. Actually, they considered an isotropic linear perturbation in the Einstein-deSitter universe that is consistent with the SNIa data, and showed that the fraction of the isotropic linear perturbation does not exceed 30% inside the past light-cone. This result implies that LTB cosmological models compatible with the observed distance-redshift relation may be studied by perturbation theory for the homogeneous and isotropic universe filled with dust at least for the inside of the past light-cone of the central observer. In this chapter, we apply this idea in studying relativistic perturbations in LTB cosmological models.

In § 3.1, we derive linear perturbation equations in LTB spacetimes, and review a previous work by February,Clarkson and Maartens [88] (FCM). In § 3.2, we consider a linearization of LTB cosmological model. We show that the CR void model which is originally described by LTB solution can be approximated to a dust-FLRW universe with an isotropic linear perturbation. In § 3.3, we analyze relativistic perturbations in the linearized LTB model and obtain density perturbations based on second order perturbations in a dust-FLRW background spacetime based on our papers [92] and [93]. In § 3.4, we compare our results with the previous work by FCM.

3.1 Perturbation equations in LTB cosmological model

3.1.1 Derivation of perturbation equations based on a spherical harmonic expansion

We review linear perturbations on LTB spacetime. Because of the spherical symmetricity of LTB spacetime, perturbations on LTB spacetime can be decoupled into two independent modes, called polar and axial modes (for details, see [87]). We are interested in the evolution of the density perturbations, and we focus on the polar mode. The infinitesimal world interval of the perturbed spacetime, in the Regge-Wheeler (RW) gauge, is written as

$$\begin{aligned} ds^2 &= -\left[1+(2\tilde{\eta}-\tilde{\chi}-\tilde{\varphi})\right]dt^2 - 2\frac{\tilde{\varsigma}a_{||}(t,r)}{\sqrt{1-k(r)}}dtdr \\ &+ \left[1+(\tilde{\chi}+\tilde{\varphi})\right]\frac{a_{||}^2(t,r)}{1-k(r)}dr^2 + a_{\perp}^2(t,r)r^2(1+\tilde{\varphi})d\Omega^2, \end{aligned} \tag{3.1}$$

where $d\Omega^2 := d\theta^2 + \sin^2\theta d\phi^2$, and $\tilde{\eta}(t,\mathbf{x})$, $\tilde{\chi}(t,\mathbf{x})$, $\tilde{\varphi}(t,\mathbf{x})$ and $\tilde{\varsigma}(t,\mathbf{x})$ are polar perturbations and equal to η, χ, φ and ς in the paper by Clarkson, Clifton and February [87] (hereafter CCF). The density and 4-velocity of the perturbed spacetime are given by

$$\rho = \rho^{\mathrm{LTB}}(t,r)\left(1+\tilde{\delta}\right), \tag{3.2}$$

$$u_\mu = \left(-1-\frac{1}{2}(2\tilde{\eta}-\tilde{\chi}-\tilde{\varphi}), \frac{a_{||}(t,r)}{\sqrt{1-k(r)}}\tilde{w}, \partial_\theta\tilde{v}, \partial_\varphi\tilde{v}\right), \tag{3.3}$$

where $\rho^{\mathrm{LTB}}(t,r)$ denotes the energy density of LTB spacetime, and $\tilde{\delta}(t,\mathbf{x})$, $\tilde{w}(t,\mathbf{x})$ and $\tilde{v}(t,\mathbf{x})$ are polar perturbations and equal to Δ, w and v in the CCF. Since the LTB spacetime has the spherical symmetricity, it is useful to expand perturbations in terms of the spherical harmonic functions, $Y^{(lm)}(\theta,\phi)$, as

$$\tilde{\varphi}(t,r,\theta,\phi) = \sum_{lm}\tilde{\varphi}^{(lm)}(t,r)Y^{(lm)}(\theta,\phi), \tag{3.4}$$

and $\tilde{\eta}$, $\tilde{\chi}$, $\tilde{\varsigma}$, $\tilde{\delta}$, $\tilde{w}$ and $\tilde{v}$ are expanded in the similar forms. Here, it should be noted that we omit the superscript in $\tilde{\varphi}^{(lm)}$ as long as there is no confusion.

By substituting the expressions (3.1), (3.2) and (3.3) into the Einstein equations, we obtain the perturbation equations as

$$-\ddot{\tilde{\chi}} + \tilde{\chi}'' - 3H_{||}\dot{\tilde{\chi}} - 2W\tilde{\chi}'$$

$$
\begin{aligned}
&+\Big[16\pi\rho^{\rm LTB}-\frac{6M}{a_\perp^3 r^3}-4H_\perp(H_{||}-H_\perp)-\frac{(l-1)(l+2)}{a_\perp^2 r^2}\Big]\tilde{\chi}\\
&\quad=-2(H_{||}-H_\perp)\tilde{\varsigma}^{'}-2\Big[H_{||}^{'}-2(H_{||}-H_\perp)W\Big]\tilde{\varsigma}+4(H_{||}-H_\perp)\dot{\tilde{\varphi}}\\
&\quad-2\Big[8\pi\rho-\frac{3M}{a_\perp^3}-2H_\perp(H_{||}-H_\perp)\Big]\tilde{\varphi},
\end{aligned}
\tag{3.5}
$$

$$
\begin{aligned}
&\ddot{\tilde{\varphi}}+4H_\perp\dot{\tilde{\varphi}}-2\Big(\frac{1}{a_\perp^2 r^2}-W^2\Big)\tilde{\varphi}\\
&\quad=-H_\perp\dot{\tilde{\chi}}+W\tilde{\chi}^{'}-\Big[2W^2-\frac{l(l+1)+2}{2a_\perp^2 r^2}\Big]\tilde{\chi}+2W(H_{||}-H_\perp)\tilde{\varsigma},
\end{aligned}
\tag{3.6}
$$

$$
\dot{\tilde{\varsigma}}+2H_{||}\tilde{\varsigma}=-\tilde{\chi}^{'},
\tag{3.7}
$$

$$
\tilde{\eta}=0,
\tag{3.8}
$$

$$
\begin{aligned}
8\pi\rho^{\rm LTB}\tilde{\delta} \;=\;& -\tilde{\varphi}^{''}-2W\tilde{\varphi}^{'}+(H_{||}+2H_\perp)\dot{\tilde{\varphi}}+W\tilde{\chi}^{'}+H_\perp\dot{\tilde{\chi}}\\
&+\Big[\frac{l(l+1)}{a_\perp^2 r^2}+2H_\perp^2+4H_{||}H_\perp-8\pi\rho^{\rm LTB}\Big](\tilde{\chi}+\tilde{\varphi})\\
&-\frac{(l-1)(l+2)}{2a_\perp^2 r^2}\tilde{\chi}+2H_\perp\tilde{\varsigma}^{'}+2(H_{||}+H_\perp)W\tilde{\varsigma},
\end{aligned}
\tag{3.9}
$$

$$
\begin{aligned}
8\pi\rho^{\rm LTB}\tilde{w} \;=\;& (\dot{\tilde{\varphi}})^{'}-(H_{||}-2H_\perp)\tilde{\varphi}^{'}-W\dot{\tilde{\chi}}+H_\perp\tilde{\chi}^{'}\\
&+\Big[\frac{l(l+1)+2}{2a_\perp^2 r^2}+H_\perp^2+2H_\perp H_{||}-W^2-4\pi\rho\Big]\tilde{\varsigma},
\end{aligned}
\tag{3.10}
$$

$$
8\pi\rho^{\rm LTB}\tilde{v}=\dot{\tilde{\varphi}}+\frac{\dot{\tilde{\chi}}}{2}+H_{||}(\tilde{\chi}+\tilde{\varphi})+\frac{\tilde{\varsigma}^{'}}{2},
\tag{3.11}
$$

where $W(t,r):=\sqrt{1-k(r)}/a_\perp(t,r)r$, an over-dot denotes differentiation with respect to t and a dash is defined as $X^{'}:=\big(\sqrt{1-k(r)}/a_{||}(t,r)\big)\partial_r X$. These equations can be found in Eqs. (40)–(46) in the CCF. We can see perturbation equations cannot be reduced to ordinary differential equations in a decoupled form. This is a very different situation from that of perturbations in the homogeneous and isotropic universe models. Since we cannot solve the perturbation equations analytically, we need to introduce an approximation scheme to solve the equations analytically.

3.1.2 Previous work by February, Clarkson and Maartens (FCM)

We review the perturbation equations in LTB cosmological model that was introduced in CCF and studied in a previous work by February, Clarkson and Maartens [88] (hereafter FCM). The FCM studied perturbations by assuming

$$\tilde{\chi} = \tilde{\varsigma} = 0. \tag{3.12}$$

In this case, the perturbation equations (3.5)–(3.11) are reduced to

$$\ddot{\tilde{\varphi}} + 4H_{\perp}\dot{\tilde{\varphi}} - \frac{2k(r)}{a_{\perp}^2 r^2}\tilde{\varphi} = 0, \tag{3.13}$$

$$4\pi a_{||}^2 \rho^{\mathrm{LTB}}\tilde{\delta} = -\frac{1}{2}\mathcal{L}^{\mathrm{FCM}}[\tilde{\varphi}], \tag{3.14}$$

where the operator $\mathcal{L}^{\mathrm{FCM}}$ is defined as

$$\begin{aligned}
\mathcal{L}^{\mathrm{FCM}} &:= (1-k(r))\partial_r^2 \\
&+ \left[\frac{2a_{||}}{a_{\perp}r} - \frac{2a_{||}}{a_{\perp}}\frac{k(r)}{r} - \frac{\partial_r k(r)}{2} - \frac{(\partial_r a_{||})}{a_{||}}(1-k(r))\right]\partial_r \\
&- \frac{a_{||}^2}{a_{\perp}^2}\left(\frac{l(l+1)}{r^2}\right) + \frac{a_{||}}{a_{\perp}}\left[\frac{\partial_r k(r)}{r} + \frac{a_{||}}{a_{\perp}}\frac{k(r)}{r^2}\right] \\
&- a_{||}^2(H_{||}+2H_{\perp})\partial_t - a_{\perp}^2 H_{\perp}(H_{\perp}+2H_{||}).
\end{aligned} \tag{3.15}$$

Eq. (3.13) can be solved analytically, and the evolution of the density perturbation $\tilde{\delta}$ can be determined by Eq. (3.14). However, it is non-trivial issue that the perturbations with the assumption Eq. (3.12) correspond to what type of perturbations in the homogeneous and isotropic universe model. We will clarify this in § 3.4.

3.2 Linearization of LTB cosmological model

3.2.1 An isotropic linear perturbation in dust-FLRW spacetimes

As mentioned, we apply linear perturbation theory in the homogeneous and isotropic dust-FLRW universe in order to approximate the LTB cosmological models. First, we briefly give a review on the dust-FLRW universe. Using the spherical polar coordinates for 3-dimensional space, the line-element of FLRW spacetime is given

by

$$ds^2 = -dt^2 + a^2(t)\left(\frac{dr^2}{1-Kr^2} + r^2 d\Omega^2\right) =: -dt^2 + a^2(t)\gamma_{ij}dx^i dx^j, \quad (3.16)$$

where $a(t)$ is the scale factor which will be determined by the Einstein equations, K is constant, $d\Omega^2$ is the 2-dimensional round metric, and, for later convenience, we have defined the background conformal 3-metric γ_{ij}. The constant K has the same sign as that of the curvature of the 3-dimensional space specified by t =constant. The stress-energy tensor of dust-FLRW universe is given by

$$T^{\mu\nu} = \rho^{\rm FLRW}(t)\bar{u}^\mu \bar{u}^\nu, \quad (3.17)$$

where $\rho^{\rm FLRW}(t)$ is the energy density, and $\bar{u}^\mu$ is the 4-velocity whose components are given by $\bar{u}^\mu = (1,0,0,0)$. The Einstein equations for the dust-FLRW universe are

$$H^2 = \frac{8\pi}{3}\rho^{\rm FLRW} - \frac{K}{a^2} \quad \text{and} \quad \frac{\ddot{a}}{a} = -\frac{4\pi}{3}\rho^{\rm FLRW}, \quad (3.18)$$

where $H(t) := \dot{a}/a$ and a dot denotes differentiation with respect to t.

Next, we review a linear isotropic perturbation in the dust-FLRW universe. We note that the isotropic perturbation generally contains only scalar perturbations. Then, by choosing the synchronous comoving gauge, the line element of the perturbed spacetime can be written in the form

$$\begin{aligned} ds^2 &= -dt^2 + a^2(t)\Big[\left(1+\kappa\, \ell^{(1)}_{||}(t,r)\right)\frac{dr^2}{1-Kr^2} \\ &\quad + \left(1+\kappa\, \ell^{(1)}_{\perp}(t,r)\right) r^2 d\Omega^2\Big] \quad (3.19) \\ &=: -dt^2 + a^2(t)\left[\gamma_{ij} + \kappa\, \ell^{(1)}_{ij}\right] dx^i dx^j, \quad (3.20) \end{aligned}$$

where we introduced a non-negative small parameter κ which characterize the amplitude of the isotropic perturbation. The perturbed stress-energy tensor is given by

$$T^{\mu\nu} = \rho^{\rm FLRW}(t)\left(1+\kappa\, \Delta^{(1)}(t,r)\right)\bar{u}^\mu \bar{u}^\nu. \quad (3.21)$$

The Einstein equations of the order κ lead:

$$\begin{aligned} \ddot{\Delta}^{(1)} + 2H\dot{\Delta}^{(1)} - 4\pi\rho^{\rm FLRW}\Delta^{(1)} &= 0, \quad (3.22) \\ r\partial_r \dot{\ell}^{(1)}_{\perp} + 3\dot{\ell}^{(1)}_{\perp} &= -2\dot{\Delta}^{(1)}, \quad (3.23) \\ \frac{\ell^{(1)}_{\parallel}}{a^2 r^2} &= -\ddot{\ell}^{(1)}_{\perp} - 3H\dot{\ell}^{(1)}_{\perp} + \frac{\ell^{(1)}_{\perp}}{a^2 r^2} + \frac{\partial_r \ell^{(1)}_{\perp}}{a^2 r}. \quad (3.24) \end{aligned}$$

General solutions for Eq. (3.22) is given by

$$\Delta^{(1)}(t,r) = \frac{D^+(t)}{D^+(t_0)}\Delta^+(r) + \frac{D^-(t)}{D^-(t_0)}\Delta^-(r), \tag{3.25}$$

where

$$D^+(t) = H\int^{a(t)} \frac{da}{a^3H^3} \quad \text{and} \quad D^-(t) = H, \tag{3.26}$$

and $\Delta^\pm$ stand for present values. D^+ and D^- represent the growing and decaying modes, respectively. where $\Delta^\pm$ are the growing and decaying modes, respectively. Once $\Delta^\pm$ are given, the metric perturbations are determined through the perturbation equations as follows. By integrating Eq. (3.23) with respect to r, we obtain

$$r^3\dot{\ell}_\perp^{(1)}(t,r) = -2\int_0^r d\tilde{r}\tilde{r}^2\dot{\Delta}^{(1)}(t,\tilde{r}), \tag{3.27}$$

where we used the regularity condition of $\dot{\ell}_\perp$ to fix the integral function. By integrating Eq. (3.27) with respect to t, we obtain

$$\ell_\perp^{(1)}(t,r) = -\frac{2}{r^3}\int_{t_0}^t d\tilde{t}\int_0^r d\tilde{r}\tilde{r}^2\dot{\Delta}^{(1)}(\tilde{t},\tilde{r}) + 2\frac{\zeta(r)}{r}, \tag{3.28}$$

where $\zeta(r)$ is an integral function. By substituting Eq. (3.28) into Eq. (3.24), we can obtain the perturbation $\ell_{||}^{(1)}(t,r)$. Here, it should be noted that we have one degree of freedom to rescale the radial coordinate r. Under the gauge transformation $r \to r + \kappa\zeta(r)$, the metric perturbations transform as

$$\ell_{||}^{(1)}(t,r) \to \ell_{||}^{(1)}(t,r) - 2\frac{d}{dr}\zeta(r), \quad \text{and} \quad \ell_\perp^{(1)}(t,r) \to \ell_\perp^{(1)}(t,r) - 2\frac{\zeta(r)}{r}, \tag{3.29}$$

and the density perturbation is invariant: $\Delta^{(1)} \to \Delta^{(1)}$.

3.2.2 Comparison with an exact LTB solution

In the case of a LTB cosmological model with homogeneous Big-Bang time $t_{\rm B}(r) = 0$, the spacetime at early time can be approximated by dust-FLRW universe with an isotropic linear perturbation. Thus, the metric and the stress energy tensor of the approximated LTB model can be represented by Eqs. (3.19) and (3.21). By choosing the initial time $t_{\rm i}$ at sufficiently early time, we give the growing mode defined in Eq. (3.25) for a given LTB model as

$$\Delta^+(r) = \frac{D^+(t_0)}{D^+(t_{\rm i})}\Delta(t_{\rm i},r), \tag{3.30}$$

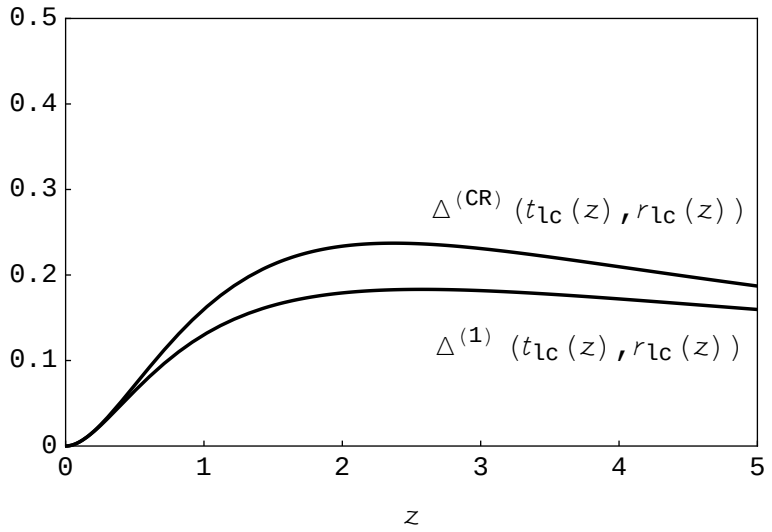

Figure 3.1: Exact density contrast $\Delta^{(\mathrm{CR})}$ and that of the linearized CR model $\Delta^{(1)}$ on the past light cone Σ_{lc}, plotted as functions of the redshift z.

where Δ is the density contrast of an exact LTB spacetime defined in Eq. (2.20). After giving the initial condition for the density perturbation by Eq. (3.30), we can compute the evolution of perturbations, $\Delta^{(1)}$, $\ell_{\parallel}^{(1)}$ and $\ell_{\perp}^{(1)}$, through linear perturbation equations (3.25), (3.27) and (3.28).

As for an example, we evaluate the accuracy of the linear approximation in the case of the CR model which was reviewed in the previous chapter. We describe the density contrast of the CR model as $\Delta^{(\mathrm{CR})}(t, r)$, of which the evolution is given by the exact LTB solution. By contrast, $\Delta^{(1)}(t, r)$ grows by the growing factor of the linear perturbation. We plot $\Delta^{(\mathrm{CR})}$ and $\Delta^{(1)}$ on the past light cone Σ_{lc} in Fig. 3.1. The relative error between the exact and linearized CR models is less than 30% on the light cone Σ_{lc}. Inside the past light cone Σ_{lc}, the error is smaller than that on the past light cone Σ_{lc}, since the CR model has only the growing mode. There is no qualitative difference between the exact and the linearized CR models, and thus we may see the qualitative behavior of linear perturbations in the CR model by the perturbation analysis of the FLRW universe based on the linearized CR model.

3.3 Analysis of perturbations in linearized LTB cosmological model

It is rather difficult to analyze the evolution of anisotropic perturbations in the LTB cosmological model, while it is much easier to study the evolution of non-

linear perturbations in the homogeneous and isotropic universe model by successive approximation. We adopt the latter approach. We introduce two-parameter perturbations with small expansion parameters κ and ϵ in a homogeneous and isotropic dust universe. The limit $\epsilon \to 0$ leads to the exact LTB solution, if we take all orders of κ into account. By contrast, the limit $\kappa \to 0$ with $0 < \epsilon \ll 1$ leads to the homogeneous and isotropic universe with small anisotropic perturbations. Then, in order to see the effect of the non-Copernican structure on the evolution of the anisotropic perturbations, we study the non-linear effects up to the order of $\kappa\epsilon$, following Ref. [99].

In the synchronous comoving gauge, the metric and stress-energy tensor of the perturbed universe model is written as

$$ds^2 = -dt^2 + a^2(t) \sum_{N=0} \kappa^N \left[\ell_{ij}^{(N)} dx^i dx^j + \epsilon \, h_{ij}^{(N+1)} dx^i dx^j + \mathcal{O}(\epsilon^2) \right], \quad (3.31)$$

and

$$T^{\mu\nu} = \rho^{\rm FLRW}(t) \bar{u}^\mu \bar{u}^\nu \sum_{N=0} \kappa^N \left[\Delta^{(N)}(t,r) + \epsilon \, \delta^{(N+1)}(t,\mathbf{x}) + \mathcal{O}(\epsilon^2) \right], \quad (3.32)$$

where $\ell_{ij}^{(0)} = \gamma_{ij}$, $\Delta^{(0)} = 1$ and $\mathbf{x} := (r, \theta, \phi)$. By substituting expressions (3.31) and (3.32) into the Einstein equations $G_{\mu\nu} = 8\pi T_{\mu\nu}$ and the equation of motion for matter $\nabla_\mu T^{\mu\nu} = 0$, and assuming the equations hold in each order with respect to κ and ϵ, we can obtain the perturbation equations order by order.

3.3.1 Perturbations of the order ϵ

Regarding the anisotropic perturbations of the order ϵ, we assume that the metric perturbation $h_{ij}^{(1)}$ is composed of the only scalar modes, and thus it is written in the form

$$h_{ij}^{(1)} = \Psi^{(1)}(t,\mathbf{x}) \bar{\gamma}_{ij} + \mathcal{D}_i \mathcal{D}_j \Phi^{(1)}(t,\mathbf{x}), \quad (3.33)$$

where $\mathcal{D}_i$ denotes covariant derivative with respect to $\bar{\gamma}_{ij}$. Note that both $\Psi^{(1)}$ and $\Phi^{(1)}$ are the scalar on a hypersurface of constant t. Then, we obtain perturbation equations of the order ϵ as

$$\dot{\Psi}^{(1)} - K \dot{\Phi}^{(1)} = 0, \quad (3.34)$$

$$\left(\mathcal{D}^i \mathcal{D}_i + 3K \right) \dot{\Phi}^{(1)} = -2\dot{\delta}^{(1)}, \quad (3.35)$$

$$\ddot{\delta}^{(1)} + 2H\dot{\delta}^{(1)} - 4\pi\rho^{\rm FLRW}\delta^{(1)} = 0. \quad (3.36)$$

General solutions for Eq. (3.36) is given by

$$\delta^{(1)}(t,\mathbf{x}) = \frac{D^+(t)}{D^+(t_0)}\delta^+(\mathbf{x}) + \frac{D^-(t)}{D^-(t_0)}\delta^-(\mathbf{x}), \tag{3.37}$$

where $\delta^{\pm}$ stand for the physical degrees of freedom of growing and decaying modes. For simplicity, we set $\delta^-(\mathbf{x}) = 0$ hereafter.

3.3.2 Perturbations of the order $\kappa\epsilon$

From perturbation equations of the order $\kappa\epsilon$, we obtain the evolution equation of the density perturbation as

$$\ddot{\delta}^{(2)} + 2H\dot{\delta}^{(2)} - 4\pi\rho^{\rm FLRW}\delta^{(2)} \;=\; S^{(2)}, \tag{3.38}$$

where $S^{(2)}$ is defined as

$$S^{(2)} := \frac{1}{2}\dot{\ell}^{(1)ij}\dot{h}^{(1)}_{ij} + 2\dot{\Delta}^{(1)}\dot{\delta}^{(1)} + \ddot{\Delta}^{(1)}\delta^{(1)} + \Delta^{(1)}\ddot{\delta}^{(1)} + 2H\dot{\Delta}^{(1)}\delta^{(1)} + 2H\Delta^{(1)}\dot{\delta}^{(1)}, \tag{3.39}$$

where $\ell^{ij} := \gamma^{ik}\gamma^{jl}\ell_{kl}$. We solve Eq. (3.38) by using the Green function method and obtain

$$\begin{aligned}\delta(t,\mathbf{x}) \;&:=\; \epsilon\,\delta^{(1)}(t,\mathbf{x}) + \kappa\epsilon\,\delta^{(2)}(t,\mathbf{x}) \\ &=\; \epsilon\,\delta^{(1)}(t,\mathbf{x}) + \kappa\epsilon\left[T_1(t)\Delta^{(1)}(t_{\rm i},r)\delta^{(1)}(t,\mathbf{x}) + T_2(t)\dot{\ell}^{(1)ij}(t_{\rm i},\mathbf{x})h^{(1)}_{ij}(t,\mathbf{x})\right],\end{aligned} \tag{3.40}$$

where

$$\begin{aligned}T_1(t) \;&:=\; [D^+(t)]^{-1}\int_{t_{\rm i}}^{t} ds G(s;t) \\ &\times\; \left(2\dot{D}^+(s)\dot{D}^+(s) + 2\ddot{D}^+(s)D^+(s) + 4H(s)\dot{D}^+(s)D^+(s)\right), \\ T_2(t) \;&:=\; \frac{1}{2}[D^+(t)\dot{D}^+(t_{\rm i})]^{-1}\int_{t_{\rm i}}^{t} ds G(s;t)\dot{D}^+(s)\dot{D}^+(s), \\ G(s;t) \;&:=\; \frac{D^-(t)D^+(s) - D^+(t)D^-(s)}{D^+(s)\dot{D}^-(s) - \dot{D}^+(s)D^-(s)}.\end{aligned}$$

For later convenience, focusing on the scalar modes on a sphere specified by the radial coordinate r, we rewrite the term $\dot{\ell}^{(1)ij}h^{(1)}_{ij}$ in the solution (3.40) as follows. By using Eq. (3.19), we first rewrite the metric perturbations of the order κ in the form

$$\ell^{(1)}_{ij}dx^i dx^j = \ell^{(1)}_{\parallel}(t,r)\frac{dr^2}{1-Kr^2} + \ell^{(1)}_{\perp}(t,r)r^2 d\Omega^2. \tag{3.41}$$

Then, we describe the radial and azimuthal Hubble parameters as

$$H_{||} := H + \kappa\psi^{(1)}_{||} + \mathcal{O}(\epsilon, \kappa^2) \quad \text{and} \quad H_{\perp} := H + \kappa\psi^{(1)}_{\perp} + \mathcal{O}(\epsilon, \kappa^2), \tag{3.42}$$

where

$$\psi^{(1)}_{||} := \frac{1}{2}\dot{\ell}^{(1)}_{||} \quad \text{and} \quad \psi^{(1)}_{\perp} := \frac{1}{2}\dot{\ell}^{(1)}_{\perp}. \tag{3.43}$$

By using the functions $\psi^{(1)}_{||}, \psi^{(1)}_{\perp}$ together with $\Phi^{(1)}$, the density contrast (3.40) is reduced to

$$\begin{aligned}
\delta(t,\mathbf{x}) &= \epsilon\,\delta^{(1)}(t,\mathbf{x}) + \kappa\epsilon\Big[T_1(t)\Delta^{\mathrm{i}}(r)\delta^{(1)}(t,\mathbf{x}) + 2T_2(t)\big\{K\left(\psi^{\mathrm{i}}_{||}(r) + 2\psi^{\mathrm{i}}_{\perp}(r)\right) \\
&+ \psi^{\mathrm{i}}_{\perp}(r)\mathcal{D}^i\mathcal{D}_i + \left(\psi^{\mathrm{i}}_{||}(r) - \psi^{\mathrm{i}}_{\perp}(r)\right)\partial_r^2\big\}\Phi^{(1)}(t,\mathbf{x})\Big] \\
&= \epsilon\,\delta^{(1)}(t,\mathbf{x}) + \kappa\epsilon\Big[\left\{T_1(t)\Delta^{\mathrm{i}}(r) - 4T_2(t)\psi^{\mathrm{i}}_{\perp}(r)\right\}\delta^{(1)}(t,\mathbf{x}) \\
&+ 2T_2(t)\left\{\psi^{\mathrm{i}}_{||}(r) - \psi^{\mathrm{i}}_{\perp}(r)\right\}\left(K + \partial_r^2\right)\Phi^{(1)}(t,\mathbf{x})\Big],
\end{aligned} \tag{3.44}$$

where the superscript i represents the initial value at $t = t_{\mathrm{i}}$. The density perturbation obtained here is one of our main result. From Eq. (3.44), we can see that the density fluctuation at the leading order, ϵ, is same to that in the homogeneous and isotropic dust universe, and the effects of the void inhomogeneity appear at the next-to-leading order, $\kappa\epsilon$, through Δ, $\psi_{\parallel}$ and $\psi_{\perp}$. We will evaluate these effects to the observations in the case of a huge void model in the next chapter.

3.4 Comparison our approach with previous work by FCM

In this section, we compare our approach for solving perturbations discussed in the previous section with previous work FCM [88]. The FCM studied perturbations in the Regge-Wheeler (RW) gauge, while we have studied in the synchronous comoving gauge. We derive perturbation equations of our approach in the RW gauge.

In order to apply our method, we regard the background LTB spacetime in Eqs. (3.1), (3.2) and (3.3) as isotropic perturbations in the Einstein-de Sitter universe model which are characterized by the book-keeping parameter κ as in section. By using $\ell^{(1)}_{||}(t,r)$, $\ell^{(1)}_{\perp}(t,r)$ and $\Delta^{(1)}(t,r)$ introduced in section, we write the the

functions $a_{||}$, $a_{\perp}$, $k(r)$ and $\rho^{\rm LTB}$ in the form

$$
\begin{aligned}
a_{||} &= a\left[1+\frac{\kappa}{2}\partial_r(r\ell_{\perp}^{(1)})\right]+\mathcal{O}(\kappa^2), && (3.45)\\
a_{\perp} &= a\left[1+\frac{\kappa}{2}\ell_{\perp}^{(1)}\right]+\mathcal{O}(\kappa^2), && (3.46)\\
k(r)r^2 &= \kappa\left[\ell_{||}^{(1)}-\partial_r(r\ell_{\perp}^{(1)})\right]+\mathcal{O}(\kappa^2), && (3.47)\\
\rho^{\rm LTB} &= \bar{\rho}\left[1+\kappa\Delta^{(1)}\right]+\mathcal{O}(\kappa^2). && (3.48)
\end{aligned}
$$

In accordance with the prescription in section, we write the polar modes of perturbations as follows:

$$
\tilde{\varphi}=\epsilon\tilde{\varphi}^{(1)}+\kappa\epsilon\tilde{\varphi}^{(2)}+\mathcal{O}(\kappa^2\epsilon), \tag{3.49}
$$

and $\tilde{\chi}$, $\tilde{\varsigma}$, $\tilde{\delta}$, $\tilde{w}$ and $\tilde{v}$ are written in the similar forms. Assuming $\epsilon \ll \kappa < 1$ and the Einstein equations hold in each order with respect to κ and ϵ, we can obtain the equations for the perturbations of the order ϵ and $\kappa\epsilon$.

First of all, we see the perturbation equations of the order ϵ. The perturbations of the order ϵ are equivalent to those of the Einstein-de Sitter universe model. As mentioned in section, we only include the scalar mode of the order ϵ in our present analysis. By contrast, the polar perturbations may be a mixture of the scalar, vector and tensor modes in the context of the perturbation theory for the Einstein-de Sitter universe model. Thus, we need to relate the polar perturbations to the scalar, vector and tensor perturbations in the Einstein-de Sitter universe model. The CCF derived these relations in Eqs. (66)–(69) in their paper, by taking the limit of the FLRW spacetimes to the LTB spacetimes. From Eqs. (67) and (68) in the CCF, we can see that $\tilde{\varsigma}^{(1)}$ and $\tilde{\chi}^{(1)}$ do not contain scalar mode but consist of the vector and tensor modes. Thus, the neglect of the vector and tensor modes leads to

$$
\tilde{\varsigma}^{(1)}=\tilde{\chi}^{(1)} = 0. \tag{3.50}
$$

In the case that Eq. (3.50) holds, the perturbed metric (3.1) becomes

$$
ds^2=-\left(1-\varphi^{(1)}\right)dt^2+a^2\left(1+\varphi^{(1)}\right)\left(dr^2+r^2d\Omega^2\right). \tag{3.51}
$$

It is clear from the above equation that the metric perturbation of the order ϵ is the scalar mode. Correspondingly, the perturbations of ρ and u^{μ} of the order ϵ must contain the only scalar mode.

By substituting the expressions (3.1), (3.2) and (3.3) into the Einstein equations and using the expansions (3.45), (3.46), (3.47), (3.48) and (3.49) together with

Eq. (3.50), we obtain the perturbation equations of the order ϵ as

$$\ddot{\tilde{\varphi}}^{(1)} + 4H\dot{\tilde{\varphi}}^{(1)} = 0, \tag{3.52}$$

$$8\pi\bar{\rho}\tilde{\delta}^{(1)} = 3H\dot{\tilde{\varphi}}^{(1)} + 3H^2\tilde{\varphi}^{(1)} - \frac{1}{a^2}\mathcal{D}^i\mathcal{D}_i\tilde{\varphi}^{(1)}, \tag{3.53}$$

$$8\pi\bar{\rho}\tilde{w}^{(1)} = \frac{\partial_r}{a}\left(\dot{\tilde{\varphi}}^{(1)} + H\tilde{\varphi}^{(1)}\right), \tag{3.54}$$

$$8\pi\bar{\rho}\tilde{v}^{(1)} = \dot{\tilde{\varphi}}^{(1)} + H\tilde{\varphi}^{(1)}. \tag{3.55}$$

Although it is non-trivial from only Eq. (3.3) that the perturbations of u_μ of the order ϵ are the scalar mode, it is clear from Eqs. (3.54) and (3.55) that it is the case. Thus, we conclude that the assumption (3.12) at the order ϵ is equal to neglecting the vector and tensor modes. We can also see that our approach for perturbations is equal to FCM's approach in the order ϵ as follows. If we apply the expansions (3.45), (3.46), (3.47), (3.48) and (3.49) to Eqs. (3.13) and (3.14), and take the limit of $\kappa \to 0$, Eqs. (3.13) and (3.14) coincide with Eqs. (3.52) and (3.53).

Next, we see the perturbation equations of the order $\kappa\epsilon$. Substituting the expressions (3.1), (3.2) and (3.3) into the Einstein equations and using the expansions (3.45), (3.46), (3.47), (3.48) and (3.49), we obtain the perturbation equations of the order $\kappa\epsilon$ as

$$\begin{aligned}
&-\ddot{\tilde{\chi}}^{(2)} - 3H\dot{\tilde{\chi}}^{(2)} + \frac{1}{a^2}\left[\mathcal{D}^i\mathcal{D}_i - 2\left(\frac{2}{r}\partial_r - \frac{1}{r^2}\right)\right]\tilde{\chi}^{(2)} = 2(\dot{\ell}_{||}^{(1)} - \dot{\ell}_{\perp}^{(1)})\dot{\tilde{\varphi}}^{(1)} \\
&\quad + 2\left[\left(\ddot{\ell}_{||}^{(1)} - \ddot{\ell}_{\perp}^{(1)}\right) + 3H\left(\dot{\ell}_{||}^{(1)} - \dot{\ell}_{\perp}^{(1)}\right)\right]\tilde{\varphi}^{(1)},
\end{aligned} \tag{3.56}$$

$$\begin{aligned}
&\ddot{\tilde{\varphi}}^{(2)} + 4H\dot{\tilde{\varphi}}^{(2)} + H\dot{\tilde{\chi}}^{(2)} + \frac{1}{2a^2}\left[\mathcal{D}^i\mathcal{D}_i - \partial_r^2 - 2\left(\frac{2}{r}\partial_r - \frac{1}{r^2}\right)\right]\tilde{\chi}^{(2)} = -2\dot{\ell}_{\perp}^{(1)}\dot{\tilde{\varphi}}^{(1)} \\
&\quad + \frac{1}{a^2r^2}\left(\ell_{||}^{(1)} - \partial_r(r\ell_{\perp}^{(1)})\right)\tilde{\varphi}^{(1)},
\end{aligned} \tag{3.57}$$

$$\dot{\tilde{\varsigma}}^{(2)} + 2H\tilde{\varsigma}^{(2)} + \frac{\partial_r\tilde{\chi}^{(2)}}{a} = 0, \tag{3.58}$$

$$\begin{aligned}
8\pi\bar{\rho}\tilde{\delta}^{(2)} &= 3H\dot{\tilde{\varphi}}^{(2)} + 3H^2\tilde{\varphi}^{(2)} - \frac{1}{a^2}\mathcal{D}^i\mathcal{D}_i\tilde{\varphi}^{(2)} \\
&+ H\dot{\tilde{\chi}}^{(2)} + \left[3H^2 + \frac{1}{2a^2}\left(\frac{2}{r}\partial_r + \frac{(l-1)(l+2)}{r^2}\right)\right]\tilde{\chi}^{(2)} + \frac{2H}{a}\left[\partial_r + \frac{2}{r}\right]\tilde{\varsigma}^{(2)} \\
&+ \frac{1}{a^2}\left(\ell_{||}^{(1)} - \ell_{\perp}^{(1)}\right)\partial_r^2\tilde{\varphi}^{(1)} + \frac{1}{a^2}\left[\frac{2}{r}\left(\ell_{||}^{(1)} - \ell_{\perp}^{(1)}\right) - \frac{1}{2}\partial_r\left(\ell_{||}^{(1)} - 2\ell_{\perp}^{(1)}\right)\right]\partial_r\tilde{\varphi}^{(1)} \\
&+ \frac{1}{a^2}\ell_{\perp}^{(1)}\mathcal{D}^i\mathcal{D}_i\tilde{\varphi}^{(1)} + \frac{1}{2}\left(\dot{\ell}_{||}^{(1)} + 2\dot{\ell}_{\perp}^{(1)}\right)\dot{\tilde{\varphi}}^{(1)} \\
&+ \left[2H\left(\dot{\ell}_{||}^{(1)} + 2\dot{\ell}_{\perp}^{(1)}\right) - 8\pi\bar{\rho}\Delta^{(1)}\right]\tilde{\varphi}^{(1)} - 8\pi\bar{\rho}\Delta^{(1)}\tilde{\delta}^{(1)},
\end{aligned} \tag{3.59}$$

$$8\pi\bar{\rho}\tilde{w}^{(2)} = \frac{\partial_r}{a}\left(\dot{\tilde{\varphi}}^{(2)} + H\tilde{\varphi}^{(2)}\right) - \frac{1}{ar}\dot{\tilde{\chi}}^{(2)} + \frac{H}{a}\partial_r\tilde{\chi}^{(2)} + \frac{1}{2a^2}\left[\partial_r^2 + \frac{2}{r}\partial_r - \mathcal{D}^i\mathcal{D}_i\right]\tilde{\varsigma}^{(2)}$$

$$
\begin{aligned}
&+ \quad \frac{3}{2}H^2\tilde{\varsigma}^{(2)} - \frac{1}{2a}\ell_{||}^{(1)}\partial_r\dot{\tilde{\varphi}}^{(1)} - \frac{1}{2a}\left[H\ell_{||}^{(1)} - (2\dot{\ell}_{\perp}^{(1)} - \dot{\ell}_{||}^{(1)})\right]\partial_r\tilde{\varphi}^{(1)} \\
&- \quad 8\pi\bar{\rho}\Delta^{(1)}\tilde{w}^{(1)},
\end{aligned}
\tag{3.60}
$$

$$
8\pi\bar{\rho}\tilde{v}^{(2)} \quad = \quad \dot{\tilde{\varphi}}^{(2)} + H\tilde{\varphi}^{(2)} + \frac{1}{2}\dot{\tilde{\chi}}^{(2)} + H\tilde{\chi}^{(2)} + \frac{1}{2a}\partial_r\tilde{\varsigma}^{(2)} + \frac{H}{2}\dot{\ell}_{||}^{(1)}\tilde{\varphi}^{(1)} - 8\pi\bar{\rho}\Delta^{(1)}\tilde{v}^{(1)}.
\tag{3.61}
$$

By defining $\tilde{y}$ as $\tilde{y} := \tilde{\chi}^{(2)}/r^2$ and the Fourier transformation of $\tilde{y}$ as

$$
\tilde{y}(t,\mathbf{x}) = \int \frac{d^3k}{(2\pi)^{3/2}} e^{i\mathbf{k}\cdot\mathbf{x}}\tilde{y}_{\mathbf{k}}(t),
\tag{3.62}
$$

Eq. (3.56) is reduced to

$$
\ddot{\tilde{y}}_{\mathbf{k}} + 3H\dot{\tilde{y}}_{\mathbf{k}} + \frac{k^2}{a^2}\tilde{y}_{\mathbf{k}} \quad = \quad S_{\mathbf{k}}(t),
\tag{3.63}
$$

where the source term $S_{\mathbf{k}}(t)$ is defined as

$$
\begin{aligned}
S_{\mathbf{k}}(t) \quad := \quad & -\int \frac{d^3x}{(2\pi)^{3/2}} e^{-i\mathbf{k}\cdot\mathbf{x}} \Bigg\{ 2(\dot{\ell}_{||}^{(1)} - \dot{\ell}_{\perp}^{(1)})\frac{\dot{\tilde{\varphi}}^{(1)}}{r^2} + 2\Big[\left(\ddot{\ell}_{||}^{(1)} - \ddot{\ell}_{\perp}^{(1)}\right) \\
& +3H\left(\dot{\ell}_{||}^{(1)} - \dot{\ell}_{\perp}^{(1)}\right)\Big]\frac{\tilde{\varphi}^{(1)}}{r^2} \Bigg\}.
\end{aligned}
\tag{3.64}
$$

We find that $\ell_{||}^{(1)} - \ell_{\perp}^{(1)} \propto a$ from the equation in the section, and the growing solution of Eq. (3.52) is $\varphi^{(1)} =$ constant. Hence, the source term $S_{\mathbf{k}}(t)$ is proportional to a^{-2}. From this, we can see that the particular solution of Eq. (3.63) is $S_{\mathbf{k}}(t_0)/k^2$. We can also see that the homogeneous solutions of Eq. (3.63) decay as time grows. Thus, we obtain the Fourier mode of the perturbation $\tilde{\chi}$ as

$$
\tilde{\chi}_{\mathbf{k}}^{(2)}(t) = \frac{r^2 S_{\mathbf{k}}(t_0)}{k^2} + (\text{decaying modes}).
\tag{3.65}
$$

By using Eqs. (3.58) and (3.65), we obtain

$$
\tilde{\varsigma}^{(2)}(t,\mathbf{x}) = -\frac{3}{5}t^{1/3}t_0^{2/3}\partial_r\tilde{\chi}^{(2)}(t,\mathbf{x}) + (\text{decaying modes}).
\tag{3.66}
$$

From Eqs. (3.65) and (3.66), we can see that $\tilde{\chi}^{(2)}$ and $\tilde{\varsigma}^{(2)}$ do not vanish but $\tilde{\chi}^{(2)} =$ constant. and $\tilde{\varsigma}^{(2)} \propto t^{1/3}$ at late time, even if we set $\tilde{\varsigma}^{(1)} = \tilde{\chi}^{(1)} = 0$ in general. Thus, the evolution of metric perturbations in our approach significantly differs from that in the FCM at the order $\kappa\epsilon$. However, it is worthwhile to notice that the effects of $\tilde{\chi}^{(2)}$ and $\tilde{\varsigma}^{(2)}$ to the density perturbation $\tilde{\delta}^{(2)}$ are not dominant compared to other effects, because the terms with respect to $\tilde{\chi}^{(2)}$ and $\tilde{\varsigma}^{(2)}$ in the right hand side of

Eq. (3.59) proportional to $t^{-4/3}$ and the terms with respect to $\tilde{\varphi}^{(1)}$ proportional to $t^{-2/3}$. Thus, the FCM's assumption $\tilde{\chi} = \tilde{\varsigma} = 0$ will be good approximation for sufficiently late time in the study of density perturbations.

The metric perturbations $\tilde{\chi}^{(2)}$ and $\tilde{\varsigma}^{(2)}$ do not exist in the case of homogeneous and isotropic FLRW models. Thus, we expect that $\tilde{\chi}^{(2)}$ and $\tilde{\varsigma}^{(2)}$ becomes important in testing LTB cosmological models from observations of large-scale structures such as weak gravitational lensing, since the photon from galaxies propagates in the spacetime with these metric perturbations. We leave the effects to the observations for a future work.

Chapter 4

Stochastic properties of density perturbations in LTB cosmological model

Theoretical cosmologies only predict stochastic properties of fluctuations rather things like the precise location of particular galaxies. Thus, observational results of the large-scale structure are commonly given by correlation functions and Power spectra which describe stochastic properties of galaxy distributions. In this chapter, to compare our results obtained in the previous chapter with observations of galaxy clustering, we study stochastic properties of the density perturbations in LTB cosmological models based on our papers [92] and [93].

In § 4.1, we derive a two-point correlation function of the density perturbations, and investigate the stochastic properties of fluctuations. In § 4.2, we discuss the Redshift Space Distortions (reviewed in § 1.3.2) in the LTB cosmological models by using two-point correlation functions. In § 4.3, we derive angular power spectrum of density perturbations, and study the evolution of density perturbations in a specific void model (the CR model) by using it. § 4.4 is devoted to conclusion and discussion of this chapter.

4.1 Two-point correlation functions of density perturbations in LTB cosmological model

4.1.1 Derivation of two-point correlation functions

To derive two-point correlation functions, it is convenient to introduce a radial coordinate χ in the metric of a dust-FLRW universe model as

$$ds^2 = -dt^2 + a^2(t)\left[d\chi^2 + S_K^2(\chi)(d\theta^2 + \sin^2\theta d\phi^2)\right], \tag{4.1}$$

where S_K is defined by

$$S_K(\chi) = \begin{cases} \sinh\left(\sqrt{-K}\chi\right)/\sqrt{-K}, & \text{for } K < 0 \\ \chi, & \text{for } K = 0 \\ \sin\left(\sqrt{K}\chi\right)/\sqrt{K}, & \text{for } K > 0 \end{cases}$$

where K is a constant that denotes spatial curvature.

In the previous chapter, we have invoked the perturbation analysis on the background dust-FLRW universe in order to clarify the evolution of density perturbations in the inhomogeneous and isotropic LTB universe model. By virtue of this treatment, we can specify the relative position of two points and the central observer by using the *comoving distance* which is the geodesic distance with respect to the background conformal metric γ_{ij}. We represent two-point correlation functions of anisotropic density perturbations in the inhomogeneous and isotropic LTB universe model in the form

$$\xi(t, \mathbf{x}_1, \mathbf{x}_2) := \langle \delta(t, \mathbf{x}_1)\delta(t, \mathbf{x}_2)\rangle = \xi(t, \chi, \chi_1, \chi_2), \tag{4.2}$$

where $\chi_{1,2}$ are the comoving distances from the central observer to the points, and χ is the comoving separation of the two points (see fig. 4.1).

By using the quantities introduced in the previous chapter, the two-point correlation function is given by

$$\begin{aligned} \xi &= \epsilon^2\langle\delta^{(1)}(t, \mathbf{x}_1)\delta^{(1)}(t, \mathbf{x}_2)\rangle \\ &+ \kappa\epsilon^2\langle\delta^{(2)}(t, \mathbf{x}_1)\delta^{(1)}(t, \mathbf{x}_2)\rangle + \kappa\epsilon^2\langle\delta^{(1)}(t, \mathbf{x}_1)\delta^{(2)}(t, \mathbf{x}_2)\rangle + \mathcal{O}(\epsilon^2\kappa^2). \end{aligned} \tag{4.3}$$

The terms of the order $\kappa\epsilon^2$ in the right hand side of the above equation represent the effects of the spherical void on the anisotropic perturbations. By using Eq. (3.44), these terms of our interest are written as follows. The second term in the right hand side of Eq. (4.3) is given by

$$\langle\delta^{(2)}(t, \mathbf{x}_1)\delta^{(1)}(t, \mathbf{x}_2)\rangle = \left[T_1(t)\Delta^{\mathrm{i}}(\chi_1) - 4T_2(t)\psi_\perp^{\mathrm{i}}(\chi_1)\right]\langle\delta^{(1)}(t, \mathbf{x}_1)\delta^{(1)}(t, \mathbf{x}_2)\rangle$$

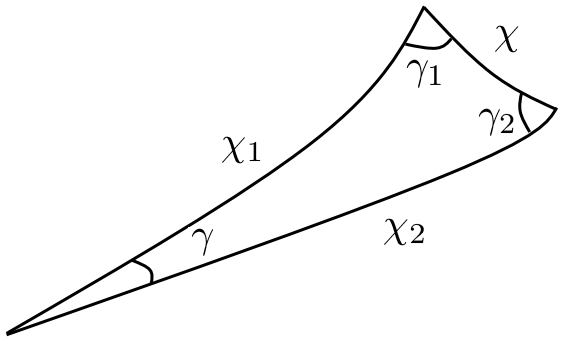

Figure 4.1: Geometry of the relative position of the observer and two points in the constant curvature space(From Ref. [100]).

$$+ 2T_2(t) \left[\psi^{\rm i}_{||}(\chi_1) - \psi^{\rm i}_{\perp}(\chi_1)\right] \left(K + \partial^2_{\chi_1}\right) \langle \Phi^{(1)}(t, \mathbf{x}_1)\delta^{(1)}(t, \mathbf{x}_2)\rangle. \quad (4.4)$$

Hereafter, we assume that the wavelength λ of the anisotropic perturbations is much smaller than the scale of the spatial curvature, $\partial_\chi \sim 1/\lambda \gg \sqrt{|K|}$, and thus we discard the term proportional to K in the above equation[1]. The third term in the right hand side of Eq. (4.3) is obtained by replacing the subscript 1 by 2 and 2 by 1, except for the subscript of T_1 and T_2, in Eq. (4.4).

Under the short-wavelength assumption, $\lambda \ll 1/\sqrt{|K|}$, the two-point correlation function of the linear density perturbations $\delta^{(1)}$ is written as[2]

$$\langle \delta^{(1)}(t, \mathbf{x}_1)\delta^{(1)}(t, \mathbf{x}_2)\rangle = \int_0^\infty \frac{dkk^2}{2\pi^2} j_0(k\chi) P^{(1)}(t, k), \quad (4.5)$$

where $P^{(1)}(t, k)$ is the so-called power spectrum in the homogeneous and isotropic universes. Here, we briefly review the power spectrum that we use. If we choose the initial time after recombination, the matter power spectrum including baryons and cold dark matter can be written as

$$\begin{aligned} P^{(1)}(t, k) &= [D^+(t)]^2 P(k), \\ P(k) &= A_0 k^n T^2(k), \end{aligned} \quad (4.6)$$

where A_0 is a positive constant which represents the amplitude for perturbations on large scales, n is constant, and $T(k)$ is the matter transfer function. In this thesis,

[1] We note that χ_1 and χ_2 can be the same order of $1/\sqrt{|K|}$.

[2] General formula which does not employ the short-wavelength approximation can be seen in Matsubara's paper [100].

we assume the Harrison-Zel'dovich spectrum $n = 1$. As for the transfer function, we adopt the fitting formula developed by Eisenstein & Hu [101]. The fitting function defined by equation (16) in Ref. [101] is determined by the four parameters as

$$T(k) = T(k; \Omega_{\rm b}, \Omega_{\rm c}, h, \Theta_{2.7}), \tag{4.7}$$

where $\Omega_{\rm b}$ and $\Omega_{\rm c}$ are the cosmological density parameter of baryons and cold dark matter, h is defined as $h = H_0/(100{\rm kms}^{-1}{\rm Mpc}^{-1})$ and the CMB temperature is written as $2.7\Theta_{2.7}K$. As an example, in the case of the CR model reviewed in §. 2.2,

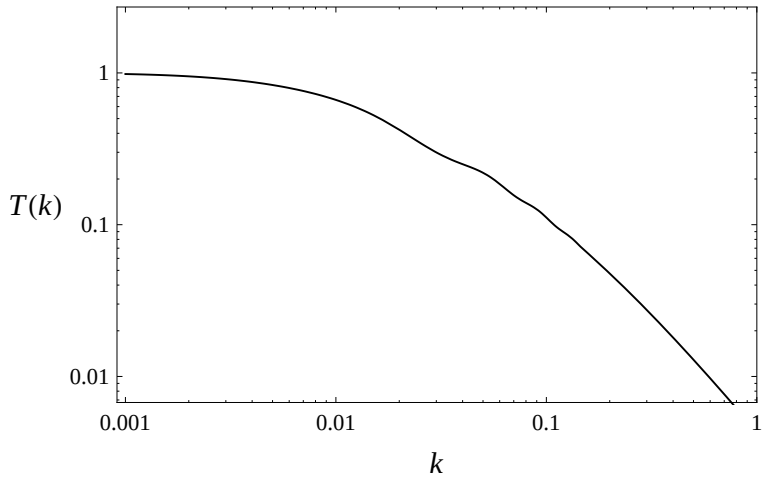

Figure 4.2: Transfer function as a function of k for the FLRW model with $\Omega_b = 0.042, \Omega_c = 0.20, h = 0.74, \Theta_{2.7} = 1.0$.

we will adopt the following values for these parameters,

$$\Omega_b = 0.042, \quad \Omega_c = 0.20, \quad h = 0.74, \quad \Theta_{2.7} = 1.0\ , \tag{4.8}$$

where Ω_b, Ω_c and h are chosen to be the same at the center of the CR model and $\Theta_{2.7} = 1.0$ is assumed. This transfer function is plotted as a function of k in Fig. 4.2.

By using Eq. (4.5) together with the relation $\delta^{(1)} \simeq -\frac{1}{2}\mathcal{D}^i\mathcal{D}_i\Phi^{(1)}$ from Eq. (3.35), we obtain

$$\langle \Phi^{(1)}(t, \mathbf{x}_1)\delta^{(1)}(t, \mathbf{x}_2)\rangle = 2\int \frac{dkk^2}{2\pi^2} j_0(k\chi)\frac{P^{(1)}(t,k)}{k^2}. \tag{4.9}$$

The remaining nontrivial term of the equation (4.4) is the derivative with respect to χ_1. To evaluate the term of the derivative with respect to χ_1 in Eq. (4.4), we use the following relations (see, for example [100]); for $K < 0$,

$$\cosh(\sqrt{-K}\chi) = \cosh(\sqrt{-K}\chi_1)\cosh(\sqrt{-K}\chi_2) - \sinh(\sqrt{-K}\chi_1)\sinh(\sqrt{-K}\chi_2)\cos\gamma; \tag{4.10}$$

for $K = 0$,

$$\chi^2 = \chi_1^2 + \chi_2^2 - 2\chi_1\chi_2 \cos\gamma; \tag{4.11}$$

for $K > 0$,

$$\cos(\sqrt{K}\chi) = \cos(\sqrt{K}\chi_1)\cos(\sqrt{K}\chi_2) + \sin(\sqrt{K}\chi_1)\sin(\sqrt{K}\chi_2)\cos\gamma. \tag{4.12}$$

Furthermore, the following relations hold

$$\cos\gamma_1 = \frac{\partial\chi}{\partial\chi_1} \qquad \text{and} \qquad \cos\gamma_2 = \frac{\partial\chi}{\partial\chi_2}, \tag{4.13}$$

where γ_1 (γ_2) is defined as an angle between the geodesics of χ_1 (χ_2) and χ (see fig. 4.1). By differentiating Eqs. (4.10)–(4.12) with respect to χ_1 with χ_2 and γ fixed, we obtain $\partial\chi/\partial\chi_1$ and $\partial^2\chi/\partial\chi_1^2$. Then, by using these results, we obtain

$$\frac{\partial^2 j_0(k\chi)}{\partial\chi_1^2} = -\frac{k^2}{3}j_0(k\chi) + \frac{k^2}{3}(3\cos^2\gamma_1 - 1)j_2(k\chi). \tag{4.14}$$

By using Eqs. (4.4), (4.5), (4.9) and (4.14), we finally obtain

$$\begin{aligned}\xi(t,\chi,\chi_1,\chi_2) &= \epsilon^2\xi_{(0)}(t,\chi) \\ &+ \kappa\epsilon^2\left[A(t,\chi_1,\chi_2)\xi_{(0)}(t,\chi) + B(t,\chi,\chi_1,\chi_2)\xi_{(2)}(t,\chi)\right] + \mathcal{O}(\kappa^2\epsilon^2),\end{aligned} \tag{4.15}$$

where $\xi_{(l)}$ is defined by

$$\xi_{(l)}(t,\chi) := \int_0^\infty \frac{dk}{2\pi^2}k^2 j_l(k\chi)P^{(1)}(t,k), \tag{4.16}$$

and, by using the Legendre polynomial of degree two, $P_2(z)$,

$$\begin{aligned}A(t,\chi_1,\chi_2) &:= T_1(t)\left[\Delta^{\rm i}(\chi_1) + \Delta^{\rm i}(\chi_2)\right] \\ &\quad -\frac{4}{3}T_2(t)\left[\psi_{||}^{\rm i}(\chi_1) + 2\psi_{\perp}^{\rm i}(\chi_1) + \psi_{||}^{\rm i}(\chi_2) + 2\psi_{\perp}^{\rm i}(\chi_2)\right], \\ B(t,\chi,\chi_1,\chi_2) &:= \frac{8}{3}T_2(t)\Big[P_2(\cos\gamma_1)\left\{\psi_{||}^{\rm i}(\chi_1) - \psi_{\perp}^{\rm i}(\chi_1)\right\} \\ &\quad +P_2(\cos\gamma_2)\left\{\psi_{||}^{\rm i}(\chi_2) - \psi_{\perp}^{\rm i}(\chi_2)\right\}\Big].\end{aligned}$$

Here, we note that $\gamma_{1,2}$ in the above equation can be represented by χ_1, χ_2 and χ (see Eqs. (4.10)–(4.12)).

4.1.2 The distant observer approximation and the long wavelength approximation

So far, we have only assumed $0 < \kappa \ll 1$ and $\partial_\chi \gg \sqrt{|K|}$. The spatial curvature K and the cosmological constant Λ have not been ignored, and further any specific spatial configurations for the isotropic perturbations have not been assumed yet. Therefore, the equation (4.15) can be used to wide class of inhomogeneous and isotropic universes.

To clarify the behavior of the two-point correlation function (4.15) in the model of huge void universe, we focus on the following situation. We consider two-point correlations whose comoving separation χ is much smaller than the comoving scale of the void $L_{\rm void}$, called the long wavelength approximation, and is much smaller than the comoving distance from the central observer to these points, χ_1 and χ_2, called the distant observer approximation. By the first assumption, $\chi \ll L_{\rm void}$, we have

$$\begin{aligned}\Delta^{(1)}(t,\chi_2) &= \Delta^{(1)}(t,\chi_1) + \sum_{n=1}\frac{1}{n!}(\chi_2-\chi_1)^n \left.\frac{\partial^n \Delta^{(1)}(t,y)}{\partial y^n}\right|_{y=\chi_1} \\ &= \left[1+\mathcal{O}\left(\frac{\chi}{L^{\rm void}}\right)\right]\Delta^{(1)}(t,\chi_1), \end{aligned} \tag{4.17}$$

where we have used $\chi \le |\chi_1-\chi_2|$ for the second equality. The similar relations as the above also hold for $\psi^{(1)}_{||}$ and $\psi^{(1)}_{\perp}$. Then, by the second assumption, $\chi \ll \chi_{1,2}$, the angle γ_2 can be approximated as $\gamma_2 \simeq \pi - \gamma_1$. By these two assumptions, the two-point correlation function (4.15) is reduced to

$$\begin{aligned}&\xi(t,\chi,\chi_1,\chi_2) \simeq \xi_{\rm ap}(t,\chi,\chi_1,\gamma_1) \\ &:= \epsilon^2\xi_{(0)}(t,\chi) + \kappa\epsilon^2\left[a(t,\chi_1)\xi_{(0)}(t,\chi) + b(t,\chi_1,\gamma_1)\xi_{(2)}(t,\chi)\right], \end{aligned} \tag{4.18}$$

where

$$\begin{aligned} a(t,\chi_1) &:= 2T_1(t)\Delta^{\rm i}(\chi_1) - \frac{8}{3}T_2(t)\left(\psi^{\rm i}_{||}(\chi_1) + 2\psi^{\rm i}_{\perp}(\chi_1)\right), \\ b(t,\chi_1,\gamma_1) &:= \frac{16}{3}T_2(t)P_2(\cos\gamma_1)\left[\psi^{\rm i}_{||}(\chi_1) - \psi^{\rm i}_{\perp}(\chi_1)\right]. \end{aligned}$$

In the the above equations, the χ_1-dependence implies the inhomogeneity of the two-point correlation function, which comes from the spherical perturbations, $\Delta^{(1)}, \psi^{(1)}_{||}$ and $\psi^{(1)}_{\perp}$. We can also see that the γ_1-dependence of $b(t,\chi_1,\gamma_1)$ corresponds to the distortions of the correlation, which results from the local anisotropy of the volume expansion rate at $\chi_1 \neq 0$, that is, $\psi^{(1)}_{||} - \psi^{(1)}_{\perp} \neq 0$. We would like to stress that the

local-FLRW approximation never predicts the existence of a term that represents the γ_1-dependence of the two-point correlation function. Since the function $T_2(t)$ is the growth factor of the second-order perturbations, the distortion of the correlation becomes important at late time.

By investigating the difference between its value of $\gamma_1 = \pi$ and of $\gamma_1 = \pi/2$, we can see whether distortion of the two-point correlation function exists. Here, it should be noted that if we take the distance up to the order κ, the comoving distance χ does not mean the same proper distance for $\gamma_1 = \pi$ and $\gamma_1 = \pi/2$. By taking this fact into account, we define the following quantity

$$\Pi(t, \chi_{\rm p}, \chi_1) := \xi_{\rm ap}\left(t, \chi_\perp, \chi_1, \pi/2\right) - \xi_{\rm ap}\left(t, \chi_{||}, \chi_1, \pi\right), \tag{4.19}$$

where $\chi_{||}$ and $\chi_\perp$ are related to the proper distance $\chi_{\rm p}$ as

$$\chi_{||} = \chi_{\rm p}\left[1 - \frac{\kappa}{2}\ell_{||}(t, \chi_1)\right] \quad \text{and} \quad \chi_\perp = \chi_{\rm p}\left[1 - \frac{\kappa}{2}\ell_\perp(t, \chi_1)\right]. \tag{4.20}$$

Substituting Eq. (4.18) into Eq. (4.19), we have

$$\begin{aligned}\Pi(t, \chi_{\rm p}, \chi_1) \;\simeq\; & \kappa\epsilon^2\left[\frac{\chi_{\rm p}}{2}\left\{\ell_{||}(t, \chi_1) - \ell_\perp(t, \chi_1)\right\}\left.\frac{\partial\xi_{(0)}(t, \chi)}{\partial\chi}\right|_{\chi=\chi_{\rm p}}\right. \\ & + \left. 8T_2(t)\left\{\psi^{\rm i}_\perp(\chi_1) - \psi^{\rm i}_{||}(\chi_1)\right\}\xi_{(2)}(t, \chi_{\rm p})\right].\end{aligned} \tag{4.21}$$

The quantity Π is a measure of the distortion of the two-point correlation function at each point.

4.1.3 Distortions of the two-point correlation functions

We investigate the distortion of the two-point correlation function ξ in a specific model of the void universe. We assume that this model approaches to the Einstein-de Sitter universe model in the spatial asymptotic region with the dimensionless Hubble parameter $h := H_0/100{\rm kms}^{-1}{\rm Mpc}^{-1} = 0.7$. In the perturbative treatment, the inhomogeneity of the void model is described by the isotropic perturbations of the order κ on the Einstein-de Sitter universe. Since we consider the void model which can be approximated by the homogeneous and isotropic universe at early stage, we neglect the decaying mode for the perturbations of the order κ. We fix the gauge degree of freedom to rescale the radial coordinate as $\ell^{(1)}_\perp(t_0, \chi) = 0$, where t_0 is present time. Then the isotropic perturbations are completely determined by the growing mode $\Delta^+(\chi)$, where the density contrast defined in Eq. (3.25) is given by

$$\Delta^{(1)}(t, \chi) = \frac{D^+(t)}{D^+(t_0)}\Delta^+(\chi). \tag{4.22}$$

We presented calculations to determine other perturbations, $\ell_{||}^{(1)}$ and $\ell_{\perp}^{(1)}$, from Δ^{+} in § 3.2. We set the function Δ^{+} as

$$\Delta^{+}(\chi_1) \;=\; -0.3 \times \frac{1-\tanh\left[(\chi_1-0.1)/\beta\right]}{1+\tanh\left[0.1/\beta\right]}, \tag{4.23}$$

where β is a parameter that determines the size of void. We set the amplitude of the isotropic density perturbation to be about 0.3 at present time. Since all inhomogeneities are assumed to be composed of the growing modes, they decrease with going back to the past. This fact implies that the amplitude of the isotropic density contrast is always less than 0.3 until the present time $t = t_0$, and therefore the linear approximation for the isotropic inhomogeneities will be valid at least in qualitative sense in our model. We show the density contrast at present time,

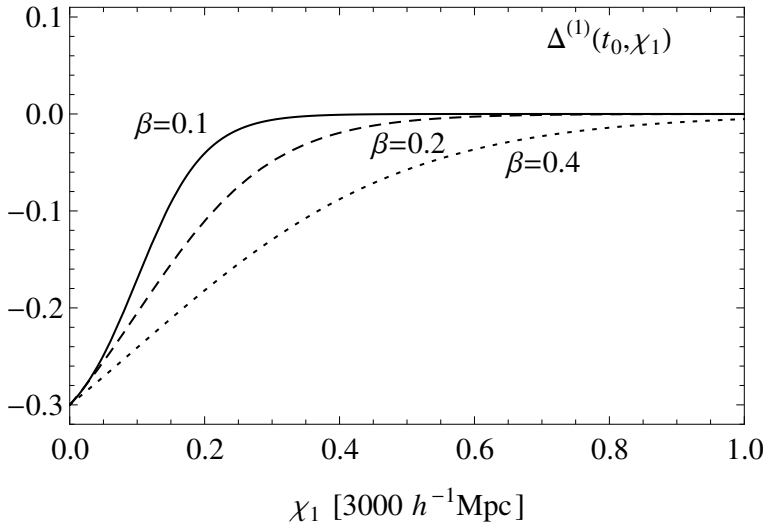

Figure 4.3: The density contrast $\Delta^{(1)}$ at present time as a function of χ_1 for three cases, $\beta = 0.1,\ 0.2$ and 0.4.

$\Delta^{(1)}(t_0, \chi_1)$, for three cases, $\beta = 0.1,\ 0.2$ and 0.4, as functions of χ_1 in Fig. 4.3 . We can see from this figure that the size of the void is about $750h^{-1}$Mpc for $\beta = 0.1$, $1500h^{-1}$Mpc for $\beta = 0.2$ and $3000h^{-1}$Mpc for $\beta = 0.4$, respectively.

Then, we depict the quantity Π defined in Eq. (4.21) at the present time $t = t_0$ as a function of χ_1 for three cases, $\beta = 0.1,\ 0.2$ and 0.4 in Fig. 4.4. Here, we have chosen the proper distance $\chi_{\rm p}$ between two points to be equal to $100h^{-1}$ Mpc, and we have used the fitting formula for the power spectrum $P^{(1)}(t, k)$ given in Eq. (4.6). We can see from Fig. 4.4 that the maximum of Π is located near the edge of the void. It is worth to notice that the magnitude of the two-point correlation function of the order ϵ^2 is $\xi_{(0)}(t_0, 100h^{-1}\text{Mpc}) \simeq -1.2 \times 10^{-4}$. Then, we can also see from Fig. 4.4 that the

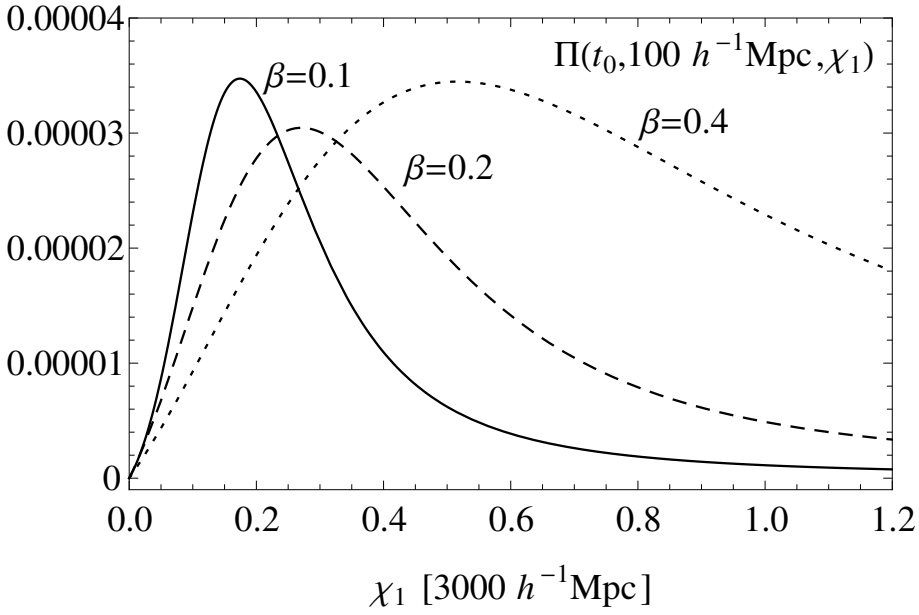

Figure 4.4: The quantity Π which represents the distortions of the two-point correlation function for $\chi_{\rm p} = 100h^{-1}$ Mpc at the present time $t = t_0$ as a function of χ_1 for cases, $\beta = 0.1,\ 0.2$ and 0.4.

function Π is about quarter of the leading order term of the two-point correlation function. So, we conclude that the distortion of the two-point correlation function is important in observationally studying the growth of the large-scale structure in a large void universe.

4.2 Redshift Space Distortions in LTB cosmological model

The distribution of galaxies is observed not in the real space but in the redshift space. Although we do not compare our results with observational data, we discuss the two-point correlation function in the redshift space and the significance of effects of the void inhomogeneity on it.

4.2.1 Effects of the real space distortions

Before studying the two-point correlation function in redshift space in the large void universe, we briefly review that in the homogeneous and isotropic model. In this case, it is known that the two-point correlation function of the density perturbations

in the redshift space is anisotropic due to the peculiar velocity field as follows [102] (see e.g. Ref. [103] for its derivation)

$$\xi^{(\mathrm{s})}(z_1,\chi,\mu) = \left(1+\frac{2}{3}f(t(z_1))+\frac{1}{5}f^2(t(z_1))\right)P_0(\mu)\xi_{(0)}\left(t(z_1),\chi\right) - \left(\frac{4}{3}f(t(z_1))+\frac{4}{7}f^2(t(z_1))\right)P_2(\mu)\xi_{(2)}\left(t(z_1),\chi\right) + \frac{8}{35}f^2(t(z_1))P_4(\mu)\xi_{(4)}\left(t(z_1),\chi\right), \tag{4.24}$$

where χ and z_1 are the comoving separation of the two points and the redshift of one of them, $f(t)$ is the growth rate of the density perturbations defined by $f(t) := d(\ln D^+(t))/d(\ln a(t))$, and $t(z_1)$ is given by

$$t(z_1) = \int_{z_1}^{\infty}\frac{dz}{(1+z)H}. \tag{4.25}$$

The redshift space distortion, namely, μ-dependence of the two-point correlation function of galaxies in the redshift space is used to estimate the growth rate $f(t)$ [104, 105]. In the homogeneous and isotropic universe, the two-point correlation function in the real space does not have the μ-dependence, and hence we can find out the growth rate $f(t)$ from the μ-dependence of the two-point correlation function of galaxies in the redshift space through Eq. (4.24) without the systematic error caused by the bias effect.

Next let us consider the case of large void universe. If there is non-Copernican inhomogeneities, as explicitly shown in Eq. (4.18), the real space correlation function has its own μ-dependence and may mislead us in determining the growth rate from the two-point correlation function in the redshift space. In general, perturbations change the propagation of photons. This fact implies that the perturbations change the mapping from the real space to the redshift space and thus the mapping between the density in the real space and that in the redshift space. Thus, to obtain the density perturbation of the order $\kappa\epsilon$ in the redshift space, we need to compute the photon propagation up to the order $\kappa\epsilon$. This is non-trivial task, and we left it for a future work. As a first step, in order to infer how significant the non-linear effects of non-Copernican inhomogeneities on the two-point correlation function in the redshift space is, we compare the quadrupole anisotropy in the two-point correlation function in the real space of the large void universe (4.18) with that in the redshift space of the homogeneous and isotropic model (4.24). The ratio α of quadrupole component in Eq. (4.18) to that in Eq. (4.24) is given in the following form,

$$\alpha(z) := \frac{\tilde{B}\left(t(z),\chi_1(z)\right)}{-\frac{4}{3}f(t(z))-\frac{4}{7}f^2(t(z))}, \tag{4.26}$$

where

$$\chi_1(z) = \int_0^z \frac{dz}{H}. \tag{4.27}$$

The ratio α in three cases $\beta = 0.1,\ 0.2$ and 0.4 is depicted as a function of the redshift in Fig. 4.5. From Fig. 4.5, we can see that the maximum of α is about 0.02 around $z = 0.2$, and this means that the error from the void structure given in Eq. (4.23) is $\mathcal{O}(0.01)$ in determining the growth rate of the density perturbation.

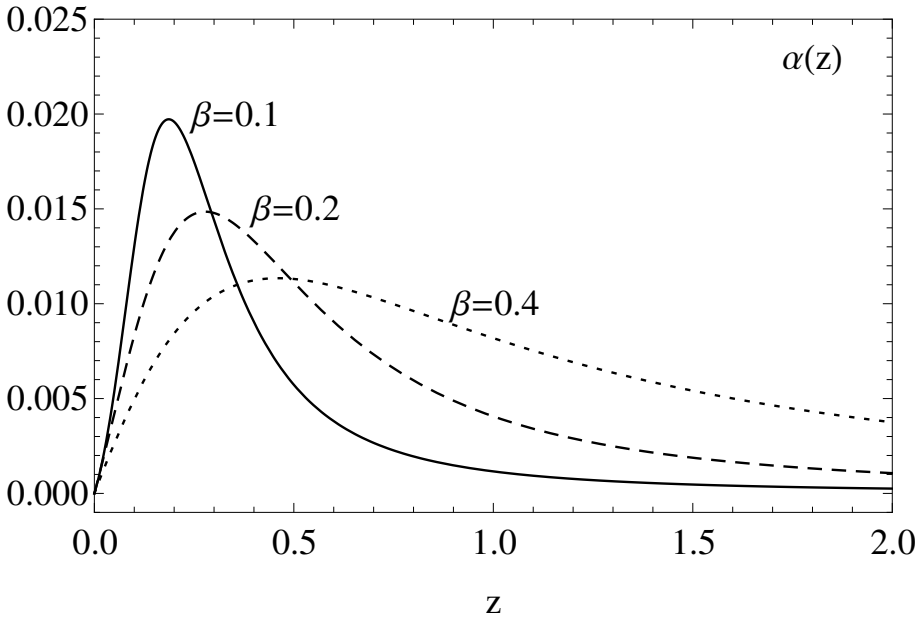

Figure 4.5: The ratio α of the quadrupole component in Eq. (4.18) to that in Eq. (4.24) as a function of the redshift.

4.2.2 Effects of the peculiar velocity fields

In the previous subsection, we neglected mapping effects for the density perturbations from the real space to the redshift space. Although we leave an estimation of mapping effects of the order $\kappa\epsilon$ for a future work, we consider mapping effects of the order ϵ by applying Newtonian approximation. It is known that only the peculiar velocity is needed when we study mapping effects in the Newtonian approximation. Thus, we only consider effects of the peculiar velocity fields of the order ϵ for simplicity.

The redshift in the perturbed universe model given in Eqs. (3.31) and (3.32) can be described as

$$1 + z \;=\; (1 + \bar{z}) \left(1 + \kappa\Delta_z^{(1)} + \epsilon\delta_z^{(1)} \;+ \mathcal{O}(\kappa^2, \kappa\epsilon, \epsilon^2)\right), \tag{4.28}$$

where $\bar{z}$ is the redshift in the homogeneous and isotropic universe model and defined as $1+\bar{z} := 1/a$, and $\Delta_z^{(1)}$ and $\delta_z^{(1)}$ are the fluctuations of the redshift produced by the perturbations and given by

$$\Delta_z^{(1)} = -\frac{1}{2}\int_{t_0}^{t} dt \dot{\ell}_{||}^{(1)}(t,\chi), \quad \delta_z^{(1)} = -\frac{1}{2}\int_{t_0}^{t} dt \left(K\dot{\Phi}^{(1)}(t,\mathbf{x}) + \partial_\chi^2 \dot{\Phi}^{(1)}(t,\mathbf{x}) \right), \quad (4.29)$$

where $\ell_{||}^{(1)}$ and $\Phi^{(1)}$ are the metric perturbations defined in Eqs. (3.19) and (3.33). Hereafter, we assume that the wavelength λ of the anisotropic perturbations of the order ϵ is much smaller than the scale of the spatial curvature K and the horizon H, and apply the Newtonian approximation for $\delta_z^{(1)}$ as

$$\delta_z^{(1)} \simeq \frac{a(t)}{2}\partial_\chi \dot{\Phi}^{(1)}(t,\chi,\theta,\varphi) - \frac{a(t_0)}{2}\partial_\chi \dot{\Phi}^{(1)}(t_0,0,0,0). \quad (4.30)$$

Here, we should note that the terms of the right hand side in Eq. (4.30) correspond to the peculiar velocities. In fact, the terms are related to the radial component of the 3-velocity in the Newtonian gauge, $v_{\rm N}^i$, as $v_{\rm N}^\chi = \partial_\chi \dot{\Phi}^{(1)}/2$. By setting the peculiar velocity at the center is zero, $v_{\rm N}^\chi(t_0,0,0,0) = 0$, and substituting Eq. (4.30) into Eq. (4.28), we obtain

$$1+z \simeq (1+\bar{z})\left(1 + \kappa\Delta_z^{(1)}(t,\chi) + \epsilon\frac{a(t)}{2}\partial_\chi\dot{\Phi}^{(1)}(t,\chi,\theta,\varphi)\right), \quad (4.31)$$

where we neglected the nonlinear terms of the order κ^2, $\kappa\epsilon$ and ϵ^2.

We have used (χ,θ,φ) as the spatial coordinate in the real space. The radial coordinate is related to the redshift of the background universe as

$$\chi = \int_0^{\bar{z}} \frac{dz'}{H(z')}. \quad (4.32)$$

Since we do not observe the redshift $\bar{z}$ in the background universe, we cannot specify the radial position of the galaxies. Then, we define the radial coordinate in the redshift space from the observed redshift z as

$$\chi_{\rm s} := \int_0^{z} \frac{dz'}{H(z')}. \quad (4.33)$$

By using Eqs. (4.31), (4.32) and (4.33), we obtain the relation of the radial coordinates in the real space and the redshift space as

$$\chi_{\rm s} \simeq \chi + \kappa\frac{\Delta_z^{(1)}}{aH} + \epsilon\frac{\partial_\chi\dot{\Phi}^{(1)}}{2H}. \quad (4.34)$$

The number density of galaxies in the redshift space $n^{(\rm s)}$ is related to that in the real space $n^{(\rm r)}$ by the number conservation as

$$n^{(\rm s)}(\chi_{\rm s},\theta,\varphi)\chi_{\rm s}^2 d\chi_{\rm s}\sin\theta d\theta d\varphi = n^{(\rm r)}(\chi,\theta,\varphi)\chi^2 d\chi\sin\theta d\theta d\varphi. \quad (4.35)$$

By using Eqs. (4.34) and (4.35), we obtain the number density in the redshift space as

$$n^{(\mathrm{s})} = \left(\frac{\chi_s^2}{\chi^2}\frac{\partial\chi_\mathrm{s}}{\partial\chi}\right)^{-1} n^{(\mathrm{r})} \simeq \left(1-\kappa\Delta_n^{(1)} - \epsilon\frac{\partial_\chi^2\dot{\Phi}^{(1)}}{2H}\right) n^{(\mathrm{r})}, \tag{4.36}$$

where in the second equality we assumed λ is much smaller than the radial distance from the central observer to the galaxies ($\lambda \ll \chi$), and $\Delta_n^{(1)}$ is defined as

$$\Delta_n^{(1)} := \left(\frac{\partial}{\partial\chi} + \frac{2}{\chi}\right)\frac{\Delta_z^{(1)}}{aH}. \tag{4.37}$$

We take an average of the number density over the volume of the galaxy survey V whose size is much larger than λ and much smaller than L^{void}, and obtain

$$\langle n^{(\mathrm{s})}\rangle_\mathrm{V} \simeq \langle n^{(\mathrm{r})}\rangle_\mathrm{V}\left(1-\kappa\langle\Delta_n^{(1)}\rangle_V\right). \tag{4.38}$$

By using Eqs. (4.36) and (4.38), we obtain the number density fluctuation in the redshift space as

$$\delta^{(\mathrm{s})} := \frac{n^{(\mathrm{s})} - \langle n^{(\mathrm{s})}\rangle_\mathrm{V}}{\langle n^{(\mathrm{s})}\rangle_\mathrm{V}} \simeq \delta^{(\mathrm{r})} - \frac{\epsilon}{2H}\partial_\chi^2\dot{\Phi}^{(1)}, \tag{4.39}$$

where $\delta^{(\mathrm{r})} := (n^{(\mathrm{r})} - \langle n^{(\mathrm{r})}\rangle_\mathrm{V})/\langle n^{(\mathrm{r})}\rangle_\mathrm{V}$, and in the second equality we used the approximation $\langle\Delta_n^{(1)}\rangle_\mathrm{V} \simeq \Delta_n^{(1)}$ because we assumed $V^{1/3} \ll L^{\mathrm{void}}$. The number density fluctuation $\delta^{(\mathrm{r})}$ is related to the energy density perturbation δ which was defined in section as $\delta^{(\mathrm{r})} = b\delta$, where b is the bias parameter. By assuming $b = 1$ and using the equations in section, $\delta^{(\mathrm{s})}$ is written as

$$\delta^{(\mathrm{s})} \simeq \epsilon\left[1 + f\frac{\partial_\chi^2}{\hat{\Delta}}\right]\delta^{(1)} + \kappa\epsilon\,\delta^{(2)}, \tag{4.40}$$

where $\hat{\Delta}$ is defined as $\hat{\Delta} := \mathcal{D}^i\mathcal{D}_i$, and f is the growth rate of the linear perturbation which is defined as $f := d(\ln D^+)/d(\ln a)$.

Then, we define the two-point correlation function of the density perturbation in the redshift space as

$$\xi^{(\mathrm{s})} := \langle\delta^{(\mathrm{s})}(t,\mathbf{x}_1)\delta^{(\mathrm{s})}(t,\mathbf{x}_2)\rangle. \tag{4.41}$$

By using the equations in section and applying the distant observer approximation, we finally obtain the correlation function as

$$\xi^{(\mathrm{s})}(t,\chi,\mu,\chi_1) \simeq \epsilon^2\xi^{(1,\mathrm{s})}(t,\chi,\mu) + 2\kappa\epsilon^2\xi^{(2,\mathrm{s})}(t,\chi,\mu,\chi_1), \tag{4.42}$$

where $\xi^{(1,s)}$ and $\xi^{(2,s)}$ are defined as

$$\begin{aligned}\xi^{(1,\mathrm{s})}(t,\chi,\mu) &:= \left(1+\frac{2}{3}f(t)+\frac{1}{5}f^2(t)\right)P_0(\mu)\xi_{(0)}(t,\chi)\\ &- \left(\frac{4}{3}f(t)+\frac{4}{7}f^2(t)\right)P_2(\mu)\xi_{(2)}(t,\chi)\\ &+ \frac{8}{35}f^2(t)P_4(\mu)\xi_{(4)}(t,\chi),\end{aligned} \tag{4.43}$$

and

$$\begin{aligned}\xi^{(2,\mathrm{s})}(t,\chi,\mu,\chi_1) &:= \left[\left(\tilde{a}(t,\chi_1)+\frac{1}{3}\tilde{b}(t,\chi_1)\right)+f(t)\left(\frac{1}{3}\tilde{a}(t,\chi_1)+\frac{1}{5}\tilde{b}(t,\chi_1)\right)\right]\\ &\times P_0(\mu)\xi_{(0)}(t,\chi)\\ &- \left[\frac{2}{3}\tilde{b}(t,\chi_1)+f(t)\left(\frac{2}{3}\tilde{a}(t,\chi_1)+\frac{4}{7}\tilde{b}(t,\chi_1)\right)\right]P_2(\mu)\xi_{(2)}(t,\chi)\\ &+ \frac{8}{35}f(t)\tilde{b}(t,\chi_1)P_4(\mu)\xi_{(4)}(t,\chi),\end{aligned} \tag{4.44}$$

where P_ℓ are the Legendre polynomials, μ is defined as $\mu := \cos\gamma_1$ (see fig. 4.1), $\xi_{(\ell)}(t,\chi)$ was defined in Eq. (4.16), and we defined $\tilde{a}$ and $\tilde{b}$ as

$$\tilde{a}(t,\chi_1) := T_1(t)\Delta^{\mathrm{i}}(\chi_1) - 4T_2(t)\psi^{\mathrm{i}}_{\perp}(\chi_1),$$

$$\tilde{b}(t,\chi_1) := -4T_2(t)\left(\psi^{\mathrm{i}}_{||}(\chi_1)-\psi^{\mathrm{i}}_{\perp}(\chi_1)\right).$$

From Eq. (4.44), we can see that the isotropic perturbations $\tilde{a}$ and $\tilde{b}$ affect to the distortion, and these terms are proportional to P_0, P_2 and P_4. This means that the isotropic perturbations may mislead us in determining the growth rate by the observation as discussed in the previous subsection. Here, we note that the terms proportional to $f(t)$ in Eq. (4.44) are involved in mapping effects from the peculiar velocity field that we have not included in the previous subsection. Then, we estimate the order of the systematic error produced by the isotropic perturbations in measuring the growth rate $f(t)$. The growth rate is $\mathcal{O}(1)$ (in fact, $f(t)=1$ in the Einstein-de Sitter universe model), and $\tilde{a}$ and $\tilde{b}$ are expected to be $\mathcal{O}(0.1)$ in the case of a void model which we have studied. Thus, from Eq. (4.43) and (4.44), we can see the order of the systematic error becomes about 10% in determining the growth rate.

4.3 Growth of density perturbations in Clarkson-Regis model

In § 4.1 and § 4.2, we have focused on the distortion of two-point correlation functions in the LTB cosmological models. The radial dependence of two-point correlation functions in the LTB models is also important in revealing stochastic properties of fluctuations. In this section, by defining an angular power spectrum, we study the radial dependence of time evolution of density perturbations in a specific void model proposed by Clarkson and Regis which we reviewed in § 2.2.

4.3.1 Angular power spectrum and angular growth rate

The LTB cosmological models have the radial inhomogeneity for the central observer in general. As a result, the evolution of perturbations in such models depends on the radial coordinate as we have shown in Eq. (4.18). To study the radial dependence of the growth of density perturbations, we use an angular power spectrum which is the simplest quantity that we can currently calculate. We define the angular power spectrum of the density contrast by

$$C_\ell(t,r) = \frac{r^2}{2\ell+1}\sum_{m=-\ell}^{\ell}\langle \delta^*_{\ell m}(t,r)\delta_{\ell m}(t,r)\rangle, \tag{4.45}$$

where $*$ denotes the complex conjugate, and $\delta_{\ell m}$ is the coefficients of the spherical harmonic expansion. By using Eq. (3.44), we obtain

$$\begin{aligned}\delta_{\ell m}(t,r) &:= \epsilon\,\delta^{(1)}_{\ell m}(t,r) + \kappa\epsilon\Big[\left\{T_1(t)\Delta^{\rm i}(r) - 4T_2(t)\psi^{\rm i}_\perp(r)\right\}\delta^{(1)}_{\ell m}(t,r) \\ &+ 2T_2(t)\left\{\psi^{\rm i}_{||}(r) - \psi^{\rm i}_\perp(r)\right\}\left(K+\partial_r^2\right)\Phi^{(1)}_{\ell m}(t,r)\Big],\end{aligned} \tag{4.46}$$

where $\delta^{(1)}_{\ell m}(t,r)$ and $\Phi^{(1)}_{\ell m}(t,r)$ are the coefficients of the spherical harmonic expansion. By using Eqs. (4.45) and (4.46), we obtain

$$\begin{aligned}C_\ell(t,r) &= \epsilon^2\,K_1(t,r,\ell) + 2\kappa\epsilon^2\left[T_1(t)\Delta^{\rm i}(r) - 4T_2(t)\psi^{\rm i}_\perp(r)\right]K_1(t,r,\ell) \\ &+ 4\kappa\epsilon^2 T_2(t)\left[\psi^{\rm i}_{||}(r) - \psi^{\rm i}_\perp(r)\right]K_2(t,r,\ell),\end{aligned} \tag{4.47}$$

where we have defined K_1 and K_2 s

$$K_1(t,r,\ell) = \left(\frac{2}{\pi}\right)\int_0^\infty dk P^{(1)}(t,k)(kr)^2 j_\ell^2(kr),$$

$$K_2(t,r,\ell) \;=\; \left(\frac{2}{\pi}\right)\int_0^\infty dk P(k)(kr)^2 j_\ell(kr)\left(\partial_r^2 j_\ell(kr)\right)\left(\frac{2}{k^2}\right).$$

To investigate the growth rates of the perturbations, we define the angular growing factor by

$$D_\ell(t,r) = \left[\frac{C_\ell(t,r)}{C_\ell(t_{\rm i},r)}\right]^{1/2}. \tag{4.48}$$

It is easy to see that the angular growing factor $D_\ell(t,r)$ is equal to $D^+(t)/D^+(t_{\rm i})$ up to order ϵ. Then, using the angular growing factor, we define the angular growth rate on the past light cone $\Sigma_{\rm lc}$ as a function of redshift z as follows:

$$f_\ell(z) = -\frac{d[\ln D_\ell(t_{\rm lc}(z), r_{\rm lc}(z))]}{d\ln(1+z)}. \tag{4.49}$$

Here, we note that the angular growing factor and the angular growth rate do not depend on the amplitude A_0. We also note that the angular growth rate up to order ϵ agrees with the growth rate usually used in the linear perturbation theory of the FLRW universe, $d(\ln D^+)/d(\ln a)$.

4.3.2 Radial dependence of the growth rate

Let us consider the evolution of the anisotropic density contrasts in the CR model introduced in § 2.2. By using the angular power spectrum $C_\ell(t,r)$ given by Eq. (4.47) and the power spectrum $P^{(1)}(t,k)$, we depict the angular growing factors $D_\ell(t,r)$'s defined by Eq. (4.48) at each comoving distance as functions of t in Fig. 4.6. Here, we introduced a useful quantity defined by

$$\tilde{k} := \frac{\ell}{r}\,. \tag{4.50}$$

Note that $\tilde{k}$ is equal to the comoving wave number of the mode ℓ at a distance r in the flat sky approximation (see e.g., Ref. [106]). In Fig. 4.6, the present time is $H_0 t_0 = 0.83$, and ℓ is chosen so that $\tilde{k} = 0.5{\rm Mpc}^{-1}$. This choice of ℓ shows us the evolution of perturbations with the size of a cluster of galaxies, i.e., $2\pi/\tilde{k} \sim 10{\rm Mpc}$. We can see from Fig. 4.6 that the larger the comoving distance of a perturbation from the symmetry center, the faster the growth of the perturbation. This result may be explained by the fact that the energy density of the CR model is a monotonically increasing function of r, since the growth rates of perturbations in the FLRW universe is a monotonically increasing function of $\Omega_{\rm M}$.

We also depict D_ℓ of the FLRW universe models with $\Omega_{\rm M} = 0.242$ and 0.7, respectively, together with that of the CR model in Fig. 4.7. We can see from this

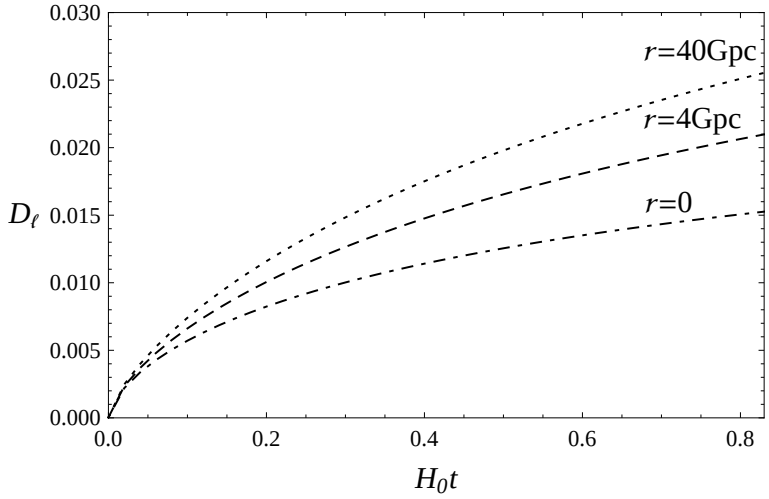

Figure 4.6: Angular growing factors D_ℓ's in the CR model at $r = 40$Gpc (dotted line), $r = 4$Gpc (dashed line) and $r = 0$ (dot-dashed line) depicted as functions of t. The present time is $H_0 t_0 = 0.83$. We choose ℓ so that $\tilde{k} = 0.5\text{Mpc}^{-1}$.

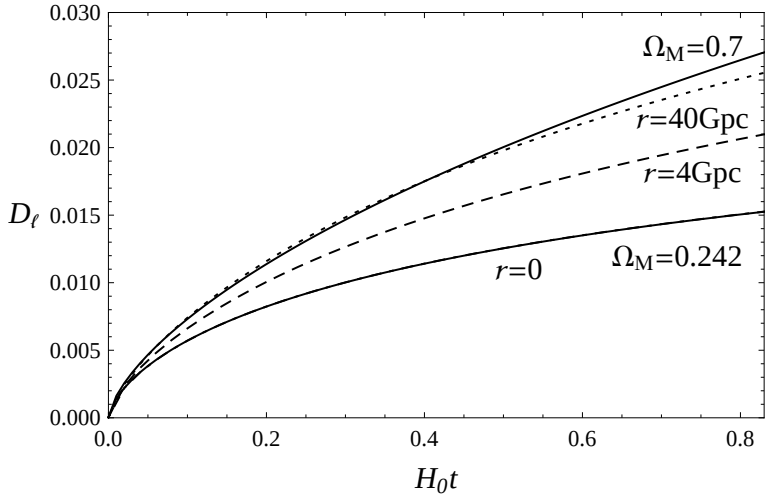

Figure 4.7: Angular growing factors D_ℓ's in the dust filled FLRW universe models with $\Omega_\text{M} = 0.242$ and $\Omega_\text{M} = 0.7$, together with that for the CR model.

figure that D_ℓ of the FLRW universe with $\Omega_{\rm M} = 0.242$ agrees with $D_\ell(t, r = 0)$ of the CR model. We note that D_ℓ in the FLRW universe with $\Omega_{\rm M} = 0.7$ does not agree with that far from the void ($r = 40$Gpc) in the CR model. This result might not be real, but rather could be an error caused by using the linearized CR model, since the error due to the linear approximation becomes larger for larger r.

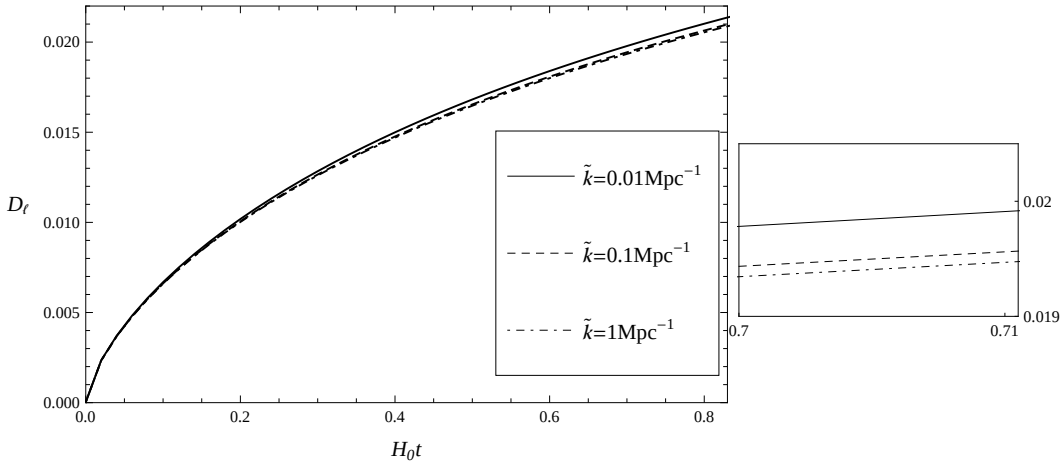

Figure 4.8: Angular growing factors $D_\ell(t, r = 4\text{Gpc})$ in the CR model for $\tilde{k} = 0.01\text{Mpc}^{-1}$ (solid line), 0.1Mpc^{-1} (dashed line) and 1Mpc^{-1} (dot-dashed line), depicted as functions of t. The right panel shows a close-up of the $0.7 < H_0t < 0.71$

.

Then, we have also investigated the dependence of D_ℓ on $\tilde{k}$. The angular growing factors $D_\ell(t, r = 4\text{Gpc})$'s with various values of ℓ, or equivalently, $\tilde{k}$ are depicted as functions of t in Fig. 4.8. We find that the dependence of $D_\ell(t, r = 4\text{Gpc})$ on $\tilde{k}$ is very small in the case of the CR model.

Next, the angular growth rate f_ℓ defined by (4.49) is plotted as a function of z for the CR model, together with those of the dust filled FLRW with $\Omega_{\rm M} = 0.242$ and $\Omega_{\rm M} = 0.7$ and the flat ΛCDM with $\Omega_{\rm M} = 0.28$ in Fig. 4.9. Lower panel shows a close-up of the region $0 < z < 1$ in. Here, ℓ is also chosen so that $\tilde{k} = 0.5\text{Mpc}^{-1}$. From Fig. 4.9, we can see that the value of f_ℓ of these models approach the value of the Einstein de-Sitter universe ($f_\ell = 1$) in the high redshift domain. We can see from Fig. 4.9 that f_ℓ at the central observer $z = 0$ of the CR model agrees with the value of the dust filled FLRW universe with $\Omega_{\rm M} = 0.242$. We can also see that f_ℓ in the CR model is significantly different from those in homogeneous and isotropic universes for redshift $0 < z \lesssim 1$.

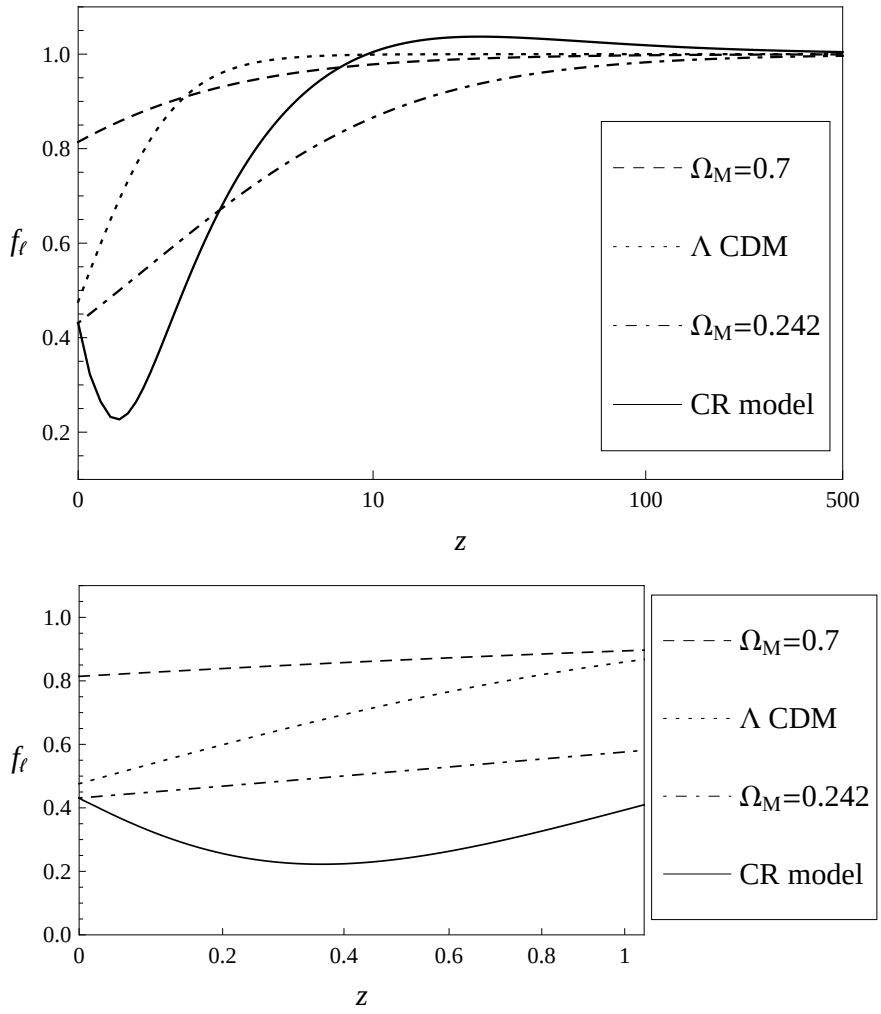

Figure 4.9: Upper panel: Angular growth rate f_ℓ in the CR model (solid line), together with those of the dust filled FLRW universe with $\Omega_{\rm M} = 0.242$ (dot-dashed line) and $\Omega_{\rm M} = 0.7$ (dashed line) and the flat ΛCDM universe with $\Omega_{\rm M} = 0.28$ (dotted line) as a function of z. ℓ is chosen so that $\tilde{k} = 0.5{\rm Mpc}^{-1}$. Lower panel: Close-up of the region $0 < z < 1$.

4.4 Conclusion and Discussion

We have studied stochastic properties of density perturbations in the LTB cosmological model, by applying the second-order perturbation theory in the homogeneous and isotropic universe which we developed in Chap 3. First of all, we have derived the general expression (4.15) for the two-point correlation function in a inhomogeneous and isotropic universe model in a form of the series expansion. Then, we have assumed the separation between two points which we take the correlation is much shorter than both the scale of the spherical inhomogeneity and the distance from the center. In these approximation, it can be explicitly shown that the two-point correlation function has the distortion as a result of the local anisotropy of the volume expansion rate. This result is very different from the prediction based on the so-called local-FLRW approximation in which sufficiently small region is assumed to be the same as the FLRW universe. Our result suggests that we should treat a large void universe model as a locally homogeneous and anisotropic universe model rather than a locally FLRW universe model. A local behavior of a huge void model will be discussed in more details in the next chapter.

We computed the distortion of the two-point correlation function for a specific model with the order of the spherical inhomogeneity being about 10%. In this model, the magnitudes of the distortions are not negligible compared to the leading order term in the real space two-point correlation function. We showed that the distortions of the correlation function in the real space contribute to the distortions in the redshift space. Hence, we may test the model of the huge void universe by the observations of the distortion of the two-point correlation function. In other words, the observational data of the two-point correlation function of galaxy distribution may contain a systematic error due to the non-Copernican inhomogeneity. In order to evaluate the net effect of the isotropic inhomogeneities on the redshift space distortion, we need to obtain the density perturbation in the redshift space of the order $\kappa\epsilon$ by computing the photon propagation up to the order $\kappa\epsilon$. This is not a trivial task and we left it for a future work.

In § 4.3, we calculated the angular growing factor using the linearized Clarkson-Regis (CR) model, which has the uniform big-bang time. From the behavior of the angular growing factor, we found that the speed of growth of a perturbation is a monotonically increasing function of the comoving distance from the center of the void. Because of this property, the angular growth rate in the CR model differs from that in the dust filled FLRW universe even for low redshift ($z < 1$). This result implies that, if we can somehow observe the angular growth rate f_ℓ, the observational data may give a strong constraint on non-Copernican universe models.

Chapter 5

Newtonian self-gravitating system in LTB cosmological model

Our universe has a well developed nonlinear structure which takes the form of galaxies, clusters and superclusters. In the standard cosmology, cosmic structure formation at subhorizon scales is commonly studied by using a Newtonian self-gravitating system in an expanding universe, where its system is governed by the equations of non-relativistic hydrodynamics and Newtonian gravitational theory for a fluid in the FLRW universe (see, for example [107]). The Newtonian equations have been solved by the cosmological N-body numerical simulation, and their results have been compared with observational results of galaxy clustering. The Newtonian equations have also been studied by some analytic approaches such as the linear approximation and the Zel'dovich approximation, and these analyses have helped us to understand the gravitational instability of the Newtonian system. However, there is no practical scheme to study Newtonian self-gravitating system in non-Copernican cosmological models. In this chapter, we propose an approximation scheme to study Newtonian self-gravitating system in the LTB cosmological models.

We consider a LTB cosmological model of a huge spherical void which is comparable to the horizon scale, and hence the curvature radius, $\mathcal{R}$, of the universe is about 1Gpc, $\mathcal{R} \sim 1$Gpc. Although LTB spacetime describing a huge void model is a relativistic and nonlinear solution of the Einstein equations, its gravitational field is weak in a sufficiently small spatial region compared to the scale of a void. In such a small region, we can approximate the metric of the LTB solution to a form of Minkowskian with small perturbations. We call the approximation a local approximation. To perform a local approximation, it is convenient to use Fermi-normal coordinates which cover a local spatial region at all times in the spacetime. Here, it should be noted that this approximation scheme is known as the tidal

approximation in the study of Newtonian self-gravitating system in the tidal field produced by relativistic structures such as Black Holes (see, for example [108]). A local approximation help us to construct Newtonian self-gravitating system in the LTB cosmological model.

To consider Newtonian self-gravitating system in the LTB model of a huge void, we assume the typical size of cosmic structures of our interest, $\ell_{\rm N}$, is much smaller than the curvature radius, $\ell_{\rm N} \ll \mathcal{R}$. We also assume the peculiar velocity of cosmic structures, $v_{\rm N}$, is much smaller than the speed of light $|v_{\rm N}| \ll c$, and the self-gravity of cosmic structures is weak. By these assumptions, we introduce two non-negative small expansion parameters as

$$\epsilon := \frac{|v_{\rm N}|}{c}, \quad \text{and} \quad \kappa := \left|\frac{\ell_{\rm N}}{\mathcal{R}}\right|. \tag{5.1}$$

Here, we note that the parameter κ is also used as an expansion parameter of a local approximation to the background LTB spacetime. By starting from the Einstein equations and by using these expansion parameters, we derive equations of non-relativistic hydrodynamics and Newtonian gravity for a fluid in the LTB cosmological model. This scheme is known as the Cosmological Post-Newtonian expansion in the study of FLRW cosmologies [109, 110, 111, 112], and thus our study can be regarded as a generalization of Cosmological Post-Newtonian expansion to the inhomogeneous cosmological models.

In § 5.1, after introducing the Fermi-normal coordinates, we apply a local approximation to the LTB cosmological model based on the Fermi-normal coordinate expansion. In § 5.2, we derive a set of equations governing Newtonian self-gravitating system in the LTB cosmological model by classifying a relation of the expansion parameters into three cases, $\epsilon > \kappa$, $\epsilon = \kappa$ and $\epsilon < \kappa$. In § 5.3, we solve the derived equations by using the linear approximation, and investigate the growth of linear vorticity fields and linear density perturbations. § 5.4 is devoted to conclusion and discussion of this chapter.

5.1 Local approximation to LTB cosmological model

5.1.1 Construction of Fermi-normal coordinates

Fermi-normal coordinates (see, for reviews [113, 114, 115, 116]) are local coordinates around a timelike geodesic[1]. We briefly review how to construct the Fermi-normal coordinate from an arbitrary coordinate, and how to compute the metric

[1]If we consider a non-geodesic worldline, the coordinates are referred to as Fermi-walker coordinates.

and stress-energy tensor of the Fermi-normal coordinate. Throughout this chapter, we represent the former coordinate as $x^{\mu'}$ and the Fermi-normal coordinate as x^{μ}.

Let γ be a timelike geodesic with a normal vector

$$u^{\mu'} = \frac{dx^{\mu'}}{d\tau}, \tag{5.2}$$

where τ denotes the proper time along γ. Then, we erect a parallel transported orthonormal tetrad $e^{\mu'}_{(\alpha)}$ on γ that satisfies

$$g_{\mu'\nu'} e^{\mu'}_{(\alpha)} e^{\nu'}_{(\beta)} = \eta_{\alpha\beta} \quad \text{and} \quad u^{\mu'} \nabla_{\mu'} e^{\nu'}_{(\alpha)} = 0, \tag{5.3}$$

where $\eta_{\alpha\beta}$ is defined as $\eta_{\alpha\beta} = (-1, 1, 1, 1)$, and we assume $e^{\mu'}_{(0)} = u^{\mu'}$. To construct the Fermi-normal coordinate of an event P neighborhood to γ, we locate an unique spacelike geodesic β that passes through P and intersects γ orthogonally, whose normal vector is given as

$$n^{\mu'} = \frac{dx^{\mu'}}{ds}, \tag{5.4}$$

where s denotes the proper length along β. We choose $s = 0$ at the point β intersects γ, and define a spatial vector Ω^i as

$$\Omega^i := n^{\mu'}\Big|_{s=0} e^{(i)}_{\mu'}, \tag{5.5}$$

where $e^{(i)}_{\mu'} := g_{\mu'\nu'} e^{\nu'}_{(i)}$ and Ω^i satisfies $\delta_{ij}\Omega^i\Omega^j = 1$. By using Eq. (5.5), the normal vector $n^{\mu'}$ at $s = 0$ can be written as

$$n^{\mu'}\Big|_{s=0} = \Omega^i e^{\mu'}_{(i)}. \tag{5.6}$$

By using the parameters τ, s and Ω^i, we define the Fermi normal coordinate as

$$t = \tau \quad \text{and} \quad x^i = s\ \Omega^i. \tag{5.7}$$

In order to relate the former coordinate $x^{\mu'}$ to the Fermi normal coordinate defined in Eq. (5.7), we solve the spacelike geodesics β order by order as follows. We start with the geodesic equation

$$\frac{d^2 x^{\mu'}}{ds^2} + \Gamma^{\mu'}_{\alpha'\beta'} \frac{dx^{\alpha'}}{ds} \frac{dx^{\beta'}}{ds} = 0. \tag{5.8}$$

Then, we expand $x^{\mu'}(s)$ and $\Gamma^{\mu'}_{\alpha'\beta'}(s)$ as

$$x^{\mu'}(s) = \sum_{N=0} \frac{s^N}{N!} \left(\frac{d}{ds^N} x^{\mu'} \right)\Big|_{s=0} =: \sum_{N=0} \frac{s^N}{N!} x^{\mu'}_{(N)}, \tag{5.9}$$

$$\Gamma^{\mu'}_{\alpha'\beta'}(s) = \sum_{N=0} \frac{s^N}{N!} \left(\frac{d}{ds^N} \Gamma^{\mu'}_{\alpha'\beta'} \right)\Big|_{s=0}. \tag{5.10}$$

From Eq. (5.6), we have

$$x^{\mu'}_{(1)} = \Omega^i e^{\mu'}_{(i)}. \tag{5.11}$$

By substituting Eqs. (5.9) and (5.10) into Eq. (5.8) and by using Eq. (5.11), we obtain $x^{\mu'}_{(2)}$ and $x^{\mu'}_{(3)}$ as

$$\begin{aligned} x^{\mu'}_{(2)} &= -\Gamma^{\mu'}_{\alpha'\beta'}\Big|_{s=0} e^{\alpha'}_{(i)} e^{\beta'}_{(j)} \Omega^i \Omega^j, & (5.12)\\ x^{\mu'}_{(3)} &= \left(2\,\Gamma^{\mu'}_{\alpha'\beta'}\Big|_{s=0}\,\Gamma^{\beta'}_{\gamma'\delta'}\Big|_{s=0} - \partial_{\delta'}\Gamma^{\mu'}_{\alpha'\gamma'}\Big|_{s=0}\right) e^{\alpha'}_{(i)} e^{\gamma'}_{(j)} e^{\delta'}_{(k)} \Omega^i\Omega^j\Omega^k. & (5.13) \end{aligned}$$

By substituting Eqs. (5.11)–(5.13) into Eq. (5.9) and by using Eq. (5.7), we obtain

$$\begin{aligned} x^{\mu'} &= x^{\mu'}_{(0)} + e^{\mu'}_{(i)} x^i - \frac{1}{2}\,\Gamma^{\mu'}_{\alpha'\beta'}\Big|_{s=0} e^{\alpha'}_{(i)} e^{\beta'}_{(j)} x^i x^j \\ &+ \frac{1}{6}\left(2\,\Gamma^{\mu'}_{\alpha'\beta'}\Big|_{s=0}\,\Gamma^{\beta'}_{\gamma'\delta'}\Big|_{s=0} - \partial_{\delta'}\Gamma^{\mu'}_{\alpha'\gamma'}\Big|_{s=0}\right) e^{\alpha'}_{(i)} e^{\gamma'}_{(j)} e^{\delta'}_{(k)} x^i x^j x^k \; + \mathcal{O}\left(x^i\right)^4. \end{aligned} \tag{5.14}$$

By differentiating Eq. (5.14) with respect to t, we obtain

$$\begin{aligned} \frac{\partial x^{\mu'}}{\partial t} &= \frac{\partial x^{\mu'}_{(0)}}{\partial t} + x^i \frac{\partial}{\partial t} e^{\mu'}_{(i)} - \frac{1}{2} x^i x^j \frac{\partial}{\partial t}\left(\Gamma^{\mu'}_{\alpha'\beta'}\Big|_{s=0} e^{\alpha'}_{(i)} e^{\beta'}_{(j)}\right) \; + \; \mathcal{O}(x^i)^3 \\ &= e^{\mu'}_{(0)} - \Gamma^{\mu'}_{\alpha'\beta'}\Big|_{s=0} e^{\alpha'}_{(0)} e^{\beta'}_{(j)} x^j + \left(\partial_{\delta'}\Gamma^{\mu'}_{\alpha'\beta'} - 2\Gamma^{\mu'}_{\alpha'\tau'}\Gamma^{\tau'}_{\delta'\beta'}\right)\Big|_{s=0} e^{\delta'}_{(0)} e^{\alpha'}_{(j)} e^{\beta'}_{(k)} x^j x^k \\ &\quad + \; \mathcal{O}(x^i)^3, \end{aligned} \tag{5.15}$$

where in the second equality we have used the relations

$$\frac{\partial}{\partial t} e^{\nu'}_{(j)} = -\Gamma^{\nu'}_{\alpha'\beta'}\Big|_{s=0} e^{\alpha'}_{(0)} e^{\beta'}_{(j)} \quad \text{and} \quad \frac{\partial}{\partial t}\,\Gamma^{\mu'}_{\alpha'\beta'}\Big|_{s=0} = e^{\delta'}_{(0)}\,\partial_{\delta'}\Gamma^{\mu'}_{\alpha'\beta'}\Big|_{s=0}. \tag{5.16}$$

By differentiating Eq. (5.14) with respect to x^i, we obtain

$$\begin{aligned} \frac{\partial x^{\mu'}}{\partial x^i} &= e^{\mu'}_{(i)} - \Gamma^{\mu'}_{\alpha'\beta'}\Big|_{s=0} e^{\alpha'}_{(i)} e^{\beta'}_{(j)} x^j \\ &+ \frac{1}{6}\left(4\Gamma^{\mu'}_{\alpha'\tau'}\Gamma^{\tau'}_{\delta'\beta'} + 2\Gamma^{\mu'}_{\delta'\tau'}\Gamma^{\tau'}_{\alpha'\beta'} - 2\partial_{\alpha'}\Gamma^{\mu'}_{\delta'\beta'} - \partial_{\delta'}\Gamma^{\mu'}_{\alpha'\beta'}\right)\Big|_{s=0} e^{\delta'}_{(i)} e^{\alpha'}_{(j)} e^{\beta'}_{(k)} x^j x^k \\ &+ \mathcal{O}(x^i)^3. \end{aligned} \tag{5.17}$$

Eqs. (5.15) and (5.17) give the coordinate transformation between the former coordinate $x^{\mu'}$ and the Fermi coordinate x^μ. Once we give the metric $g_{\mu'\nu'}$ and choose the tetrad $e^{\mu'}_{(\nu)}$ in the former coordinate, we can construct the Fermi normal coordinate by using the transformation (5.15) and (5.17).

5.1.2 Metric and stress-energy tensor in Fermi normal coordinates

We compute the metric and stress-energy tensor of dust $T^{\mu\nu} = \rho u^\mu u^\nu$ in Fermi normal coordinates by using the coordinate transformation (5.15) and (5.17). As an example for the computations, we derive the 4-velocity u_μ in the Fermi coordinate. Under the coordinate transformation, the u_μ transforms as

$$u_\mu = \frac{\partial x^{\nu'}}{\partial x^\mu} u_{\nu'}. \tag{5.18}$$

The $u_{\nu'}$ can be expanded around $s = 0$ as

$$u_{\nu'} = u_{\nu'}|_{s=0} + \partial_{\alpha'} u_{\nu'}|_{s=0}\, \delta x^{\alpha'} + \partial_{\alpha'}\partial_{\beta'} u_{\nu'}|_{s=0}\, \delta x^{\alpha'} \delta x^{\beta'} + \cdots, \tag{5.19}$$

where $\delta x^{\alpha'}$ is defined as $\delta x^{\alpha'} := x^{\alpha'} - x^{\alpha'}\big|_{s=0}$ and by using Eq. (5.14) is given as

$$\delta x^{\alpha'} = e^{\alpha'}_{(j)} x^j - \frac{1}{2}\Gamma^{\alpha'}_{\tau'\rho'} e^{\tau'}_{(j)} e^{\rho'}_{(k)} x^j x^k + \mathcal{O}(x^i)^3. \tag{5.20}$$

By substituting Eqs. (5.15), (5.17), (5.19) and (5.20) into Eq. (5.18), we obtain the u_μ in the Fermi coordinate as

$$u_\mu \;=\; u_{\alpha'}|_{s=0}\, e^{\alpha'}_{(\mu)} + \left(\partial_{\beta'} u_{\alpha'} - \Gamma^{\tau'}_{\alpha'\beta'} u_{\tau'}\right)\Big|_{s=0} e^{\alpha'}_{(\mu)} e^{\beta'}_{(j)} x^j + \mathcal{O}\left(x^i\right)^2. \tag{5.21}$$

The energy density ρ in the Fermi coordinate is given as

$$\begin{aligned} \rho(x^\mu) &= \rho(x^{\mu'})\Big|_{s=0} + \partial_{\alpha'}\rho(x^{\mu'})\Big|_{s=0} \delta x^{\alpha'} + \cdots \\ &= \rho(x^{\mu'})\Big|_{s=0} + \partial_{\alpha'}\rho(x^{\mu'})\Big|_{s=0} e^{\alpha'}_{(j)} x^j + \mathcal{O}(x^i)^2, \end{aligned} \tag{5.22}$$

where we have used Eq. (5.20) in the second equality.

As for the metric in the Fermi coordinate, after lengthy but straightforward calculations, we obtain

$$g_{00} = -1 - \hat{R}_{0i0j} x^i x^j + \mathcal{O}\left(x^i\right)^3, \tag{5.23a}$$

$$g_{0i} = -\frac{2}{3}\hat{R}_{0jik} x^j x^k + \mathcal{O}\left(x^i\right)^3, \tag{5.23b}$$

$$g_{ij} = \delta_{ij} - \frac{1}{3}\hat{R}_{ikjl} x^k x^l + \mathcal{O}\left(x^i\right)^3, \tag{5.23c}$$

where $\hat{R}_{\mu\nu\rho\sigma}$ is defined as

$$\hat{R}_{\mu\nu\rho\sigma}(t) \;:=\; e^{\alpha'}_{(\mu)} e^{\beta'}_{(\nu)} e^{\gamma'}_{(\rho)} e^{\delta'}_{(\sigma)} R_{\alpha'\beta'\gamma'\delta'}, \tag{5.24}$$

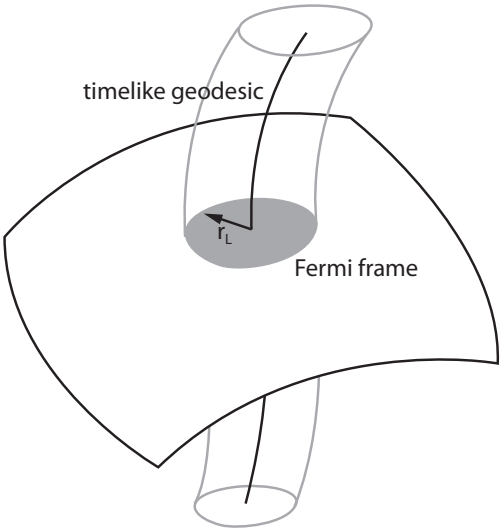

Figure 5.1: A local cylindrical region in the spacetime covered by the Fermi-normal coordinate (From Ref. [113]).

where $R_{\alpha'\beta'\gamma'\delta'}$ is the Riemann tensor of the prior metric. For later convenience, we define $h^{\rm B}_{\mu\nu}$ as

$$h^{\rm B}_{00} := -\hat{R}_{0i0j}x^i x^j, \quad h^{\rm B}_{0i} := -\frac{2}{3}\hat{R}_{0jik}x^j x^k, \quad h^{\rm B}_{ij} := -\frac{1}{3}\hat{R}_{ikjl}x^k x^l. \tag{5.25}$$

We represent the order of $h^{\rm B}_{\mu\nu}$ as

$$\mathcal{O}\left(h^{\rm B}_{\mu\nu}\right) = \mathcal{O}\left(\frac{|\mathbf{x}|}{\mathcal{R}}\right)^2 =: \kappa^2, \tag{5.26}$$

where $\mathcal{R}$ is the curvature radius of the spacetime we consider. Here, we have introduced a dimensionless parameter κ which was defined in Eq. (5.1). Although the definition of κ in Eq. (5.1) is different from that in Eq. (5.26), we will consider a situation $|\mathbf{x}| \sim \ell_{\rm N}$ in the next section. Then, we rewrite the metric in Eqs. (5.23a)–(5.23c) by using Eqs. (5.25) and (5.26) as

$$g_{\mu\nu} \;=\; \eta_{\mu\nu} + \kappa^2\, h^{\rm B}_{\mu\nu} + \mathcal{O}(\kappa^3). \tag{5.27}$$

As far as $\kappa \ll 1$, the Fermi-normal coordinate is admissible for all times. Fig. 5.1 shows a cylindrical region in the spacetime covered by the Fermi-normal coordinate.

5.1.3 LTB cosmological model in Fermi normal coordinates

We apply the Fermi-normal coordinate expansion to the LTB cosmological model. We consider the synchronous comoving coordinate as the prior coordinate $x^{\mu'}$. As

seen in Chap. 2, the line element and the stress-energy tensor of the LTB spacetime, in the synchronous comoving coordinate, are given by

$$ds^2 = -dt'^2 + \frac{(\partial_{r'} R(t', r'))^2}{1 - k(r')} dr'^2 + R^2(t', r') \left(d\theta'^2 + \sin^2 \theta' d\phi'^2 \right), \quad (5.28)$$

$$T^{\mu'\nu'} = \rho(t', r') u^{\mu'} u^{\nu'}, \quad (5.29)$$

where we denote the former coordinate as (t', r', θ', ϕ'). To construct the Fermi coordinate, we choose a worldline of a dust which stays at a constant spatial coordinate $(r', \theta', \phi') = (r'_0, \theta'_0, \phi'_0)$ as the fundamental timelike geodesic γ in the Fermi-normal coordinate. In this situation, we can naturally choose the parallel transported tetrad which satisfies Eq. (5.3) as

$$e^{\mu'}_{(0)} = u^{\mu'} = (1, 0, 0, 0), \quad (5.30a)$$

$$e^{\mu'}_{(1)} = \left(0, \sqrt{1 - k(r'_0)} / \partial_{r'} R(t', r'_0), 0, 0 \right), \quad (5.30b)$$

$$e^{\mu'}_{(2)} = (0, 0, 1/R(t', r'_0), 0), \quad (5.30c)$$

$$e^{\mu'}_{(3)} = (0, 0, 0, 1/R(t', r'_0) \sin \theta'_0). \quad (5.30d)$$

By substituting Eqs. (5.29) and (5.30a)–(5.30d) into Eq. (5.22), we obtain the energy density in the Fermi coordinate as

$$\begin{aligned} \rho(t, \mathbf{x}) &= \rho|_{r'_0, \theta'_0, \phi'_0} + x^1 \left[\left(\frac{\sqrt{1 - k(r')}}{\partial_{r'} R(t', r')} \right) \partial_{r'} \rho \right] \Bigg|_{r'_0, \theta'_0, \phi'_0} + \mathcal{O}(x^i)^2 \\ &=: \rho^{\mathrm{L}}(t) + x^1 \left[\left(\frac{\sqrt{1 - k(r')}}{R(t', r')} \right) \partial_{r'} \rho \right] \Bigg|_{r'_0, \theta'_0, \phi'_0} + \mathcal{O}(x^i)^2, \end{aligned} \quad (5.31)$$

where we defined a local density $\rho^{\mathrm{L}}(t)$ which depends only on the time coordinate. By substituting Eqs. (5.29) and (5.30a)–(5.30d) into Eq. (5.21), we obtain the 4-velocity in the Fermi coordinate as

$$u^0(t, x^i) = 1 + \mathcal{O}(x^i)^2, \quad (5.32a)$$

$$u^1(t, x^i) = H_{\parallel}\big|_{r'_0, \theta'_0, \phi'_0} x^1 + \mathcal{O}(x^i)^2 =: H^{\mathrm{L}}_{\parallel}(t) x^1 + \mathcal{O}(x^i)^2, \quad (5.32b)$$

$$u^2(t, x^i) = H_{\perp}|_{r'_0, \theta'_0, \phi'_0} x^2 + \mathcal{O}(x^i)^2 =: H^{\mathrm{L}}_{\perp}(t) x^2 + \mathcal{O}(x^i)^2, \quad (5.32c)$$

$$u^3(t, x^i) = H_{\perp}|_{r'_0, \theta'_0, \phi'_0} x^3 + \mathcal{O}(x^i)^2 =: H^{\mathrm{L}}_{\perp}(t) x^3 + \mathcal{O}(x^i)^2, \quad (5.32d)$$

where we defined a local Hubble functions $H^{\mathrm{L}}_{\parallel}(t)$ and $H^{\mathrm{L}}_{\perp}(t)$ which depend only on the time coordinate. By using Eqs. (5.32a)–(5.32d), the 3-velocity v^i in the Fermi coordinate is given as

$$v^i = \frac{u^i}{u^0} = H_{ij}(t) x^j + \mathcal{O}(x^i)^2, \quad (5.33)$$

where we define H_{ij} as

$$H_{ij}(t) = \begin{pmatrix} H_{\parallel}^{\mathrm{L}}(t) & 0 & 0 \\ 0 & H_{\perp}^{\mathrm{L}}(t) & 0 \\ 0 & 0 & H_{\perp}^{\mathrm{L}}(t) \end{pmatrix}. \tag{5.34}$$

As for the metric, by substituting Eqs. (5.28) and (5.30a)–(5.30d) into Eq. (5.25) and by computing Riemann tensors in the former coordinate, we obtain $h_{\mu\nu}^{\mathrm{B}}$ as

$$h_{00}^{\mathrm{B}} = -K_1(t)(x^1)^2 - K_2(t)\left[(x^2)^2 + (x^3)^2\right], \tag{5.35a}$$

$$h_{11}^{\mathrm{B}} = -\frac{1}{3}K_3(t)\left[(x^2)^2 + (x^3)^2\right], \tag{5.35b}$$

$$h_{12}^{\mathrm{B}} = \frac{1}{3}K_3(t)x^1x^2, \tag{5.35c}$$

$$h_{13}^{\mathrm{B}} = \frac{1}{3}K_3(t)x^1x^3, \tag{5.35d}$$

$$h_{22}^{\mathrm{B}} = -\frac{1}{3}K_3(t)(x^1)^2 - \frac{1}{3}K_4(t)(x^3)^2, \tag{5.35e}$$

$$h_{23}^{\mathrm{B}} = \frac{1}{3}K_4(t)x^2x^3, \tag{5.35f}$$

$$h_{33}^{\mathrm{B}} = -\frac{1}{3}K_3(t)(x^1)^2 - \frac{1}{3}K_4(t)(x^2)^2, \tag{5.35g}$$

and $h_{0i}^{\mathrm{B}} = 0$, where $K_1(t)$, $K_2(t)$, $K_3(t)$ and $K_4(t)$ are defined as

$$K_1(t) = -\left.\frac{\partial_t^2\partial_r R}{\partial_r R}\right|_{r'_0,\theta'_0,\phi'_0}, \tag{5.36a}$$

$$K_2(t) = -\left.\frac{\partial_t^2 R}{R}\right|_{r'_0,\theta'_0,\phi'_0}, \tag{5.36b}$$

$$K_3(t) = \left.\left(H_{||}H_{\perp} + \frac{\partial_r k}{2R\partial_r R}\right)\right|_{r'_0,\theta'_0,\phi'_0}, \tag{5.36c}$$

$$K_4(t) = \left.\left(H_{\perp}^2 + \frac{k}{R^2}\right)\right|_{r'_0,\theta'_0,\phi'_0}. \tag{5.36d}$$

From Eq. (5.14), the former coordinate is related to the Fermi coordinate as

$$t' = t_{\mathrm{F}} - \frac{1}{2}(x^1)^2 H_{\parallel}^{\mathrm{L}}(t) - \frac{1}{2}\left[(x^2)^2 + (x^3)^2\right] H_{\perp}^{\mathrm{L}}(t) + \mathcal{O}\left(x^i\right)^3, \tag{5.37a}$$

$$r' - r'_0 = \left.\left(\frac{\sqrt{1-k(r')}}{\partial_{r'}R(t',r')}\right)\right|_{r'_0,\theta'_0,\phi'_0} x^1 + \mathcal{O}\left(x^i\right)^2, \tag{5.37b}$$

$$\theta' - \theta'_0 = \left.\left(\frac{1}{R(t',r')}\right)\right|_{r'_0,\theta'_0,\phi'_0} x^2 + \mathcal{O}\left(x^i\right)^2, \tag{5.37c}$$

$$\phi' - \phi'_0 = \left.\left(\frac{1}{R(t',r')\sin\theta'}\right)\right|_{r'_0,\theta'_0,\phi'_0} x^2 + \mathcal{O}\left(x^i\right)^2. \tag{5.37d}$$

To see the local behavior of the LTB spacetime, we introduce a local 3-velocity $v^i_{\rm L}$ and a local Potential $\Phi^{\rm L}$ from Eqs. (5.33) and (5.35a) as

$$v^i_{\rm L}(t,x^i) := H_{ij}(t)x^j, \quad \text{and} \quad \Phi^{\rm L}(t,x^i) := -\frac{1}{2}h^{\rm B}_{00}. \tag{5.38}$$

If we neglect higher corrections of the Fermi-normal coordinate expansion, the local behavior of the LTB spacetime is determined by the local quantities $\rho^{\rm L}$, $v^i_{\rm L}$ and $\Phi^{\rm L}$, as we will see below. From the conservation in the LTB spacetime given in Eq. (2.19), the local density and the local 3-velocity are related as

$$\frac{\partial}{\partial t}\rho^{\rm L} + \frac{\partial}{\partial x^j}\left(\rho^{\rm L}v^j_{\rm L}\right) = 0. \tag{5.39}$$

By using Eqs. (5.34) and (5.35a), we obtain the relation between $v^i_{\rm L}$ and $\Phi^{\rm L}$ as

$$\frac{\partial}{\partial t}v^i_{\rm L} + v^j_{\rm L}\frac{\partial}{\partial x^j}v^i_{\rm L} = -\frac{\partial}{\partial x^i}\Phi^{\rm L}. \tag{5.40}$$

By using the relation given in Eq. (2.18), we obtain the relation between $\rho^{\rm L}$ and $\Phi^{\rm L}$ as

$$\nabla^2\Phi^{\rm L} = 4\pi\rho^{\rm L}, \tag{5.41}$$

where we define $\nabla^2 = \delta^{ij}\partial^2/\partial x^i\partial x^j$. From Eqs. (5.39), (5.40) and (5.41), we can see that the relations of the local quantities have the same form to the equations of a Newtonian self-gravitating system of a non-relativistic fluid, where the Continuity equation (5.39), the Euler equation (5.40) and the Poisson equation (5.41). This means that the LTB cosmological model under a local approximation can be regarded as a solution of Newtonian hydrodynamics. Since the local density only depends on the time coordinate, we expect that the LTB cosmological model with local approximation corresponds to a Newtonian fluid with a homogeneous density $\rho = \rho(t)$. From the property of local quantities, we conclude that the LTB cosmological model can be reduced to an universe with homogeneous density and anisotropic volume expansion under a local approximation.

It is worthwhile to write down the metric of the LTB spacetime with weak field approximation in a spherical Fermi-normal coordinate. We define a spherical Fermi-normal coordinate $(r_{\rm F}, \Theta, \Phi)$ from the Fermi-normal coordinate x^μ as

$$x^1 = r_{\rm F}\cos\Theta, \quad x^2 = r_{\rm F}\sin\Theta\sin\Phi, \quad x^3 = r_{\rm F}\sin\Theta\cos\Phi. \tag{5.42}$$

The metric in the spherical Fermi-normal coordinate (see also [117]) is given by

$$ds^2 = -\left(1 + K_1(t)r^2_{\rm F}\cos^2\Theta + K_2(t)r^2_{\rm F}\sin^2\Theta\right)dt^2$$

$$
\begin{aligned}
&+ \quad dr_{\rm F}^2 + \left[1 - \frac{1}{3}\left(H_{||}H_{\perp} + \frac{\partial_{r'}k(r')}{2r'a_{||}a_{\perp}}\right)\Big|_{r_0'\theta_0'\phi_0'} r_{\rm F}^2\right] r_{\rm F}^2\left(d\Theta^2 + \sin^2\Theta d\Phi^2\right) \\
&+ \quad \frac{1}{3}\left(H_{||}H_{\perp} - H_{\perp}^2 + \frac{\partial_{r'}k(r')}{2r'a_{||}a_{\perp}} - \frac{k(r')}{a_{\perp}^2}\right)\Big|_{r_0'\theta_0'\phi_0'} r_{\rm F}^4 \sin^2\Theta d\Phi^2 \ + \mathcal{O}(\kappa)^3,
\end{aligned}
\tag{5.43}
$$

If we take the limit to FLRW universes, the functions approach $k(r) \to Kr^2$ and $a_{\parallel,\perp} \to a$, and accordingly the metric (5.43) is reduced to

$$
\begin{aligned}
ds^2 &= -\left(1 - \frac{\ddot{a}}{a}r_{\rm F}^2\right)dt^2 \\
&+ \quad dr_{\rm F}^2 + \left[1 - \frac{1}{3}\left(H^2 + \frac{K}{a^2}\right)r_{\rm F}^2\right] r_{\rm F}^2\left(d\Theta^2 + \sin^2\Theta d\Phi^2\right) + \mathcal{O}(\kappa)^3.
\end{aligned}
\tag{5.44}
$$

From Eq. (5.44), we can see that gravitational fields of the FLRW universe appear as small corrections of the order $r_{\rm F}^2 H^2$ in the local coordinate.

5.2 Derivation of Newtonian hydrodynamical equations in LTB cosmological model under the local approximation

The purpose of this section is to derive field equations governing Newtonian self-gravitating system in the LTB cosmological model. To perform this, we add local inhomogeneities which represent the cosmic structures such as galaxies and clusters to the background LTB spacetime. The metric and stress-energy tensor of the LTB cosmological model with the cosmic structures are given as

$$
g_{\mu\nu} = g^{\rm B}_{\mu\nu} + h^{\rm N}_{\mu\nu}, \tag{5.45}
$$

$$
T^{\mu\nu} = T^{\mu\nu}_{\rm B} + T^{\mu\nu}_{\rm N}, \tag{5.46}
$$

where $g^{\rm B}_{\mu\nu}$ and $T^{\mu\nu}_{\rm B}$ denote the metric and the stress-energy tensor of the background LTB cosmological model in the Fermi-normal coordinate and are given as

$$
\begin{aligned}
g^{\rm B}_{\mu\nu} &= \eta_{\mu\nu} + \kappa^2\, h^{\rm B}_{\mu\nu} + \mathcal{O}(\kappa)^3, && (5.47)\\
T^{00}_{\rm B} &= \rho^{\rm L} + \mathcal{O}(\kappa), && (5.48)\\
T^{0i}_{\rm B} &= \kappa\, \rho^{\rm L} v^i_{\rm L} + \mathcal{O}(\kappa^2), && (5.49)\\
T^{ij}_{\rm B} &= \kappa^2\, \rho^{\rm L} v^i_{\rm L} v^j_{\rm L} + \mathcal{O}(\kappa^3), && (5.50)
\end{aligned}
$$

and $h^{\rm N}_{\mu\nu}$ and $T^{\mu\nu}_{\rm N}$ represent the metric and the stress-energy tensor coming from the cosmic structures which is well described by the Cosmological Newtonian approximation.

5.2.1 Expansion parameters and gauge fixing

As discussed above, the local inhomogeneities coming from the cosmic structures are characterized by two expansion parameters ϵ and κ given in Eq. (5.1). Since the size of the structures $\ell_{\rm N}$ is much smaller than the curvature radius $\mathcal{R}$, we only need a local coordinate that sufficiently cover a region contains the local structures. In this situation, the small parameter κ introduced in Eq. (5.26) coincides with the κ in Eq. (5.1):

$$\kappa = \mathcal{O}\left(\frac{|\mathbf{x}|}{\mathcal{R}}\right) \sim \mathcal{O}\left(\frac{\ell_{\rm N}}{\mathcal{R}}\right). \tag{5.51}$$

In other words, κ is used in expanding both the background and the local inhomogeneities.

We have two time-scales in this system: one is the cosmic time-scale and the other comes from the local inhomogeneities which are defined as

$$T_{\rm age} := \frac{\mathcal{R}}{c} \quad \text{and} \quad t_{\rm N} := \frac{\ell_{\rm N}}{v_{\rm N}}. \tag{5.52}$$

These time-scales are important since they are related to a ratio of the two parameters as

$$\frac{T_{\rm age}}{t_{\rm N}} = \frac{\epsilon}{\kappa}. \tag{5.53}$$

From this, we assume that the order of time derivative for the local inhomogeneities is related to that of spatial derivative as

$$\mathcal{O}\left(\frac{\partial}{c\partial t}\phi\right) = \epsilon \times \mathcal{O}\left(\frac{\partial}{\partial x}\phi\right) \quad \text{for} \quad \epsilon > \kappa, \tag{5.54a}$$

$$\mathcal{O}\left(\frac{\partial}{c\partial t}\phi\right) = \kappa \times \mathcal{O}\left(\frac{\partial}{\partial x}\phi\right) \quad \text{for} \quad \epsilon < \kappa, \tag{5.54b}$$

where we introduced ϕ as a representative quantity describe the local inhomogeneities. This means that the ordering for the system depends on the magnitude relationship between ϵ and κ. In the next subsection, we consider the system dividing into three cases: $\epsilon > \kappa$, $\epsilon = \kappa$ and $\epsilon < \kappa$, depending on physical situations under consideration.

Here, we briefly review magnitudes of ϵ and κ in three cases. If we focus on the solar system, the orbital speed of the earth is about $v_{\rm N} \sim 30$km/s and we have $\epsilon \sim 10^{-4}$. The order of the κ is estimated as $\kappa = 1{\rm AU}/3{\rm Gpc} \sim 0.2 \times 10^{-14}$, where we assumed the curvature radius is 3Gpc. Thus the solar system is the case of $\epsilon \gg \kappa$. If we see clusters of galaxies whose velocity dispersion is about 1000km/s and spatial scale is about 10Mpc, we have $\epsilon \sim \kappa \sim 0.3 \times 10^{-2}$. If we consider the scale of the BAO, the velocity dispersion is about 600km/s and the spatial scale is about 100Mpc. Thus we have $\epsilon \sim 0.2 \times 10^{-2} < \kappa \sim 0.3 \times 10^{-1}$.

We give the order of the stress energy tensor $T^{\mu\nu}_{\rm N}$. Since we consider dust-filled universe, $T^{\mu\nu}_{\rm N}$ is given as

$$T^{\mu\nu}_{\rm N} = \rho_{\rm N} u^\mu_{\rm N} u^\nu_{\rm N}. \tag{5.55}$$

Then we define the density perturbation $\delta_{\rm N}$, the peculiar velocity $v^i_{\rm N}$ and the Gamma factor $\Gamma_{\rm N}$ of the local structures as

$$\delta_{\rm N} = \frac{\rho_{\rm N}}{\rho^{\rm B}}, \quad v^i_{\rm N} = \frac{u^i_{\rm N}}{u^0_{\rm N}}, \quad \Gamma_{\rm N} = u^0. \tag{5.56}$$

We assume the order of $v^i_{\rm N}$ and $\Gamma_{\rm N}$ as

$$v^i_{\rm N} = \epsilon\ v^i_{\rm N}, \ \text{ and } \ \Gamma_{\rm N} = 1\ + \mathcal{O}(\epsilon)^2. \tag{5.57}$$

The order of $\delta_{\rm N}$ is a little complicated. To estimate the order of the density contrast $\delta_{\rm N}$, we assume the Newtonian relation

$$\frac{G\rho|\mathbf{x}|^2}{c^2} \sim \frac{|\mathbf{v}|^2}{c^2}, \tag{5.58}$$

for the whole system. By applying Eq. (5.58), we obtain

$$\left(\kappa^2 \frac{G\rho^{\rm B}|\mathbf{x}|^2}{c^2}\right)(1+\delta_{\rm N}) \sim \left(\kappa \frac{v_{\rm B}}{c} + \epsilon \frac{v_{\rm N}}{c}\right)^2$$

$$\Rightarrow \quad \delta_{\rm N} = \mathcal{O}(\epsilon\kappa^{-1}) + \mathcal{O}(\epsilon^2\kappa^{-2}), \tag{5.59}$$

where we have used the relation $G\rho^{\rm B} \sim c^2\mathcal{R}^{-2}$. From this, we assume the magnitude of the density contrast as

$$\delta_{\rm N} = \kappa^{-2}\epsilon^2\ \delta_{\rm N} \quad \text{for} \quad \epsilon > \kappa, \tag{5.60a}$$

$$\delta_{\rm N} = \kappa^{-1}\epsilon\ \delta_{\rm N} \quad \text{for} \quad \epsilon < \kappa. \tag{5.60b}$$

From Eqs. (5.60a) and (5.60b), we can see the density contrast becomes $\delta_{\rm N} \ll 1$ when $\epsilon \ll \kappa$ is satisfied. This corresponds to the case of linear perturbations, as we will see it later.

As for the metric $h^{\rm N}_{\mu\nu}$, the order of magnitude is determined through the Einstein equations, and we will see it in the next subsection. We give the gauge condition as follows. Since we assume the self-gravity of the local structure is weak $|h^{\rm N}_{\mu\nu}| \ll 1$, we neglect the nonlinear terms about $h^{\rm N}_{\mu\nu}$. By this assumption, the gauge transformation for $h^{\rm N}_{\mu\nu}$ is written as

$$h^{\rm N}_{\mu\nu} \to \;\; = \;\; h^{\rm N}_{\mu\nu} + \partial_\mu \xi_\nu + \partial_\nu \xi_\mu - 2\, {}^{\rm B}\Gamma^\alpha_{\mu\nu}\xi_\alpha, \tag{5.61}$$

where ξ_μ represents the gauge field and ${}^{\rm B}\Gamma^\alpha_{\mu\nu}$ is the connection of the background metric $g^{\rm B}_{\mu\nu}$. Since we use the Fermi coordinate for the background, we have ${}^{\rm B}\Gamma^\alpha_{\mu\nu} = \kappa^2\ {}^{\rm B}\Gamma^\alpha_{\mu\nu}$. We neglect the higher orders of κ and the gauge transformation is reduced to

$$h^{\rm N}_{\mu\nu} \to h^{\rm N}_{\mu\nu} + \partial_\mu \xi_\nu + \partial_\nu \xi_\mu. \tag{5.62}$$

Then, we can fix the gauge condition in the same way that on the Minkowski spacetime as [2]

$$\partial^\mu \bar{h}^{\rm N}_{\mu\nu} = 0, \tag{5.63}$$

where we defined the trace-reversed tensor as $\bar{h}^{\rm N}_{\mu\nu} := h^{\rm N}_{\mu\nu} - \frac{1}{2}\eta_{\mu\nu}(\eta^{\alpha\beta}h^{\rm N}_{\alpha\beta})$. The Einstein tensor can be decomposed as $G_{\mu\nu} = G^{\rm B}_{\mu\nu} + \delta G_{\mu\nu}$, where $G^{\rm B}_{\mu\nu}$ and $\delta G_{\mu\nu}$ denote the background part and the perturbed part, respectively. We write them schematically:

$$G^{\rm B}_{\mu\nu} \;\; = \;\; G_{\mu\nu}\left[\partial^2 h^{\rm B}\right] + G_{\mu\nu}\left[\partial^2\left(h^{\rm B}h^{\rm B}\right)\right] + \cdots, \tag{5.64}$$

$$\delta G_{\mu\nu} \;\; = \;\; G_{\mu\nu}\left[\partial^2 h^{\rm N}\right] + G_{\mu\nu}\left[\partial^2\left(h^{\rm B}h^{\rm N}\right)\right] + G_{\mu\nu}\left[\partial^2\left(h^{\rm N}h^{\rm N}\right)\right] + \cdots. \tag{5.65}$$

We can see the first term of the right hand side in Eq. (5.64) is of the order of $\mathcal{R}^{-2}\kappa^2$, and larger than other parts as far as $\kappa < 1$. We can also see that the first term of the right hand side in Eq. (5.65) is of the order of $\ell_{\rm N}^{-2}h^{\rm N}$, and larger than other parts as far as $\kappa < 1$ and $|h^{\rm N}_{\mu\nu}| < 1$. We only consider the first terms of the right hand sides in Eqs. (5.64) and (5.64), in the range of the Newtonian approximation. Under the gauge condition (5.63), the dominant term of the perturbed Einstein tensor in Eq. (5.65) can be written as

$$G_{\mu\nu}[\partial^2 h] = -\frac{1}{2}\left(-\frac{\partial^2}{\partial t^2} + \delta^{ij}\frac{\partial^2}{\partial x^i \partial x^j}\right)\bar{h}^{\rm N}_{\mu\nu} \simeq -\frac{1}{2}\nabla^2 \bar{h}^{\rm N}_{\mu\nu}, \tag{5.66}$$

where we have neglected time derivative by using Eqs. (5.54a) and (5.54b).

[2]Fixing the gauge condition in the Newtonian order is guaranteed by the uniqueness of the solution for the equation $\nabla^2\xi_\mu + \partial^j \bar{h}_{\mu j} = 0$ with a suitable boundary condition [118].

5.2.2 Case analysis of Newtonian self-gravitating system

In the previous subsection, we showed that the ordering of ∂_t and $\delta_{\rm N}$ concerning the local inhomogeneities depends on the ratio of ϵ/κ. In this subsection, we derive the Newtonian equations by classifying the system into three cases, $\epsilon > \kappa$, $\epsilon = \kappa$ and $\epsilon < \kappa$.

In the case of $\epsilon > \kappa$

First we derive Newtonian equations for the local inhomogeneities in the case of $\epsilon > \kappa$. By using Eqs. (5.55), (5.56) and (5.66), the perturbed part of the Einstein equations are given, at leading order, as

$$\nabla^2 \bar{h}^{\rm N}_{00} = -16\pi G \rho_{\rm B} \delta_{\rm N}, \tag{5.67a}$$

$$\nabla^2 \bar{h}^{\rm N}_{0i} = -16\pi G \rho_{\rm B} \delta_{\rm N} v^i_{\rm N}, \tag{5.67b}$$

$$\nabla^2 \bar{h}^{\rm N}_{ij} = -16\pi G \rho_{\rm B} \delta_{\rm N} v^i_{\rm N} v^j_{\rm N}. \tag{5.67c}$$

From Eqs. (5.67a)–(5.67c) together with Eqs. (5.57) and (5.60a), we obtain the ordering of each components of $h^{\rm N}_{\mu\nu}$ as

$$h^{\rm N}_{00} = \mathcal{O}(\epsilon^2), \quad h^{\rm N}_{0i} = \mathcal{O}(\epsilon^3), \quad h^{\rm T} = \mathcal{O}(\epsilon^2), \quad h^{\rm TL}_{ij} = \mathcal{O}(\epsilon^4), \tag{5.68}$$

where $h^{\rm T}$ and $h^{\rm TL}_{ij}$ are trace part and traceless part of $h^{\rm N}_{ij}$ and given as $h_{ij} = \frac{1}{3} h^{\rm T} \delta_{ij} + h^{\rm TL}_{ij}$. When we derive the field equations at the leading order, we only need the conservation low $\nabla_\mu T^{\mu\nu} = 0$ and (00) component of the Einstein equation:

$$\partial_0 \rho + \partial_i (\rho v^i) = \rho \left[-\Gamma^\mu_{\mu 0} - \Gamma^\mu_{\mu i} v^i + \left(\Gamma^0_{00} + 2\Gamma^0_{0i} v^i + \Gamma^0_{ij} v^i v^j \right) \right], \tag{5.69a}$$

$$\partial_0 v^i + v^j \partial_j v^i = -\Gamma^i_{00} - 2\Gamma^i_{0j} v^j - \Gamma^i_{jk} v^j v^k + \left(\Gamma^0_{00} + 2\Gamma^0_{0j} v^j + \Gamma^0_{jk} v^j v^k \right) v^i, \tag{5.69b}$$

$$G_{00} = 8\pi G \; T_{00}, \tag{5.69c}$$

By substituting Eqs. (5.45) and (5.46) into Eqs. (5.69a)–(5.69c) and subtracting the background part governed by Eqs. (5.39), (5.40) and (5.41), we obtain, under the ordering (5.54a), (5.57), (5.60a) and (5.68), field equations governing the local inhomogeneities as

$$\left[\epsilon \frac{\partial}{\partial t} + \kappa \; v^i_{\rm B} \frac{\partial}{\partial x^i} \right] \kappa^{-2} \epsilon^2 \delta_{\rm N} + \frac{\partial}{\partial x^i} \left[(1 + \kappa^{-2} \epsilon^2 \delta_{\rm N}) \epsilon \; v^i_{\rm N} \right] + \mathcal{O}(\epsilon^2) = 0, \tag{5.70a}$$

$$\left[\epsilon \frac{\partial}{\partial t} + \kappa \; v^j_{\rm B} \frac{\partial}{\partial x^j} \right] \epsilon \; v^i_{\rm N} + \epsilon \; v^j_{\rm N} \frac{\partial}{\partial x^j} \kappa \; v^i_{\rm B} + \epsilon \; v^j_{\rm N} \frac{\partial}{\partial x^j} \epsilon \; v^i_{\rm N} + \mathcal{O}(\epsilon\kappa^2) = -\frac{\partial}{\partial x^i} \epsilon^2 \phi_{\rm N}, \tag{5.70b}$$

$$\epsilon^2 \phi_{\rm N} + \mathcal{O}(\epsilon^2 \kappa) = \epsilon^2 \; \nabla^{-2} 4\pi G \; \rho_{\rm B} \delta_{\rm N}, \tag{5.70c}$$

where $\phi_{\rm N}$ denotes Newtonian potential which is defined as $\phi_{\rm N} := -\frac{1}{2}h^{\rm N}_{00}$, and we introduced the inverse Laplacian ∇^{-2} to clarify the ordering of the derived equation.

Then, we see the structure of the derived equations (5.70a)–(5.70c). If we neglect higher-order terms and only include the leading terms in Eqs. (5.70a)–(5.70c), the equations are reduced to

$$\kappa^{-2}\epsilon^3\frac{\partial}{\partial t}\delta_{\rm N} + \kappa^{-2}\epsilon^3\frac{\partial}{\partial x^i}(\delta_{\rm N}v^i_{\rm N}) = 0, \tag{5.71a}$$

$$\epsilon^2\frac{\partial}{\partial t}v^i_{\rm N} + \epsilon^2 v^j_{\rm N}\frac{\partial}{\partial x^j}v^i_{\rm N} = -\epsilon^2\frac{\partial}{\partial x^i}\phi_{\rm N}, \tag{5.71b}$$

$$\epsilon^2\phi_{\rm N} = \epsilon^2\nabla^{-2}4\pi G\rho_{\rm B}\delta_{\rm N}. \tag{5.71c}$$

We can see that Eqs. (5.71a)–(5.71c) are same to Newtonian equations for the self-gravitating system in Minkowski spacetime, as we expected. The effects of the background spacetimes appear when we go to next orders. Including next-to-leading orders in Eqs. (5.70a)–(5.70c), we obtain

$$\left[\epsilon\frac{\partial}{\partial t} + \kappa\ v^i_{\rm B}\frac{\partial}{\partial x^i}\right]\kappa^{-2}\epsilon^2\delta_{\rm N} + \frac{\partial}{\partial x^i}\left[(1+\kappa^{-2}\epsilon^2\delta_{\rm N})\epsilon\ v^i_{\rm N}\right] = 0, \tag{5.72a}$$

$$\left[\epsilon\frac{\partial}{\partial t} + \kappa\ v^j_{\rm B}\frac{\partial}{\partial x^j}\right]\epsilon\ v^i_{\rm N} + \epsilon\ v^j_{\rm N}\frac{\partial}{\partial x^j}\kappa\ v^i_{\rm B} + \epsilon\ v^j_{\rm N}\frac{\partial}{\partial x^j}\epsilon\ v^i_{\rm N} = -\frac{\partial}{\partial x^i}\epsilon^2\phi_{\rm N}, \tag{5.72b}$$

$$\epsilon^2\phi_{\rm N} = \epsilon^2\ \nabla^{-2}4\pi G\ \rho_{\rm B}\delta_{\rm N}, \tag{5.72c}$$

where we have neglected corrections of $\mathcal{O}(\epsilon^2)$ in Eq. (5.70a), $\mathcal{O}(\epsilon\kappa^2)$ in Eq. (5.70b) and $\mathcal{O}(\epsilon^2\kappa)$ in Eq. (5.70c), since they are still higher-order terms than the terms we have included. Eqs. (5.72a)–(5.72c) govern dynamics of the local inhomogeneities affected by the background LTB universe in the range of the Newtonian approximation. We can see that the effects of the background appear as the velocity field $v^i_{\rm B}$ and the density $\rho_{\rm B}$, and they become important when κ approaches to ϵ.

In the case of $\epsilon = \kappa$

Second we derive the Newtonian equations in the case of $\epsilon = \kappa$. In this case, we can describe inhomogeneities with one small-parameter ϵ, by setting $\kappa = \epsilon$. By taking the limit of $\kappa \to \epsilon$ in Eqs. (5.70a)–(5.70c), we obtain field equations as

$$\left[\epsilon\frac{\partial}{\partial t} + \epsilon\ v^i_{\rm B}\frac{\partial}{\partial x^i}\right]\delta_{\rm N} + \frac{\partial}{\partial x^i}\left[(1+\delta_{\rm N})\epsilon\ v^i_{\rm N}\right] + \mathcal{O}(\epsilon^2) = 0, \tag{5.73a}$$

$$\left[\epsilon\frac{\partial}{\partial t} + \epsilon\ v^j_{\rm B}\frac{\partial}{\partial x^j}\right]\epsilon\ v^i_{\rm N} + \epsilon\ v^j_{\rm N}\frac{\partial}{\partial x^j}\epsilon\ v^i_{\rm B} + \epsilon\ v^j_{\rm N}\frac{\partial}{\partial x^j}\epsilon\ v^i_{\rm N} + \mathcal{O}(\epsilon^3) = -\frac{\partial}{\partial x^i}\epsilon^2\phi_{\rm N}, \tag{5.73b}$$

$$\epsilon^2\phi_{\rm N} + \mathcal{O}(\epsilon^3) = \epsilon^2\ \nabla^{-2}4\pi G\ \rho_{\rm B}\delta_{\rm N}, \tag{5.73c}$$

When we neglect higher orders in Eqs. (5.73a)–(5.73c), we obtain field equations, at leading order, as

$$\left[\epsilon\frac{\partial}{\partial t}+\epsilon\ v^i_{\rm B}\frac{\partial}{\partial x^i}\right]\delta_{\rm N}+\frac{\partial}{\partial x^i}\left[(1+\delta_{\rm N})\epsilon\ v^i_{\rm N}\right]=0, \tag{5.74a}$$

$$\left[\epsilon\frac{\partial}{\partial t}+\epsilon\ v^j_{\rm B}\frac{\partial}{\partial x^j}\right]\epsilon\ v^i_{\rm N}+\epsilon\ v^j_{\rm N}\frac{\partial}{\partial x^j}\epsilon\ v^i_{\rm B}+\epsilon\ v^j_{\rm N}\frac{\partial}{\partial x^j}\epsilon\ v^i_{\rm N}=-\frac{\partial}{\partial x^i}\epsilon^2\phi_{\rm N}, \tag{5.74b}$$

$$\epsilon^2\phi_{\rm N}=\epsilon^2\ \nabla^{-2}4\pi G\ \rho_{\rm B}\delta_{\rm N}, \tag{5.74c}$$

From Eqs. (5.74a)–(5.74c), we can see the effects of the background spacetimes appear at leading-order, which is different from the previous case. Since we cannot neglect the background effects, we expect that the evolution of structures strongly reflects the background LTB universes through the velocity field $v^i_{\rm B}$ and the energy density $\rho_{\rm B}$.

In the case of $\epsilon<\kappa$

Third we derive Newtonian equations in the case of $\epsilon<\kappa$. In this case, the ordering for the the local inhomogeneities is quite different from that in the previous two cases. By using Eqs. (5.55), (5.56) and (5.66), the perturbed part of the Einstein equations are given, at leading order, as

$$\nabla^2\bar{h}^{\rm N}_{00}=-16\pi G\rho_{\rm B}\delta_{\rm N}, \tag{5.75a}$$

$$\nabla^2\bar{h}^{\rm N}_{0i}=-16\pi G\rho_{\rm B}\left(v^i_{\rm N}+\delta_{\rm N}v^i_{\rm B}\right), \tag{5.75b}$$

$$\nabla^2\bar{h}^{\rm N}_{ij}=-16\pi G\rho_{\rm B}\left[v^i_{\rm B}\left(v^j_{\rm N}+\delta_{\rm N}v^j_{\rm B}\right)+v^j_{\rm B}\left(v^i_{\rm N}+\delta_{\rm N}v^i_{\rm B}\right)\right]. \tag{5.75c}$$

By using Eqs. (5.75a)–(5.75c) together with the ordering given in Eqs. (5.48), (5.49), (5.50), (5.57) and (5.60b), we obtain the ordering of $h^{\rm N}_{\mu\nu}$ as

$$h^{\rm N}_{00}=\mathcal{O}(\kappa\epsilon),\quad h^{\rm N}_{0i}=\mathcal{O}(\kappa^2\epsilon),\quad h^{\rm T}=\mathcal{O}(\kappa\epsilon),\quad h^{\rm TL}_{ij}=\mathcal{O}(\kappa^3\epsilon). \tag{5.76}$$

Here, we should note that the ordering of $h_{\mu\nu}$ in Eq. (5.76) is quite different from that in Eq. (5.68). By substituting Eqs. (5.45) and (5.46) into Eqs. (5.69a)–(5.69c) and subtracting the background part governed by Eqs. (5.39), (5.40) and (5.41), we obtain field equations governing the local inhomogeneities, under the ordering (5.54b),

(5.57), (5.60b) and (5.76), as

$$\left[\kappa\frac{\partial}{\partial t}+\kappa\ v^i_{\rm B}\frac{\partial}{\partial x^i}\right]\kappa^{-1}\epsilon\ \delta_{\rm N}+\frac{\partial}{\partial x^i}\left[(1+\kappa^{-1}\epsilon\ \delta_{\rm N})\epsilon\ v^i_{\rm N}\right]+\mathcal{O}(\kappa\epsilon)=0, \tag{5.77a}$$

$$\left[\kappa\frac{\partial}{\partial t}+\kappa\ v^j_{\rm B}\frac{\partial}{\partial x^j}\right]\epsilon\ v^i_{\rm N}+\epsilon\ v^j_{\rm N}\frac{\partial}{\partial x^j}\kappa\ v^i_{\rm B}+\epsilon\ v^j_{\rm N}\frac{\partial}{\partial x^j}\epsilon\ v^i_{\rm N}+\mathcal{O}(\kappa^2\epsilon)=-\frac{\partial}{\partial x^i}\kappa\epsilon\ \phi_{\rm N}, \tag{5.77b}$$

$$\kappa\epsilon\ \phi_{\rm N}+\mathcal{O}(\kappa^2\epsilon^2)=\kappa\epsilon\ \nabla^{-2}4\pi G\rho_{\rm B}\delta_{\rm N}. \tag{5.77c}$$

If we neglect higher-orders in Eqs. (5.77a)–(5.77c), we obtain field equations, at leading-order, as

$$\epsilon\left[\frac{\partial}{\partial t}+v^i_{\rm B}\frac{\partial}{\partial x^i}\right]\delta_{\rm N}+\epsilon\frac{\partial}{\partial x^i}v^i_{\rm N}=0, \tag{5.78a}$$

$$\kappa\epsilon\left[\frac{\partial}{\partial t}+v^j_{\rm B}\frac{\partial}{\partial x^j}\right]v^i_{\rm N}+\kappa\epsilon\ v^j_{\rm N}\frac{\partial}{\partial x^j}v^i_{\rm B}=-\kappa\epsilon\ \frac{\partial}{\partial x^i}\phi_{\rm N}, \tag{5.78b}$$

$$\kappa\epsilon\ \phi_{\rm N}=\kappa\epsilon\ \nabla^{-2}4\pi G\rho_{\rm B}\delta_{\rm N}. \tag{5.78c}$$

From Eqs. (5.78a)–(5.78c), we can see that the background effects appear through $v^i_{\rm B}$ and $\rho_{\rm B}$, and the equations are linearized about the variables $\delta_{\rm N}$, $v^i_{\rm N}$ and $\phi_{\rm N}$. We will show that the equations can be reduced to ordinary differential equations in a decoupled form, by performing the Fourier transformation to the perturbations. If we include the terms of next-to-leading order in Eqs. (5.78a)–(5.78c), we obtain the field equations

$$\left[\kappa\frac{\partial}{\partial t}+\kappa\ v^i_{\rm B}\frac{\partial}{\partial x^i}\right]\kappa^{-1}\epsilon\ \delta_{\rm N}+\frac{\partial}{\partial x^i}\left[(1+\kappa^{-1}\epsilon\ \delta_{\rm N})\epsilon\ v^i_{\rm N}\right]=0, \tag{5.79a}$$

$$\left[\kappa\frac{\partial}{\partial t}+\kappa\ v^j_{\rm B}\frac{\partial}{\partial x^j}\right]\epsilon\ v^i_{\rm N}+\epsilon\ v^j_{\rm N}\frac{\partial}{\partial x^j}\kappa\ v^i_{\rm B}+\epsilon\ v^j_{\rm N}\frac{\partial}{\partial x^j}\epsilon\ v^i_{\rm N}=-\frac{\partial}{\partial x^i}\kappa\epsilon\ \phi_{\rm N}, \tag{5.79b}$$

$$\kappa\epsilon\ \phi_{\rm N}=\kappa\epsilon\ \nabla^{-2}4\pi G\rho_{\rm B}\delta_{\rm N}. \tag{5.79c}$$

5.2.3 On the limit to FLRW universe model

To understand the derived equations more clearly, we take the limit of the LTB cosmological models to the FLRW models as follows. Although we have derived Newtonian equations about three cases, the derived equations about three cases coincide with each other if we take the next-to-leading order terms into account. Accordingly, we rewrite Eqs. (5.72a)–(5.72c), Eqs. (5.74a)–(5.74c) and Eqs. (5.79a)–

(5.79c) as

$$\left[\frac{\partial}{\partial t}+v^i_{\rm B}\frac{\partial}{\partial x^i}\right]\delta_{\rm N}+\frac{\partial}{\partial x^i}\left[(1+\delta_{\rm N})v^i_{\rm N}\right]=0, \tag{5.80a}$$

$$\left[\frac{\partial}{\partial t}+v^j_{\rm B}\frac{\partial}{\partial x^j}\right]v^i_{\rm N}+v^j_{\rm N}\frac{\partial}{\partial x^j}v^i_{\rm B}+v^j_{\rm N}\frac{\partial}{\partial x^j}v^i_{\rm N}=-\frac{\partial}{\partial x^i}\phi_{\rm N}, \tag{5.80b}$$

$$\phi_{\rm N}=\nabla^{-2}4\pi G\rho_{\rm B}\delta_{\rm N}, \tag{5.80c}$$

where we omitted the small parameters ϵ and κ. This is our main result in this chapter. The equations (5.80a)–(5.80c) govern Newtonian self-gravitating system in the LTB cosmological model. From Eqs. (5.80a)–(5.80c), we can see that effects of the background universe appear through $\rho_{\rm B}$ and $v^i_{\rm B}$ which represent the homogeneous density and the anisotropic volume expansion. Thus, we conclude that Newtonian structures feel gravitational fields of the background universe like those of a homogeneous and anisotropic universe.

To take the limit to the case of FLRW universes, we introduce a comoving coordinate $x^i_{\rm c}$ as

$$x^1=a^{\rm L}_{\parallel}(t)x^1_{\rm c},\qquad x^2=a^{\rm L}_{\perp}(t)x^2_{\rm c},\qquad x^3=a^{\rm L}_{\perp}(t)x^3_{\rm c}, \tag{5.81}$$

where x^i denotes the Fermi-normal coordinate and $a^{\rm L}_{\parallel,\perp}$ are defined as $a^{\rm L}_{\parallel,\perp}(t)=a_{\parallel,\perp}(t,r_0)$, where $a_{\parallel,\perp}(t,r)$ denote the scale factors of LTB spacetimes defined in Eq. (2.14). By using Eq. (5.81), Eqs. (5.80a)–(5.80c) are transformed as

$$\frac{\partial}{\partial t}\delta_{\rm N}+\frac{1}{a^{\rm L}_{||}(t)}\frac{\partial}{\partial x^1_{\rm c}}\left[(1+\delta_{\rm N})v^1_{\rm N}\right]+\frac{1}{a^{\rm L}_{\perp}(t)}\frac{\partial}{\partial x^I_{\rm c}}\left[(1+\delta_{\rm N})v^I_{\rm N}\right]=0, \tag{5.82a}$$

$$\frac{\partial}{\partial t}v^1_{\rm N}+H^{\rm L}_{\parallel}(t)v^1_{\rm N}+\left[\frac{1}{a^{\rm L}_{||}(t)}v^1_{\rm N}\frac{\partial}{\partial x^1_{\rm c}}+\frac{1}{a^{\rm L}_{\perp}(t)}v^J_{\rm N}\frac{\partial}{\partial x^J_{\rm c}}\right]v^1_{\rm N}=-\frac{1}{a^{\rm L}_{\parallel}(t)}\frac{\partial}{\partial x^1_{\rm c}}\phi_{\rm N}, \tag{5.82b}$$

$$\frac{\partial}{\partial t}v^I_{\rm N}+H^{\rm L}_{\perp}(t)v^I_{\rm N}+\left[\frac{1}{a^{\rm L}_{||}(t)}v^1_{\rm N}\frac{\partial}{\partial x^1_{\rm c}}+\frac{1}{a^{\rm L}_{\perp}(t)}v^J_{\rm N}\frac{\partial}{\partial x^J_{\rm c}}\right]v^I_{\rm N}=-\frac{1}{a^{\rm L}_{\perp}(t)}\frac{\partial}{\partial x^I_{\rm c}}\phi_{\rm N}, \tag{5.82c}$$

$$\left[\frac{1}{\left(a^{\rm L}_{\parallel}(t)\right)^2}\frac{\partial^2}{\partial x^1_{\rm c}\partial x^1_{\rm c}}+\frac{1}{\left(a^{\rm L}_{\perp}(t)\right)^2}\delta^{IJ}\frac{\partial^2}{\partial x^I_{\rm c}\partial x^J_{\rm c}}\right]\phi_{\rm N}=4\pi G\rho_{\rm B}(t)\delta_{\rm N}, \tag{5.82d}$$

where we have used the relation

$$\left.\frac{\partial}{\partial t}\right|_{x^i_{\rm c}=\text{const.}}=\frac{\partial}{\partial t}+v^j_{\rm B}\frac{\partial}{\partial x^j}. \tag{5.83}$$

By taking the limit of $a_{\parallel,\perp}\to a$, $H^{\rm L}_{\parallel,\perp}\to H$ and $\rho_{\rm B}\to\rho^{\rm FLRW}$ for the equa-

tions (5.82a)–(5.82d), we obtain

$$\frac{\partial}{\partial t}\delta_{\rm N} + \frac{1}{a(t)}\frac{\partial}{\partial x^i_{\rm c}}\left[(1+\delta_{\rm N})v^i_{\rm N}\right] = 0, \tag{5.84a}$$

$$\frac{\partial}{\partial t}v^j_{\rm N} + H(t)v^j_{\rm N} + \frac{1}{a(t)}v^i_{\rm N}\frac{\partial}{\partial x^i_{\rm c}}v^j_{\rm N} = -\frac{1}{a(t)}\frac{\partial}{\partial x^j_{\rm c}}\phi_{\rm N}, \tag{5.84b}$$

$$\frac{1}{a^2(t)}\delta^{ij}\frac{\partial^2}{\partial x^i_{\rm c}\partial x^j_{\rm c}}\phi_{\rm N} = 4\pi G\rho^{\rm FLRW}(t)\delta_{\rm N}. \tag{5.84c}$$

The equations (5.84a)–(5.84c) are none other than well-known Newtonian equations in FLRW universes. Thus, our results given in Eqs. (5.82a)–(5.82d) can be recognized as a generalization of Newtonian equations of a fluid with self-gravity in homogeneous and isotropic universes to the case of the inhomogeneous universe.

5.2.4 On the N-body simulations

We have to study the numerical N-body simulations to solve the derived nonlinear equations (5.80a)–(5.80c). Although this is left for a future work, we derive equations of motion of particles in the N-body simulations. First, we assume the energy density as

$$\rho(t,x^i) = \rho_{\rm B}(t)\left(1+\delta_{\rm N}(t,x^i)\right) = m\sum_{I=1}^{N}\delta^{(3)}_{\rm D}\left(x^i - x^i_{(I)}(t)\right), \tag{5.85}$$

where the subscript (I) denotes a label of each particles, m denotes the mass of each particles and $\delta^{(3)}_{\rm D}$ represents the Dirac's delta function. By solving the Poisson equation (5.80c), we have a solution

$$\phi_{\rm N}(t,\mathbf{x}) = -G\int d^3x'\frac{\rho_{\rm B}(t)\delta_{\rm N}(t,\mathbf{x}')}{|\mathbf{x}-\mathbf{x}'|}. \tag{5.86}$$

By substituting Eqs. (5.85) and (5.86) into the Euler equation (5.80b), we obtain equation of motion of particle (I) as

$$\frac{d}{dt}x^i_{(I)} = H_{ij}(t,r_0)x^j_{(I)} + v^i_{{\rm N}(I)}, \tag{5.87}$$

$$\frac{d}{dt}v^i_{{\rm N}(I)} = -H_{ij}(t,r_0)v^j_{{\rm N}(I)} + g^i_{(I)}, \tag{5.88}$$

$$g^i_{(I)} = Gm\sum_{J(J\neq I)}\frac{x^i_{(I)} - x^i_{(J)}}{\left|x^i_{(I)} - x^i_{(J)}\right|^3}, \tag{5.89}$$

where we have used the total time derivative defined as

$$\frac{d}{dt} = \frac{\partial}{\partial t} + v^i_{\rm B}\frac{\partial}{\partial x^i} + v^i_{\rm N}\frac{\partial}{\partial x^i}.$$

From the equation (5.87), we can see that the velocity of particles contains the Hubble flow of the LTB cosmological model, $H_{ij}x^j$, and the peculiar velocity, $v^i_{\rm N}$. From the equations (5.88) and (5.89), we can see that the volume expansion, H_{ij}, appears as a friction term of the equation of motion and the gravitational field, $g^i_{(I)}$, denotes the Newtonian gravitational force from all other particles.

If we take the limit of $H_{ij}(t, r_0) \to H(t)\delta_{ij}$, Eqs. (5.87)–(5.89) can be reduced to the equations of motion in the N-body simulations in the homogeneous and isotropic FLRW universes. This implies that we can apply the well-developed method of the N-body simulations in the FLRW universes to the case of our interest. As for the initial condition, since we consider a huge void model which approaches to a FLRW universe at sufficiently early times, we assume that the initial particle positions are governed by the power spectrum in the FLRW universe. Here, it should be noted that r_0 is a parameter of the simulation. If we practice numerical simulations for each local patch characterized by the parameter r_0, we obtain a result of cosmic structure formation of all spatial region in the LTB void universe model.

5.3 Analysis of linear perturbations

5.3.1 Linear perturbation equations

We solve the derived equations of Newtonian self-gravitating system in the LTB cosmological model by using a linear approximation. By linearizing the equations (5.80a)–(5.80c) about the quantities $\delta_{\rm N}$, $v^i_{\rm N}$ and $\phi_{\rm N}$, we obtain

$$\left(\frac{\partial}{\partial t} + v^j_{\rm B}\frac{\partial}{\partial x^j}\right)\delta_{\rm N} + \frac{\partial}{\partial x^j}v^j_{\rm N} = 0, \tag{5.90}$$

$$\left(\frac{\partial}{\partial t} + v^j_{\rm B}\frac{\partial}{\partial x^j}\right)v^i_{\rm N} + H_{ij}v^j_{\rm N} = -\frac{\partial}{\partial x^i}\phi_{\rm N}, \tag{5.91}$$

$$\nabla^2\phi_{\rm N} = 4\pi G\rho_{\rm B}\delta_{\rm N}, \tag{5.92}$$

where $H_{ij}(t)$ denotes the local volume expansion of the background model defined in Eq. (5.34). Here, we note that Eqs. (5.90), (5.91) and (5.92) are equivalent to the equations (5.78a)–(5.78c). To solve the linearized equations, we introduce the kinematic quantities about the 3-velocity v^i as

$$\frac{\partial}{\partial x^j}v^i = \partial_j v_i = \frac{1}{3}\theta\delta_{ij} + \sigma_{ij} + \omega_{ij}, \tag{5.93}$$

where θ, σ_{ij} and ω_{ij} describe the expansion, shear and vorticity of the fluid flow and are defined as

$$\theta = \partial^j v_j, \tag{5.94}$$

$$\sigma_{ij} = \sigma_{\langle ij\rangle} = \frac{1}{2}\left(\partial_j v_i + \partial_i v_j\right) - \frac{1}{3}\theta\delta_{ij}, \tag{5.95}$$

$$\omega_{ij} = \omega_{[ij]} = \frac{1}{2}\left(\partial_j v_i - \partial_i v_j\right). \tag{5.96}$$

Here, we note that the 3-velocity includes both the background and Newtonian 3-velocities, $v^i = v^i_{\rm B} + v^i_{\rm N}$. By using Eqs. (5.34), (5.38) and (5.93), the kinematic quantities of the background fluid $v^i_{\rm B}$ are obtained as

$$\theta_{\rm B}(t) = H^{\rm L}_{\parallel}(t) + 2H^{\rm L}_{\perp}(t), \tag{5.97}$$

$$\sigma^{\rm B}_{ij}(t) = \begin{pmatrix} \frac{2}{3}\left(H^{\rm L}_{\parallel}(t) - H^{\rm L}_{\perp}(t)\right) & 0 & 0 \\ 0 & -\frac{1}{2}\sigma^{\rm B}_{11} & 0 \\ 0 & 0 & -\frac{1}{2}\sigma^{\rm B}_{11} \end{pmatrix}, \tag{5.98}$$

and

$$\omega^{\rm B}_{ij}(t) = 0. \tag{5.99}$$

We introduce the total time derivative along the fluid flow as

$$\frac{d}{dt} := \frac{\partial}{\partial t} + v^j\frac{\partial}{\partial x^j}. \tag{5.100}$$

By using Eqs. (5.93), (5.94), (5.95), (5.96), (5.97), (5.98), (5.99) and (5.100), the linear perturbation equations (5.90)–(5.92) are reduced to

$$\frac{d}{dt}\delta_{\rm (N)} = -\theta_{\rm (N)}, \tag{5.101a}$$

$$\frac{d}{dt}\theta_{\rm (N)} = -\frac{2}{3}\theta_{\rm (B)}\theta_{\rm (N)} - 2\sigma_{{\rm (B)}ij}\sigma_{{\rm (N)}ji} - 4\pi G\rho_{\rm (B)}\delta_{\rm (N)}, \tag{5.101b}$$

$$\frac{d}{dt}\sigma_{{\rm (N)}ij} = -\frac{2}{3}\theta_{\rm (B)}\sigma_{{\rm (N)}ij} - \frac{2}{3}\theta_{\rm (N)}\sigma_{{\rm (B)}ij} - \left(\sigma_{{\rm (B)}ki}\sigma_{{\rm (N)}jk} + \sigma_{{\rm (B)}kj}\sigma_{{\rm (N)}ik}\right)^{\rm TL} - \partial^{\rm TL}_{ij}\phi_{\rm N}, \tag{5.101c}$$

$$\frac{d}{dt}\omega_{{\rm (N)}ij} = -\frac{2}{3}\theta_{\rm (B)}\omega_{{\rm (N)}ij} + \sigma_{{\rm (B)}ki}\omega_{{\rm (N)}jk} - \sigma_{{\rm (B)}kj}\omega_{{\rm (N)}ik}, \tag{5.101d}$$

$$\nabla^2\phi_{\rm (N)} = 4\pi G\rho_{\rm (B)}\delta_{\rm (N)}, \tag{5.101e}$$

where the subscripts (B) and (N) represent the quantities of the background and the perturbation, respectively, and the superscript TL denotes the traceless of the symmetric tensor defined as

$$\begin{aligned}\left(\sigma_{(\mathrm{B})ki}\sigma_{(\mathrm{N})jk}+\sigma_{(\mathrm{B})kj}\sigma_{(\mathrm{N})ik}\right)^{\mathrm{TL}} &= \left(\sigma_{(\mathrm{B})ki}\sigma_{(\mathrm{N})jk}+\sigma_{(\mathrm{B})kj}\sigma_{(\mathrm{N})ik}\right)-\frac{2}{3}\sigma_{(\mathrm{B})kl}\sigma_{(\mathrm{N})lk}\delta_{ij},\\ \partial_{ij}^{\mathrm{TL}}\phi_{\mathrm{N}} &= \left(\partial_i\partial_j-\frac{1}{3}\nabla^2\delta_{ij}\right)\phi_{\mathrm{N}}.\end{aligned}$$

To solve the equations (5.101a)–(5.101e), we assume a periodic boundary condition about the perturbations. Then, we perform the Fourier transform for the linear perturbations as

$$\delta_{\mathrm{N}}(t,x^i)=\int\frac{d^3k}{(2\pi)^{3/2}}e^{i\mathbf{k}\cdot\mathbf{x}}\tilde{\delta}_{\mathrm{N}}(t,k^i), \tag{5.102}$$

and θ_{N}, σ^{N}_{ij}, ω^{N}_{ij} and ϕ_{N} are transformed in the similar way. By performing the Fourier transform (5.102) to the equations (5.101a)–(5.101e), we obtain

$$\frac{d}{dt}\tilde{\delta}_{(\mathrm{N})}=-\tilde{\theta}_{(\mathrm{N})}, \tag{5.103a}$$

$$\frac{d}{dt}\tilde{\theta}_{(\mathrm{N})}=-\frac{2}{3}\theta_{(\mathrm{B})}\tilde{\theta}_{(\mathrm{N})}-2\sigma_{(\mathrm{B})ij}\tilde{\sigma}_{(\mathrm{N})ji}-4\pi G\rho_{(\mathrm{B})}\tilde{\delta}_{(\mathrm{N})}, \tag{5.103b}$$

$$\begin{aligned}\frac{d}{dt}\tilde{\sigma}_{(\mathrm{N})ij}=&-\frac{2}{3}\theta_{(\mathrm{B})}\tilde{\sigma}_{(\mathrm{N})ij}-\frac{2}{3}\tilde{\theta}_{(\mathrm{N})}\sigma_{(\mathrm{B})ij}-\left(\sigma_{(\mathrm{B})ki}\tilde{\sigma}_{(\mathrm{N})jk}+\sigma_{(\mathrm{B})kj}\tilde{\sigma}_{(\mathrm{N})ik}\right)^{\mathrm{TL}}\\ &+\left(k^ik^j-\frac{1}{3}k^2\delta^{ij}\right)\tilde{\phi}_{\mathrm{N}},\end{aligned} \tag{5.103c}$$

$$\frac{d}{dt}\tilde{\omega}_{(\mathrm{N})ij}=-\frac{2}{3}\theta_{(\mathrm{B})}\tilde{\omega}_{(\mathrm{N})ij}+\sigma_{(\mathrm{B})ki}\tilde{\omega}_{(\mathrm{N})jk}-\sigma_{(\mathrm{B})kj}\tilde{\omega}_{(\mathrm{N})ik}, \tag{5.103d}$$

$$-k^2\tilde{\phi}_{(\mathrm{N})}=4\pi G\rho_{(\mathrm{B})}\tilde{\delta}_{(\mathrm{N})}, \tag{5.103e}$$

where k is defined as $k^2=\delta_{ij}k^ik^j$. From Eqs. (5.103a)–(5.103e), we can see that the linear perturbation equations are reduced to a decoupled set of ordinary differential equations about each Fourier modes. This is a very different result from the case of relativistic linear perturbations in LTB models discussed in § 3.1. This is because that the background quantities, ρ_{B}, θ_{B} and $\sigma_{(\mathrm{B})ij}$, only depend on the time coordinate. Although background quantities in LTB spacetimes are functions of the time

and the radial coordinate in general, we neglected the radial dependence of them by applying the local approximation in § 5.1. This is a main point of our approximation to the Newtonian structure formation in the LTB cosmological model.

5.3.2 Evolution of vorticity fields

We solve the linear perturbation equations (5.103a)–(5.103e). First, we consider the vorticity $\omega_{ij}^{\rm N}$. From Eq. (5.103d), we can see that the vorticity is decoupled to other perturbation quantities. This is because the vorticity of the background is zero as shown in Eq. (5.99). By using Eqs. (5.97) and (5.98), the evolution equation (5.103d) is written as

$$\frac{d}{dt}\tilde{\omega}_{12}^{\rm N} = -\left(H_{\parallel}^{\rm L}(t)+H_{\perp}^{\rm L}(t)\right)\tilde{\omega}_{12}^{\rm N}, \tag{5.104}$$

$$\frac{d}{dt}\tilde{\omega}_{13}^{\rm N} = -\left(H_{\parallel}^{\rm L}(t)+H_{\perp}^{\rm L}(t)\right)\tilde{\omega}_{13}^{\rm N}, \tag{5.105}$$

$$\frac{d}{dt}\tilde{\omega}_{23}^{\rm N} = -2H_{\perp}^{\rm L}(t)\tilde{\omega}_{23}^{\rm N}. \tag{5.106}$$

By solving Eqs. (5.104) and (5.105), we obtain

$$\tilde{\omega}_{12}^{\rm N}(t,\mathbf{k}) = \frac{C_{12}(\mathbf{k})}{a_{\parallel}^{\rm L}(t)a_{\perp}^{\rm L}(t)}, \quad \text{and} \quad \tilde{\omega}_{13}^{\rm N}(t,\mathbf{k}) = \frac{C_{13}(\mathbf{k})}{a_{\parallel}^{\rm L}(t)a_{\perp}^{\rm L}(t)}, \tag{5.107}$$

where C_{12} and C_{13} are arbitrary functions of k^i. Similarly, by solving Eq. (5.106), we obtain

$$\tilde{\omega}_{23}^{\rm N}(t,\mathbf{k}) = \frac{C_{23}(\mathbf{k})}{\left(a_{\perp}^{\rm L}(t)\right)^2}, \tag{5.108}$$

where C_{23} is an arbitrary function of k^i. From the solutions (5.107) and (5.108), we can see that the vorticity decays as time grows, since both scale factors grows as time grows in the LTB universe model. In the case of FLRW cosmological models, it is known that the linear vorticity decays as $\omega_{ij} \propto a^{-2}(t)$. Since the evolution of scale factors in the LTB models is significantly different from that in the FLRW models, we conclude that the evolution of the linear vorticity fields in the LTB models differs from that in the homogeneous and isotropic universes.

Here, we note that the vorticity corresponds to the vector mode of the 3-velocity. As is well known, the irreducible scalar and vector decomposition of v^i is given as

$$v^i = \frac{\partial}{\partial x^i}S + V^i; \quad \text{where} \quad \frac{\partial}{\partial x^i}V^i = 0. \tag{5.109}$$

By using Eqs. (5.96) and (5.109), we can see that

$$\omega_{ij} = \frac{1}{2}\left(\partial_j V_i - \partial_i V_j\right). \tag{5.110}$$

Thus, we conclude that the vector mode, V^i, of the Newtonian 3-velocity $v^i_{\rm N}$ decays as the universe expands in the LTB cosmological models.

5.3.3 Evolution of density perturbations

As we saw in the previous subsection, the vorticity field is decoupled from other perturbations. By contrast, we can see from Eqs. (5.103a)–(5.103e) that other perturbations, $\delta_{\rm N}$, $\theta_{\rm N}$, $\sigma^{\rm N}_{ij}$ and $\phi_{\rm N}$, are coupled each other. In this subsection, we solve the coupled equations numerically and study the growth of density perturbations. By using Eqs. (5.98) and (5.103a)–(5.103e), we obtain the evolution equations for the density perturbations as

$$\frac{d}{dt}\tilde{\delta}_{\rm N} = -\tilde{\theta}_{\rm N}, \tag{5.111}$$

$$\frac{d}{dt}\tilde{\theta}_{\rm N} = -\frac{2}{3}\theta_{\rm B}\tilde{\theta}_{\rm N} - 3\sigma^{\rm B}_{11}\tilde{\sigma}^{\rm N}_{11} - 4\pi G\rho_{\rm B}\tilde{\delta}_{\rm N}, \tag{5.112}$$

$$\frac{d}{dt}\tilde{\sigma}^{\rm N}_{11} = -\frac{2}{3}\sigma^{\rm B}_{11}\tilde{\theta}_{\rm N} - \frac{2}{3}\theta_{\rm B}\tilde{\sigma}^{\rm N}_{11} - \sigma^{\rm B}_{11}\tilde{\sigma}^{\rm N}_{11} - 4\pi G\rho_{\rm B}\left(\mu^2 - \frac{1}{3}\right)\tilde{\delta}_{\rm N}, \tag{5.113}$$

where μ is defined as $\mu = k^1/k$. We can obtain the perturbations $\delta_{\rm N}$, $\theta_{\rm N}$ and $\sigma^{\rm N}_{11}$ by solving a set of the coupled equations (5.111), (5.112) and (5.113). Once $\delta_{\rm N}$, $\theta_{\rm N}$ and $\sigma^{\rm N}_{11}$ are obtained, other components of the shear $\sigma^{\rm N}_{ij}$ and the Newtonian potential $\phi_{\rm N}$ can be determined through Eqs. (5.103c) and (5.103e).

To solve the ordinary differential equations (5.111), (5.112) and (5.113), we assume the initial conditions as follows. We consider a huge void universe model which has the uniform Big-Bang time $t_{\rm B}(r) = 0$ and approaches to the Einstein de-Sitter universe model at $r \to \infty$. Then we assume the power spectrum of perturbations in a huge void model is same to that in the Einstein de-Sitter universe model at sufficiently early time. By neglecting the decaying mode for perturbations, we set the initial conditions as

$$\tilde{\delta}_{\rm N}(t_{\rm i}, \mathbf{k}) = t_{\rm i}^{2/3}\delta^{\rm i}(\mathbf{k}), \tag{5.114}$$

$$\tilde{\theta}_{N}(t_{\rm i}, \mathbf{k}) = -\frac{2}{3}t_{\rm i}^{-1/3}\delta^{\rm i}(\mathbf{k}), \tag{5.115}$$

$$\tilde{\sigma}_{N11}(t_{\rm i}, \mathbf{k}) = -\frac{2}{3}t_{\rm i}^{-1/3}\left(\mu^2 - \frac{1}{3}\right)\delta^{\rm i}(\mathbf{k}), \tag{5.116}$$

where $t_{\rm i}$ denotes the initial time, and $\delta^{\rm i}(\mathbf{k})$ represents the density perturbation at the initial time and has the stochastic property

$$\langle \delta^{\rm i}(\mathbf{k})\delta^{\rm i}(\mathbf{k}')\rangle = P(k)\delta^3_{\rm D}(\mathbf{k} - \mathbf{k}'), \tag{5.117}$$

where $\delta_{\rm D}$ denotes the Dirac's delta function, and $P(k)$ represents the power spectrum defined in Eq. (4.6). From Eqs. (5.111)–(5.113) and the conditions (5.114)–(5.116), the density perturbation can be described as

$$\tilde{\delta}_{\rm N}(t, \mathbf{k}) \;=\; D^{+}(t, \mu)\delta^{\rm i}(\mathbf{k}), \tag{5.118}$$

where we defined $D^{+}(t, \mu)$ as a growth factor of the density perturbations in the LTB model. The μ dependence of the growth factor comes from the term of the right hand side in Eq. (5.113). Since the evolution of the shear perturbation $\sigma^{\rm N}_{11}$ depends on μ and the density perturbation couples to the shear perturbation $\sigma^{\rm N}_{11}$ due to the existence of $\sigma^{\rm B}_{11}$, we can see that the μ dependence of the growth factor is originally from the anisotropy of the volume expansion, that is, the existence of the background shear.

Here, we recall that we have a parameter r_0 for the background quantities in the local approximation, that is, $\rho_{\rm B}(t) = \rho_{\rm B}(t; r_0)$ and $H^{\rm B}_{\parallel,\perp}(t) = H^{\rm B}_{\parallel,\perp}(t; r_0)$. Thus, the growth factor defined in Eq. (5.118) should be represented as

$$\tilde{\delta}_{\rm N}(t, \mathbf{k}; r_0) \;=\; D^{+}(t, \mu; r_0)\delta^{\rm i}(\mathbf{k}). \tag{5.119}$$

The r_0 dependence of the growth factor comes from the radial inhomogeneity of the background LTB cosmological models.

In order to study the evolution of growth factors $D^{+}(t, \mu; r_0)$, we consider a toy LTB model that has the uniform Big-Bang time and the density-parameter function $\Omega_{\rm M}(r)$ defined in Eq. (2.16) is given as

$$\Omega_{\rm M}(r) = \Omega_{\rm out} - (\Omega_{\rm out} - \Omega_{\rm in})\, e^{-r^2/(2\sigma^2)}, \tag{5.120}$$

where $\Omega_{\rm out} = 1.0$, $\Omega_{\rm in} = 0.3$ and $\sigma = 0.5$. In fig. 5.2, we plot the energy density divided by its value at the center in a toy LTB model on the spacelike hypersurface for $t = t_0$ as a function of the radial coordinate. We can see that a toy model has a void structure whose size is about $0.7\, r/(ct_0)$ and amplitude becomes nonlinear at the present time. The vicinity of the center is locally the dust filled FLRW model with the cosmological parameter $\Omega_{\rm M} = 0.3$, whereas the asymptotic region is almost the same as the dust filled FLRW model with $\Omega_{\rm M} = 1.0$. In fig. 5.3, we plot the Hubble functions, $H_{\parallel}(t, r)$ and $H_{\perp}(t, r)$, in a toy LTB model on the spacelike hypersurface for $t = t_0$ as functions of the radial coordinate. From fig. 5.3, we can see that The Hubble functions at the center is larger than those at off central region, since the matter density at the center is least. In fig. 5.4, we plot the normalized shear, $\Delta_{\sigma}(t, r)$ defined in Eq. (2.22), in a toy LTB model on the spacelike hypersurfaces for $t = t_0$, as a function of r. From fig. 5.4, we can see that the peak position of the normalized shear is located around the edge of the void structure.

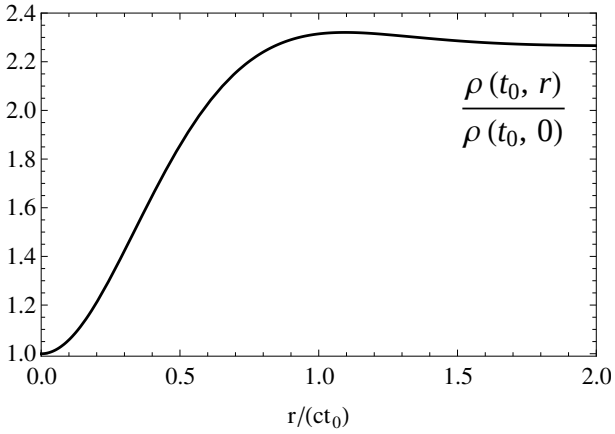

Figure 5.2: The energy density in a toy LTB model on the spacelike hypersurface for $t = t_0$ as a function of the radial coordinate.

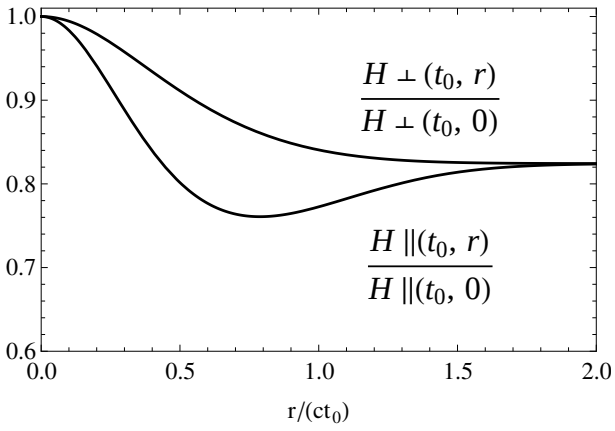

Figure 5.3: The Hubble functions, $H_{\parallel}(t, r)$ and $H_{\perp}(t, r)$, in a toy LTB model on the spacelike hypersurface for $t = t_0$ as functions of the radial coordinate.

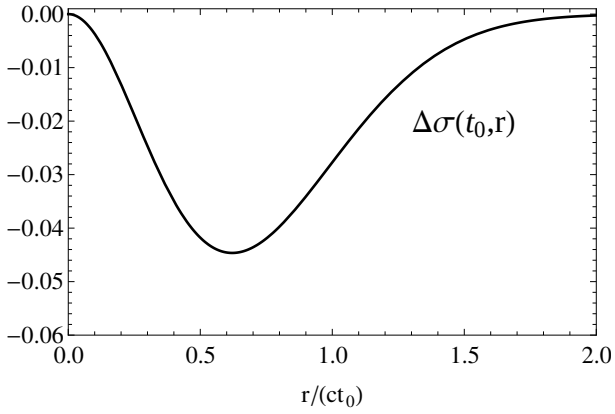

Figure 5.4: The normalized shear, $\Delta_\sigma(t, r)$, in a toy LTB model on the spacelike hypersurfaces for $t = t_0$, as a function of r.

By numerically solving the perturbation equations (5.111)–(5.113) with the initial conditions (5.114)–(5.116) for the LTB model (5.120), we obtained the growth factors $D^+(t, \mu; r_0)$ in the LTB model. In fig. 5.5, we plot the growth factors, $D^+(t, \mu; r_0)$, at $r_0 = 0.6c^{-1}t_0^{-1}$ as functions on μ on $t = 0.01t_0$, $t = 0.5t_0$ and $t = t_0$. From fig 5.5, we can see that the anisotropy of the growth factor, that

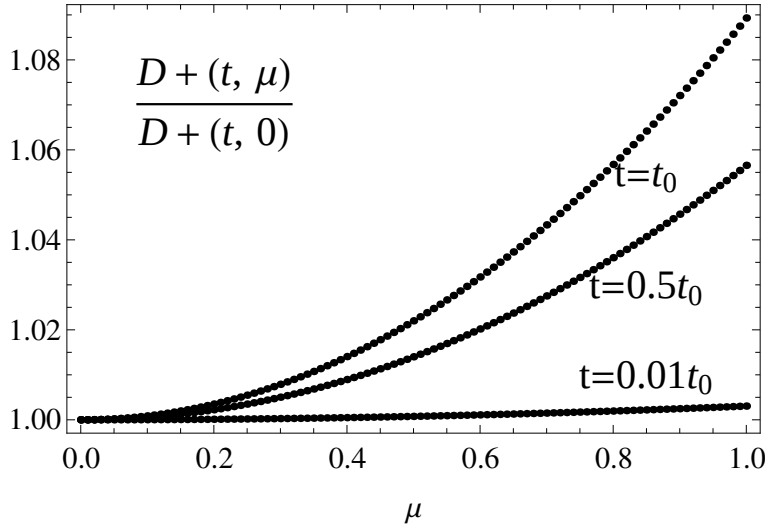

Figure 5.5: The growth factors, $D^+(t, \mu; r_0)$, in a toy LTB model at $r_0 = 0.6$ as functions on μ on $t = 0.01t_0$, $t = 0.5t_0$ and $t = t_0$.

is, the μ dependence of the growth factors, grows as time grows. At the present time, the anisotropy of the growth factor is about 10%. Thus, we conclude that non-negligible effects on the anisotropy for the growth factors appear in a typical

void universe model. From fig 5.5, we can also see that the growth factors of $\mu = 1$ is larger that that of $\mu = 0$. This means that the growth of density perturbations in the radial direction for the central observer is faster than that in the transverse direction. This is because that the volume expansion rate of the radial direction, $H_{\parallel}$, which disturbs the growth of structures is smaller than that of the transverse direction, $H_{\perp}$, in the LTB model (see fig. 5.4). In fig. 5.6, we plot the growth factors, $D^{+}(t, \mu; r_0)$, for $\mu = 0$ as functions of t/t_0 at $r_0 = 0$, $r_0 = 0.4c^{-1}t_0^{-1}$, $r_0 = 0.8c^{-1}t_0^{-1}$ and $r_0 = 1.2c^{-1}t_0^{-1}$. From fig 5.6, we can see that the speed of growth is an increas-

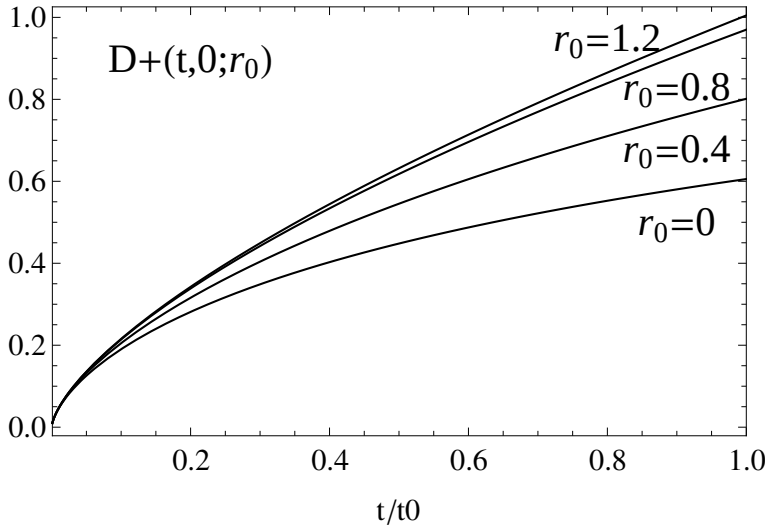

Figure 5.6: The growth factors, $D^{+}(t, \mu; r_0)$, for $\mu = 0$ in a toy LTB model as functions of t/t_0 at $r_0 = 0$, $r_0 = 0.4c^{-1}t_0^{-1}$, $r_0 = 0.8c^{-1}t_0^{-1}$ and $r_0 = 1.2c^{-1}t_0^{-1}$.

ing function of the radial distance from the center of the void. This can be explained by the fact that the background matter density in the void model is a monotonically increasing function of r, because the growth rates of perturbations in dust-FLRW models are monotonically increasing function of Ω_{M}.

5.4 Conclusion and Discussion

We have studied a Newtonian self-gravitating system in the LTB cosmological models by applying a local approximation to the background LTB models and a Cosmological Newtonian approximation to the perturbations. First, we introduced a local approximation which is applicable to a small spatial region in the universe based on the Fermi-normal coordinate expansion. Then, we have shown that the background LTB models can be reduced to a locally homogeneous and anisotropic dust universe

under the local approximation from Eqs. (5.39)–(5.41). This result shows that a local FLRW approximation in which sufficiently small region is assumed to be the same as the FLRW universe is not applicable to the LTB cosmological models.

Next, we have added Newtonian inhomogeneities in the LTB models under the local approximation. By using a Cosmological Newtonian approximation which is characterized by two small expansion parameters, ϵ and κ, defined in Eq. (5.1), we derived Newtonian hydrodynamical equations of a self-gravitating system in the LTB models for the first time in Eqs. (5.80a)–(5.80c). We expect that the evolution of Newtonian structures in the LTB models can significantly differ from that in the homogeneous and isotropic universes, because the anisotropy of the background volume expansion appears in the derived equations. We expect that the derived equations can be used to a N-body numerical simulation in the LTB cosmological models. If we solve the numerical simulation and compare the results with observations of galaxy distributions, we may give a strong constraint to non-Copernican cosmological models from cosmic structure formation at subhorizon scales. We leave it for a future work.

We have linearized the derived Newtonian equations about the perturbations. Thanks to the local approximation, the linearized equations are reduced to a set of ordinary differential equations in a decoupled form for each Fourier modes as shown in Eqs. (5.103a)–(5.103e). Since relativistic linear perturbation equations in the LTB models cannot be reduced to a set of ordinary differential equations as discussed in § 3.1, we conclude that our approximation scheme developed here simplified perturbation equations to a form of easy to handle. Then we solved the linear perturbation equations numerically, and revealed the evolution of vorticity fields and density perturbations. We have shown that the vorticity fields decays as the universe expands, and this means the vector mode in the Newtonian perturbations only contains the decaying mode. Since the weak lensing B-mode discussed in Chap. 1 is produced only by the vector mode in the Newtonian approximation, we expect that the B-mode in the LTB cosmological models is quite small at small scales. The analysis of gravitational weak lensing based on our approach is left for a future work.

We have found that the growth factor of density perturbations significantly depends on the direction of the wave vector of perturbations, μ, and the radial coordinate of the LTB models, r_0.as shown in figs. 5.5 and 5.6. We have shown that the μ dependence reflects of the anisotropic volume expansion and the r_0 dependence is a result of the radial inhomogeneity of a huge void. These properties of the evolution of density perturbations are consistent with the results obtained in Chap 4. Since

the growth factor in the FLRW models is only a function of t, the μ-dependence and r_0-dependence of the growth factor in the LTB models can become a strong discriminator for these two models.

Here, we should mention about a geometric approximation which was discussed in Chap. 1 for the BAO scales. We showed that perturbations of each Fourier modes in the comoving coordinate (5.81) are decoupled each other. This means the wavelength of each modes expands following the volume expansion. Therefore, our result shows that the geometric approximation is applicable to the cosmic structures at subhorizon scales, includes the BAO scales. By using our analysis, we can test the LTB cosmological models through observations of the BAO scales. This is left for a future work.

In Chap. 3 and Chap. 4, we studied relativistic linear perturbations in the LTB cosmological models, by restricting ourselves to the linearized LTB model which is described by a dust-FLRW universe with an isotropic linear perturbation. Thus, the analysis developed in Chap. 3 cannot be applied for LTB cosmological models that have nonlinear spherical inhomogeneity, although many LTB cosmological models proposed as an alternative to Dark Energy have nonlinear inhomogeneity at the present time as shown in § 2.2. By contrast, a method developed in this chapter can be used for perturbations in non-linear LTB cosmological models, as long as the wavelength of perturbations is so small that the Cosmological Newtonian approximation is applicable.

Here, we discuss a relation between the analysis for perturbations developed in Chap. 3 and that in this chapter. In fig. 5.7, we showed a schematic picture representing the relation between the two independent approaches. Here, $\mathcal{A}$ denotes the amplitude of radial inhomogeneity which exists in the background LTB model, and $\lambda/\mathcal{R}$ denotes the ratio between the wavelength of perturbations and the curvature radius of the background LTB model. Region 1 (dotted line) in fig. 5.7 shows a region that the analysis proposed in Chap. 3 can cover, where the inhomogeneity of the LTB model is small ($\mathcal{A} \ll 1$) and the linearized LTB model is applicable. Region 2 (dashed line) shows a region that the analysis proposed in this chapter can cover, where the wavelength of perturbations is much smaller than the curvature radius ($\lambda \ll \mathcal{R}$) and the Newtonian approximation is applicable, and the local approximation can be used for the background LTB model. From fig. 5.7, we can see that there exists a region covered by both Region 1 and Region 2, where the wavelength of fluctuations is small ($\lambda \ll \mathcal{R}$) and the background inhomogeneity is small ($\mathcal{A} \ll 1$). We have shown that in such a region the growth of density perturbations obtained by the analysis in Region 2 is consistent with that in Region

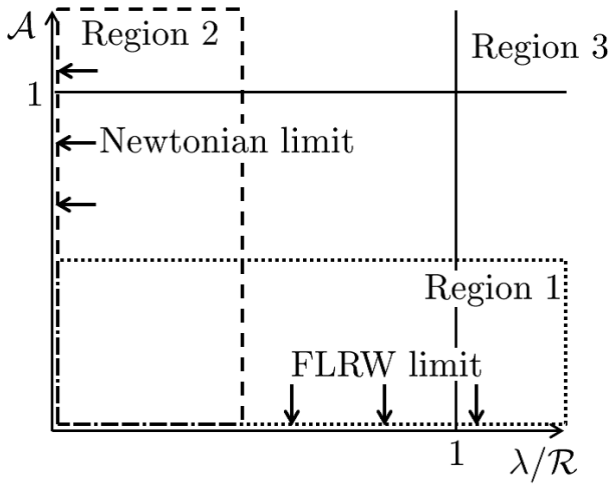

Figure 5.7: A schematic picture representing a relation between the analysis for perturbations developed in Chap. 3 and that in this chapter, where $\mathcal{A}$, λ and $\mathcal{R}$ denote the amplitude of inhomogeneity of the LTB background, the wavelength of perturbations and the curvature radius of the LTB background. Region 1 (dotted line) and Region 2 (dashed line) represent regions covered by the analysis proposed in Chap. 3 and this chapter, respectively.

1. From fig. 5.7, we can see that Region 3 is an uncovered region by our methods, where the system is composed of relativistic perturbations in the highly non-linear LTB models. Analysis of perturbations in Region 3 seems to be more difficult, and we leave it for a future work.

Chapter 6

Summary

In this thesis, we have studied the evolution of cosmic structures in a non-Copernican cosmological model based on cosmological perturbation theory. We have considered a LTB cosmological model which is the most popular model among non-Copernican cosmological models. In Chap. 2, we have summarized physical properties of LTB spacetimes, and given a brief review on LTB cosmological models of a huge void proposed by some authors as an alternative to dark energy.

In Chap. 3, we have studied relativistic linear perturbations in LTB cosmological models. First, we have seen that linear perturbation equations in LTB spacetimes cannot be reduced to a set of ordinary differential equations in a decoupled form, since isometries in LTB spacetimes are less than those in FLRW spacetimes. Then, to avoid the difficulty, we have assumed a LTB cosmological model of which radial inhomogeneity is not so large inside the past light cone of the central observer, and linearized it around a homogeneous and isotropic FLRW model. Then, we have added anisotropic fluctuations with a random phase Gaussian probability distribution which seed all cosmic structures to the linearized LTB model. In this case, linear perturbation equations in a LTB model are reduced to nonlinear perturbation equations in a FLRW universe model. We solved the nonlinear perturbation equations up to the second order, and obtained anisotropic density fluctuations. We have compared our approximation method with an approximation scheme used in a paper by February, Clarkson and Maartens (FCM) [88]. We have shown that metric perturbations $\tilde{\chi}$ and $\tilde{\varsigma}$, which are assumed to be zero in FCM, do not decay as time grows at the second order of our expansion method. This suggests that FCM's assumption of $\tilde{\chi} = \tilde{\varsigma} = 0$ is not applicable at late times, where cosmic structures are well developed.

In Chap. 4, we have studied stochastic properties of anisotropic density perturbations obtained in Chap. 3. We have computed the two-point correlation function

of the density perturbations in a huge void model, and shown that it has the distortion coming from the tidal field of LTB cosmological models. Then we have shown that the distortion of the two-point correlation function has a non-negligible effect both for the real space and the redshift space galaxy distributions in the off-center region of LTB models. Thus, observations of galaxy clustering such as Redshift Space Distortions may give a strong constraint for non-Copernican cosmological models. We have computed the angular power spectrum of density perturbations in the Clarkson-Regis void model, and have shown that the angular growth rates are significantly different from those in the ΛCDM model even for low redshifts. This implies that we can test the void model by observing of the angular growth rates.

In Chap. 5, we have considered nonlinear structure formation at subhorizon scales in the LTB cosmological model of a huge void. First, by applying the local approximation to the LTB model based on the Fermi-normal coordinate expansion, we have shown that the LTB model can be considered as a locally homogeneous and anisotropic universe of a dust fluid. Then, by using the Cosmological Newtonian approximation to perturbations, we have derived equations of non-relativistic hydrodynamics and Newtonian gravity for perturbations in a locally homogeneous and anisotropic universe. The derived equations govern Newtonian self-gravitating system in the LTB cosmological model, and enable us to study numerical N-body simulation in these models. Then, we analyzed linear perturbations of the Newtonian structure formation, and showed that the local anisotropy of volume expansion in the LTB model significantly affects to the density perturbations at small scales. Our result suggests that observations involved in the Newtonian structure formation at small scales, such as dark halos and galaxies, can be used as a test of non-Copernican cosmological models.

References

[1] G. F. R. Ellis, "Cosmology and verifiability," Q. Jl. astr. Soc. **16**, 245 (1975).

[2] G. F. R. Ellis, "Cosmology and verifiability," Gen. Rel. Grav. **11**, 281 (1979).

[3] C. Clarkson and R. Maartens, "Inhomogeneity and the foundations of concordance cosmology," Class. Quant. Grav. **27**, 124008 (2010) [arXiv:1005.2165 [astro-ph.CO]].

[4] G. F. R. Ellis, "Inhomogeneity effects in Cosmology," arXiv:1103.2335 [astro-ph.CO].

[5] R. Maartens, "Is the Universe homogeneous?," Phil. Trans. Roy. Soc. Lond. A **369**, 5115 (2011) [arXiv:1104.1300 [astro-ph.CO]].

[6] C. Clarkson, B. Bassett and T. H. -C. Lu, "A general test of the Copernican Principle," Phys. Rev. Lett. **101**, 011301 (2008) [arXiv:0712.3457 [astro-ph]].

[7] J. Goodman, "Geocentrism reexamined," Phys. Rev. D **52**, 1821 (1995) [astro-ph/9506068].

[8] J. -P. Uzan, C. Clarkson and G. F. R. Ellis, "Time drift of cosmological redshifts as a test of the Copernican principle," Phys. Rev. Lett. **100**, 191303 (2008) [arXiv:0801.0068 [astro-ph]].

[9] G. Lemaitre, Gen. Rel. Grav. **29** (1997), 641.

[10] R. C. Tolman, Proc. Nat. Acad. Sci. **20** (1934), 169.

[11] H. Bondi, Mon. Not. R. Astron. Soc. **107** (1947), 410.

[12] H. Alnes and M. Amarzguioui, "CMB anisotropies seen by an off-center observer in a spherically symmetric inhomogeneous Universe," Phys. Rev. D **74**, 103520 (2006) [arXiv:astro-ph/0607334].

[13] H. Kodama, K. Saito and A. Ishibashi, "Analytic formulae for the off-center CMB anisotropy in a general spherically symmetric universe," Prog. Theor. Phys. **124**, 163 (2010) [arXiv:1004.3089 [astro-ph.CO]].

[14] A. G. Riess *et al.* [Supernova Search Team Collaboration], "Observational evidence from supernovae for an accelerating universe and a cosmological constant," Astron. J. **116**, 1009 (1998) [astro-ph/9805201].

[15] S. Perlmutter *et al.* [Supernova Cosmology Project Collaboration], "Measurements of Omega and Lambda from 42 high redshift supernovae," Astrophys. J. **517**, 565 (1999) [astro-ph/9812133].

[16] R. A. Knop *et al.* [Supernova Cosmology Project Collaboration], "New constraints on Omega(M), Omega(lambda), and w from an independent set of eleven high-redshift supernovae observed with HST," Astrophys. J. **598**, 102 (2003) [astro-ph/0309368].

[17] A. G. Riess *et al.* [Supernova Search Team Collaboration], "Type Ia supernova discoveries at $z > 1$ from the Hubble Space Telescope: Evidence for past deceleration and constraints on dark energy evolution," Astrophys. J. **607**, 665 (2004) [astro-ph/0402512].

[18] P. Bull and T. Clifton, "Local and non-local measures of acceleration in cosmology," Phys. Rev. D **85**, 103512 (2012) [arXiv:1203.4479 [astro-ph.CO]].

[19] M. N. Celerier, "Do we really see a cosmological constant in the supernovae data?," Astron. Astrophys. **353**, 63 (2000) [arXiv:astro-ph/9907206].

[20] M. N. Celerier, K. Bolejko and A. Krasinski, "A (giant) void is not mandatory to explain away dark energy with a Lemaitre – Tolman model," Astron. Astrophys. **518**, A21 (2010) [arXiv:0906.0905 [astro-ph.CO]].

[21] T. Clifton, P. G. Ferreira and K. Land, "Living in a Void: Testing the Copernican Principle with Distant Supernovae," Phys. Rev. Lett. **101**, 131302 (2008) [arXiv:0807.1443 [astro-ph]].

[22] S. P. Goodwin, P. A. Thomas, A. J. Barber, J. Gribbin and L. I. Onuora, "The local to global H_0 ratio and the SNe Ia results," arXiv:astro-ph/9906187.

[23] H. Iguchi, T. Nakamura and K. i. Nakao, "Is dark energy the only solution to the apparent acceleration of the present universe?," Prog. Theor. Phys. **108**, 809 (2002) [arXiv:astro-ph/0112419].

[24] E. W. Kolb and C. R. Lamb, "Light-cone observations and cosmological models: implications for inhomogeneous models mimicking dark energy," arXiv:0911.3852 [astro-ph.CO].

[25] N. Mustapha, C. Hellaby, G. F. R. Ellis, "Large scale inhomogeneity versus source evolution: Can we distinguish them observationally?," Mon. Not. Roy. Astron. Soc. **292**, 817-830 (1997). [gr-qc/9808079].

[26] K. Tomita, "Distances and lensing in cosmological void models," Astrophys. J. **529**, 38 (2000) [arXiv:astro-ph/9906027].

[27] K. Tomita, "A local void and the accelerating universe," Mon. Not. Roy. Astron. Soc. **326**, 287 (2001) [arXiv:astro-ph/0011484].

[28] K. Tomita, "Analyses of type Ia supernova data in cosmological models with a local void," Prog. Theor. Phys. **106**, 929 (2001) [arXiv:astro-ph/0104141].

[29] R. A. Vanderveld, E. E. Flanagan and I. Wasserman, "Mimicking dark energy with Lemaitre-Tolman-Bondi models: Weak central singularities and critical points," Phys. Rev. D **74**, 023506 (2006) [arXiv:astro-ph/0602476].

[30] C. M. Yoo, T. Kai and K. i. Nakao, "Solving Inverse Problem with Inhomogeneous Universe," Prog. Theor. Phys. **120**, 937 (2008) [arXiv:0807.0932 [astro-ph]].

[31] C. -M. Yoo, "A Note on the Inverse Problem with LTB Universes," Prog. Theor. Phys. **124**, 645-665 (2010). [arXiv:1010.0530 [astro-ph.CO]].

[32] S. Alexander, T. Biswas, A. Notari and D. Vaid, "Local Void vs Dark Energy: Confrontation with WMAP and Type Ia Supernovae," JCAP **0909**, 025 (2009) [arXiv:0712.0370 [astro-ph]].

[33] H. Alnes, M. Amarzguioui and O. Gron, "An inhomogeneous alternative to dark energy?," Phys. Rev. D **73**, 083519 (2006) [arXiv:astro-ph/0512006].

[34] T. Biswas, A. Notari and W. Valkenburg, "Testing the Void against Cosmological data: fitting CMB, BAO, SN and H0," JCAP **1011**, 030 (2010) [arXiv:1007.3065 [astro-ph.CO]].

[35] K. Bolejko and J. S. B. Wyithe, "Testing the Copernican Principle Via Cosmological Observations," JCAP **0902**, 020 (2009) [arXiv:0807.2891 [astro-ph]].

[36] C. Clarkson and M. Regis, "The Cosmic Microwave Background in an Inhomogeneous Universe - why void models of dark energy are only weakly constrained by the CMB," JCAP **1102**, 013 (2011) [arXiv:1007.3443 [astro-ph.CO]].

[37] J. Garcia-Bellido and T. Haugboelle, "Confronting Lemaitre-Tolman-Bondi models with Observational Cosmology," JCAP **0804**, 003 (2008) [arXiv:0802.1523 [astro-ph]].

[38] V. Marra and A. Notari, "Observational constraints on inhomogeneous cosmological models without dark energy," arXiv:1102.1015 [astro-ph.CO].

[39] V. Marra and M. Paakkonen, "Observational constraints on the LLTB model," JCAP **1012**, 021 (2010) [arXiv:1009.4193 [astro-ph.CO]].

[40] A. Moss, J. P. Zibin and D. Scott, "Precision Cosmology Defeats Void Models for Acceleration," Phys. Rev. D **83**, 103515 (2011) [arXiv:1007.3725 [astro-ph.CO]].

[41] S. Nadathur and S. Sarkar, "Reconciling the local void with the CMB," Phys. Rev. D **83**, 063506 (2011) [arXiv:1012.3460 [astro-ph.CO]].

[42] C. M. Yoo, K. i. Nakao and M. Sasaki, "CMB observations in LTB universes: Part I: Matching peak positions in the JCAP **1007**, 012 (2010) [arXiv:1005.0048 [astro-ph.CO]].

[43] J. P. Zibin, A. Moss and D. Scott, "Can we avoid dark energy?," Phys. Rev. Lett. **101**, 251303 (2008) [arXiv:0809.3761 [astro-ph]].

[44] J. Garcia-Bellido and T. Haugboelle, "The radial BAO scale and Cosmic Shear, a new observable for Inhomogeneous Cosmologies," JCAP **0909**, 028 (2009) [arXiv:0810.4939 [astro-ph]].

[45] M. Zumalacarregui, J. Garcia-Bellido and P. Ruiz-Lapuente, "Tension in the Void: Cosmic Rulers Strain Inhomogeneous Cosmologies," JCAP **1210**, 009 (2012) [arXiv:1201.2790 [astro-ph.CO]].

[46] P. Bull, T. Clifton and P. G. Ferreira, "The kSZ effect as a test of general radial inhomogeneity in LTB cosmology," arXiv:1108.2222 [astro-ph.CO].

[47] J. Garcia-Bellido and T. Haugboelle, "Looking the void in the eyes - the kSZ effect in LTB models," JCAP **0809**, 016 (2008) [arXiv:0807.1326 [astro-ph]].

[48] A. Moss and J. P. Zibin, "Linear kinetic Sunyaev-Zel'dovich effect and void models for acceleration," arXiv:1105.0909 [astro-ph.CO].

[49] C. M. Yoo, K. i. Nakao and M. Sasaki, "CMB observations in LTB universes: Part II – the kSZ effect in an LTB universe," JCAP **1010**, 011 (2010) [arXiv:1008.0469 [astro-ph.CO]].

[50] P. Zhang and A. Stebbins, "Confirmation of the Copernican principle at Gpc radial scale and above from the kinetic Sunyaev Zel'dovich effect power spectrum," arXiv:1009.3967 [astro-ph.CO].

[51] P. A. R. Ade *et al.* [Planck Collaboration], "Planck intermediate results. XIII. Constraints on peculiar velocities," [arXiv:1303.5090 [astro-ph.CO]].

[52] M. Adachi and M. Kasai, "An analytical approximation of the luminosity distance in flat cosmologies with a cosmological constant," Prog. Theor. Phys. **127**, 145 (2012) [arXiv:1111.6396 [astro-ph.CO]].

[53] H. Alnes and M. Amarzguioui, "The supernova Hubble diagram for off-center observers in a spherically symmetric inhomogeneous Universe," Phys. Rev. D **75**, 023506 (2007) [arXiv:astro-ph/0610331].

[54] K. Bolejko, M. -N. Celerier and A. Krasinski, "Inhomogeneous cosmological models: Exact solutions and their applications," Class. Quant. Grav. **28**, 164002 (2011) [arXiv:1102.1449 [astro-ph.CO]].

[55] K. Bolejko, "Supernovae ia observations in the lemaitre-tolman model," PMC Phys. A **2**, 1 (2008) [arXiv:astro-ph/0512103].

[56] R. R. Caldwell and N. A. Maksimova, "Spectral Distortion in a Radially Inhomogeneous Cosmology," arXiv:1309.4454 [astro-ph.CO].

[57] M. -N. Celerier, "Effects of inhomogeneities on the expansion of the Universe: a challenge to dark energy?," arXiv:1203.2814 [astro-ph.CO].

[58] C. Clarkson, "Establishing homogeneity of the universe in the shadow of dark energy," Comptes Rendus Physique **13**, 682 (2012) [arXiv:1204.5505 [astro-ph.CO]].

[59] R. de Putter, L. Verde and R. Jimenez, "Testing LTB Void Models Without the Cosmic Microwave Background or Large Scale Structure: New Constraints from Galaxy Ages," arXiv:1208.4534 [astro-ph.CO].

[60] P. Dunsby, N. Goheer, B. Osano and J. P. Uzan, "How close can an Inhomogeneous Universe mimic the Concordance Model?," JCAP **1006**, 017 (2010) [arXiv:1002.2397 [astro-ph.CO]].

[61] K. Enqvist, M. Mattsson and G. Rigopoulos, "Supernovae data and perturbative deviation from homogeneity," JCAP **0909**, 022 (2009) [arXiv:0907.4003 [astro-ph.CO]].

[62] K. Enqvist and T. Mattsson, "The effect of inhomogeneous expansion on the supernova observations," JCAP **0702**, 019 (2007) [arXiv:astro-ph/0609120].

[63] H. Goto and H. Kodama, "The Gravitational Lensing Effect on the CMB Polarisation Anisotropy in the Lambda-LTB Model," Prog. Theor. Phys. **125**, 815 (2011) [arXiv:1101.0476 [astro-ph.CO]].

[64] A. F. Heavens, R. Jimenez and R. Maartens, "Testing homogeneity with the fossil record of galaxies," JCAP **1109**, 035 (2011) [arXiv:1107.5910 [astro-ph.CO]].

[65] M. Quartin and L. Amendola, "Distinguishing Between Void Models and Dark Energy with Cosmic Parallax and Redshift Drift," Phys. Rev. D **81**, 043522 (2010) [arXiv:0909.4954 [astro-ph.CO]].

[66] M. Regis and C. Clarkson, "Do primordial Lithium abundances imply there's no Dark Energy?," arXiv:1003.1043 [astro-ph.CO].

[67] A. E. Romano, "Mimicking the cosmological constant for more than one observable with large scale inhomogeneities," Phys. Rev. D **82**, 123528 (2010) [arXiv:0912.4108 [astro-ph.CO]].

[68] A. E. Romano, M. Sasaki and A. A. Starobinsky, "Effects of inhomogeneities on apparent cosmological observables: 'fake" evolving dark energy," arXiv:1006.4735 [astro-ph.CO].

[69] A. E. Romano and P. Chen, "Corrections to the apparent value of the cosmological constant due to local inhomogeneities," JCAP **1110**, 016 (2011) [arXiv:1104.0730 [astro-ph.CO]].

[70] M. Tanimoto, Y. Nambu and K. Iwata, "The Role of Anisotropy in the Void Models without Dark Energy," arXiv:0906.4857 [astro-ph.CO].

[71] K. Tomita, "On astrophysical explanations due to cosmological inhomogeneities for the observational acceleration," arXiv:0906.1325 [astro-ph.CO].

[72] K. Yagi, A. Nishizawa and C. -M. Yoo, "Probing the Inhomogeneous Universe with Gravitational Wave Cosmology," J. Phys. Conf. Ser. **363**, 012056 (2012) [arXiv:1204.1670 [astro-ph.CO]].

[73] J. P. Zibin, "Can decaying modes save void models for acceleration?," arXiv:1108.3068 [astro-ph.CO].

[74] P. Mishra, M. -N. Celerier and T. P. Singh, "Redshift drift as a test for discriminating between different cosmological models," arXiv:1206.6026 [astro-ph.CO].

[75] C. M. Yoo, T. Kai and K. i. Nakao, "Redshift Drift in LTB Void Universes," Phys. Rev. D **83**, 043527 (2011) [arXiv:1010.0091 [astro-ph.CO]].

[76] A. D. Linde, D. A. Linde and A. Mezhlumian, "Do we live in the center of the world?," Phys. Lett. B **345**, 203 (1995) [hep-th/9411111].

[77] W. Valkenburg, M. Kunz and V. Marra, "Intrinsic uncertainty on the nature of dark energy," arXiv:1302.6588 [astro-ph.CO].

[78] W. Valkenburg, V. Marra and C. Clarkson, "Testing the Copernican principle by constraining spatial homogeneity," arXiv:1209.4078 [astro-ph.CO].

[79] C. Blake, T. Davis, G. Poole, D. Parkinson, S. Brough, M. Colless, C. Contreras and W. Couch *et al.*, "The WiggleZ Dark Energy Survey: testing the cosmological model with baryon acoustic oscillations at z=0.6," Mon. Not. Roy. Astron. Soc. **415**, 2892 (2011) [arXiv:1105.2862 [astro-ph.CO]].

[80] N. Kaiser, "Clustering in real space and in redshift space," Mon. Not. Roy. Astron. Soc. **227**, 1 (1987).

[81] A. J. S. Hamilton, "Linear redshift distortions: A Review," astro-ph/9708102.

[82] S. Tsujikawa, A. De Felice and J. Alcaniz, "Testing for dynamical dark energy models with redshift-space distortions," JCAP **1301**, 030 (2013) [arXiv:1210.4239 [astro-ph.CO]].

[83] L. Fu, E. Semboloni, H. Hoekstra, M. Kilbinger, L. van Waerbeke, I. Tereno, Y. Mellier and C. Heymans *et al.*, "Very weak lensing in the CFHTLS Wide: Cosmology from cosmic shear in the linear regime," Astron. Astrophys. **479**, 9 (2008) [arXiv:0712.0884 [astro-ph]].

[84] U.H. Gerlach and U.K. Sengupta, "Gauge-invariant perturbations on most general spherically symmetric space-times" Phys. Rev. D **19**, 2268 (1979).

[85] D. Alonso, J. Garcia-Bellido, T. Haugboelle and A. Knebe, "Halo abundances and shear in void models," arXiv:1204.3532 [astro-ph.CO].

[86] D. Alonso, J. Garcia-Bellido, T. Haugbolle and J. Vicente, "Large scale structure simulations of inhomogeneous LTB void models," Phys. Rev. D **82**, 123530 (2010) [arXiv:1010.3453 [astro-ph.CO]].

[87] C. Clarkson, T. Clifton and S. February, "Perturbation Theory in Lemaitre-Tolman-Bondi Cosmology," JCAP **0906**, 025 (2009) [arXiv:0903.5040 [astro-ph.CO]].

[88] S. February, C. Clarkson and R. Maartens, "Galaxy correlations and the BAO in a void universe: structure formation as a test of the Copernican Principle," arXiv:1206.1602 [astro-ph.CO].

[89] S. February, J. Larena, C. Clarkson and D. Pollney, "Evolution of linear perturbations in spherically symmetric dust models," arXiv:1311.5241 [astro-ph.CO].

[90] J. P. Zibin, "Scalar Perturbations on Lemaitre-Tolman-Bondi Spacetimes," Phys. Rev. D **78**, 043504 (2008) [arXiv:0804.1787 [astro-ph]].

[91] E. Bertschinger and A. J. S. Hamilton, "Lagrangian evolution of the Weyl tensor," Astrophys. J. **435**, 1 (1994) [astro-ph/9403016].

[92] R. Nishikawa, C. -M. Yoo and K. -i. Nakao, "Evolution of density perturbations in large void universe," Phys. Rev. D **85**, 103511 (2012) [arXiv:1202.1582 [astro-ph.CO]].

[93] R. Nishikawa, C. -M. Yoo and K. -i. Nakao, "Two-point correlation function of density perturbations in a large void universe," Phys. Rev. D **88**, 123520 (2013) [arXiv:1306.5131 [astro-ph.CO]].

[94] R. Nishikawa, C. -M. Yoo and K. -i. Nakao, in preparation.

[95] G. F. R. Ellis and H. van Elst, "Cosmological models: Cargese lectures 1998," NATO Adv. Study Inst. Ser. C. Math. Phys. Sci. **541**, 1 (1999) [gr-qc/9812046].

[96] R. Maartens, T. Gebbie and G. F. R. Ellis, "Covariant cosmic microwave background anisotropies. 2. Nonlinear dynamics," Phys. Rev. D **59**, 083506 (1999) [astro-ph/9808163].

[97] C. G. Tsagas, A. Challinor and R. Maartens, "Relativistic cosmology and large-scale structure," Phys. Rept. **465**, 61 (2008) [arXiv:0705.4397 [astro-ph]].

[98] H. van Elst and C. Uggla, "General relativistic (1+3) orthonormal frame approach revisited," Class. Quant. Grav. **14**, 2673 (1997) [gr-qc/9603026].

[99] K. Tomita, "Non-Linear Theory of Gravitational Instability in the Expanding Universe," Prog. Theor. Phys. **37**, 831 (1967)

[100] T. Matsubara, "The Correlation function in redshift space: General formula with wide angle effects and cosmological distortions," [astro-ph/9908056].

[101] D. J. Eisenstein and W. Hu, "Baryonic features in the matter transfer function," Astrophys. J. **496**, 605 (1998) [arXiv:astro-ph/9709112].

[102] N. Kaiser, "Clustering in real space and in redshift space," Mon. Not. Roy. Astron. Soc. **227**, 1 (1987).

[103] T. Matsubara and Y. Suto, "Cosmological redshift distortion of correlation functions as a probe of the density parameter and the cosmological constant," Astrophys. J. **470**, L1 (1996) [astro-ph/9604142].

[104] L. Guzzo *et al.*, "A test of the nature of cosmic acceleration using galaxy redshift Nature **451**, 541 (2008) [arXiv:0802.1944 [astro-ph]].

[105] C. Blake, S. Brough, M. Colless, C. Contreras, W. Couch, S. Croom, T. Davis and M. J. Drinkwater *et al.*, "The WiggleZ Dark Energy Survey: the growth rate of cosmic structure since redshift z=0.9," Mon. Not. Roy. Astron. Soc. **415**, 2876 (2011) [arXiv:1104.2948 [astro-ph.CO]].

[106] D. H. Lyth and A. R. Liddle, "The primordial density perturbation: cosmology, inflation and the origin of structure," Cambridge University Press, U.K. (2009) 156 p.

[107] P. J. E. Peebles, "The Large-Scale Structure of the Universe," (Princeton University Press, Princeton, 1980).

[108] M. Ishii, M. Shibata and Y. Mino, "Black hole tidal problem in the Fermi normal coordinates," Phys. Rev. D **71**, 044017 (2005) [gr-qc/0501084].

[109] T. Futamase, "An approximation scheme for constructing inhomogeneous universes in general relativity," Mon. Not. Roy. Astron. Soc. **237**, 187 (1989).

[110] J. -C. Hwang, H. Noh and D. Puetzfeld, "Cosmological nonlinear hydrodynamics with post-Newtonian corrections," JCAP **0803**, 010 (2008) [astro-ph/0507085].

[111] M. Shibata and H. Asada, "PostNewtonian equations of motion in the flat universe," Prog. Theor. Phys. **94**, 11 (1995).

[112] K. Tomita, "Post-Newtonian equations of motion in an Expanding Universe," Prog. Theor. Phys. **79**, 2 (1988).

[113] T. Baldauf, U. Seljak, L. Senatore and M. Zaldarriaga, "Galaxy Bias and non-Linear Structure Formation in General Relativity," JCAP **1110**, 031 (2011) [arXiv:1106.5507 [astro-ph.CO]].

[114] D. Klein and P. Collas, "General Transformation Formulas for Fermi-Walker Coordinates," Class. Quant. Grav. **25**, 145019 (2008) [arXiv:0712.3838 [gr-qc]].

[115] E. Poisson, "A relativist's toolkit," (Cambridge University Press, Cambridge, 2004).

[116] F. Schmidt and D. Jeong, "Large-Scale Structure with Gravitational Waves II: Shear," Phys. Rev. D **86**, 083513 (2012) [arXiv:1205.1514 [astro-ph.CO]].

[117] B. Mashhoon, N. Mobed and D. Singh, "Tidal dynamics in cosmological space-times," Class. Quant. Grav. **24**, 5031 (2007) [arXiv:0705.1312 [gr-qc]].

[118] R. M. Wald, "General Relativity," (The University of Chicago Press, Chicago, 1984).